Effect of Heat Treatment on Stability of Adiabatic Shear Bands in 4340 Steel

By

Solomon Boakye-Yiadom

A Thesis Submitted to the Faculty of Graduate Studies of

The University of Manitoba

In Partial Fulfillment of the Requirements for the Degree of

MASTER OF SCIENCE

Department of Mechanical and Manufacturing Engineering

University of Manitoba

Winnipeg, Manitoba

Canada

ABSTRACT

The fingerprint of deformation in materials at large strains and at high strain rates is the formation of adiabatic shear bands. Adiabatic shear bands lead to unexpected failure of materials during service. This study investigated the possibility of eliminating adiabatic shear bands from materials subjected to severe deformation at high strain rates by post impact heat treatment.

Five groups of cylindrical AISI 4340 steel samples were impacted using the Direct Impact Hopkinson Pressure Bar (DIHPB) developed at the University of Manitoba. Metallographic analyses carried out on the impacted steel samples revealed that adiabatic shear bands are very hard and brittle and exhibit a tendency to brittle fracture.

Selected impacted samples with distinct transformed shear bands were soaked at 350 ^{O}C to 850 ^{O}C for periods ranging from 30 minutes to 4 hours to investigate how temperature and time affects the properties and structure of the shear bands.

Annealing the shear bands at 350^{O}C resulted in an increase in hardness of the shear bands and the surrounding material outside the shear bands regardless of the heat treatment before impact, amount of deformation, and the time of annealing.

Significant decrease in hardness of the shear bands occurred after post impact annealing at 650 ^{O}C for 30 minutes and 2 hours. Hardness of the shear bands reduced to the same level as that of the impacted material outside the shear bands. However, the initial path of the shear bands in the impacted steel samples could be traced through a “signature” left after the annealing.

Post-impact annealing of the steel samples at 750 ^{O}C and 850 ^{O}C resulted in a homogenous microstructure with no trace of the shear bands. The “signatures” which were used to trace the

path of the shear bands in impacted samples annealed at 650 ^{O}C disappeared and the hardness across the samples became uniform.

The observations from this study show that adiabatic shear bands in typical steel can be eliminated by annealing heat treatment. The temperature of annealing is the most critical parameter and the annealing should be performed above 650 ^{O}C.

ACKNOWLEDGEMENTS

I want to take this opportunity to thank all those who helped me and guided me throughout this work. First, I am most grateful to God who gives wisdom to the wise and knowledge to those who have understanding. Without Him, I can do nothing.

My gratitude goes to my mum Cynthia Agnes Rothe and my inspiration Sylvia Yiadom-Boakye for their prayers, advice and encouragement which has brought me this far.

I am also very grateful to my supervisor who I have taken as my dad, Professor M. N. Bassim, for his persistent support and advice even when he was at the hospital. Without him and his wise counsel, this work would never have been a success.

My thanks and appreciation goes to Dr. Akindele Odeshi for his help, support and guidance that made this work a success. I am very grateful to Mr. J. P Burak who helped and guided me through most of my experiments at the high strain rate studies laboratory. I would also want to thank the enormous help and support I received from Ian Polyzois, Ghaznafar Nazimuddin and Jeff Delorme that made this work a success.

I thank the Department of National Defense of Canada (DND), and the Natural Sciences and Engineering Research Council of Canada (NSERC) for the funds they provided for this work.

My gratitude goes to all the staff and technicians at the department of Mechanical and Manufacturing Engineering for their advice, help and support in making this work a success. My sincere gratitude goes to all my committee members for their support and advice in reading through this work. My appreciation also goes to all the Ghanaian students at the University of Manitoba especially Jonathan Mawuli Tsikata for their help, support and encouragement. Finally, my warmest gratitude goes to everyone who helped me to make this project a success.

TABLE OF CONTENT

LIST OF FIGURES

LIST OF TABLES

CHAPTER 1.0: INTRODUCTION

The behavior of materials and their mechanical properties at high strain rates of deformation differ considerably from that observed at quasi-static or intermediate strain rates. Deformation of materials at quasi-static or intermediate strain rates is characterized by slip and twinning mechanisms. However, at high strain rates, plastic deformation is characterized by strain localization along narrow bands. These bands during deformation at large strains and high strain rates occur because of adiabatic heating.

During deformation of materials, most of the deformation energy or work is spent as heat. Only a very small portion of the deformation energy is stored in the defected structure of the deformed material. During quasi-static loading and loading at low strain rates, there is enough time for the conduction of heat away from the material being deformed. Conversely, at high strain rates of deformation, there is insufficient time for the dissipation of heat away from the material to the atmosphere or the surrounding components. The heat produced is retained in the zone where it was formed. This leads to a localized increase in the temperature of the material in these zones. A rise in temperature causes a thermal softening effect on the material and a condition of mechanical instability that leads to stress collapse. Once this mechanical instability is reached, deformation becomes localized in narrow bands leading to the formation of adiabatic shear bands.

High strain rate deformations of metals such as steels are mostly characterized by the formation of adiabatic shear bands. Adiabatic shear bands are very hard and brittle compared to the surrounding materials. Their hard and brittle nature makes them susceptible to crack initiation and propagation. The performance of materials is compromised after adiabatic shear bands are

introduced in them. Material fragmentation at high strain rates are preceded by the formation of adiabatic shear bands. The width of an adiabatic shear band is very narrow usually between 10μm and 300μm.

Deformed adiabatic shear bands, which are zones of intense deformation and shearing of the original material, and transformed adiabatic shear bands, in which the material appears to have undergone a permanent change in structure, are the two types of adiabatic shear bands reported in the literature. Deformed bands consist of highly distorted and elongated grains whilst transformed bands consist of very fine equiaxed sub-grains with high dislocation density. Transformed shear bands appear white when etched with nital solution and observed under the microscope whilst deformed shear bands appear as a dark or black band. The formation of either a deformed band or a transformed band depends on the type of material, its properties and the loading conditions. In general, transformed shear bands are harder and more brittle than deformed shear bands. Cracks usually initiate and propagate in transformed shear bands and may lead to fracture during deformation.

Several investigators have studied the mechanisms of formation of adiabatic shear bands, and the failure modes of deformed materials containing adiabatic shear bands. There has been little effort to investigate if these adiabatic shear bands are stable or could be eliminated when they are formed in materials during high strain rate deformations. Recently, Sahar Al-Ameeri addressed the stability of adiabatic shear bands [26].

The current study investigated the stability of adiabatic shear bands in typical heat treatable steel. The objectives of this study were to

(1) Generate adiabatic shear bands in AISI 4340 steel samples

(2) Eliminate the adiabatic shear bands from the steel samples

(3) Study the conditions under which the shear bands disappear

To achieve these objectives, experiments were conducted on AISI 4340 steel samples to investigate the stability of adiabatic shear bands. Three groups of cylindrical AISI 4340 steel samples were austenitized, oil quenched and tempered at 315^{O}C, 425 ^{O}C, and 620 ^{O}C respectively for 2 hours, followed by air cooling. Additional two groups of AISI 4340 steel samples were austenitized, oil quenched and tempered at 315^{O}C and 425 ^{O}C respectively for 1 hour, followed by air cooling. These groups of steel samples were impacted at large strains and high strain rates to generate adiabatic shear bands using the Direct Impact Hopkinson Pressure Bar (DIHPB). The Direct Impact Hopkinson Pressure Bar was used to generate adiabatic shear bands in samples in the current study due to its advantages of ensuring homogeneous compression whilst extensively straining the material at high strain rates. This extensive straining at high strain rates ensured the development of adiabatic shear bands. Metallographic analyses were performed on the impacted steel samples to observe the occurrence of adiabatic shear bands. The width and hardness of the shear bands were measured using the Zeiss Optical Microscope.

Selected impacted steel samples with distinct transformed shear bands were soaked at 350 ^{O}C to 850 ^{O}C for periods ranging from 30 minutes to 4 hours to investigate how temperature and time affects the presence and the structure of the adiabatic shear bands. Metallographic analyses were performed on the steel samples to observe how the shear bands appear after each post impact annealing process.

The literature review in chapter 2 considers the studies carried out by other investigators on the mechanism of formation of adiabatic shear bands, their appearance and properties, and how they lead to failure. The importance of deformation at large strains and at high strain rates to generate adiabatic shear bands is reviewed in chapter 2. The stability of shear bands is also assessed in this chapter.

The experimental procedures described in chapter 3 were adopted to generate adiabatic shear bands in the steel samples and to eliminate the shear bands. The Direct Impact Hopkinson Pressure Bar (DIHPB) used for deforming the samples at large strains and high strain rates to generate adiabatic shear bands was described in this chapter. Metallographic analysis to study the properties of the shear bands and the surrounding impacted material were performed using the Zeiss Optical Microscope. Post impact heat treatment was used to investigate the stability of shear bands and how they respond to temperature and time. The flow resistance curves and the strain rates for the samples during impact were generated from the data obtained in the experimental procedure.

The experimental results and observations were presented in chapter 4. The stress resistance graphs that describe how the steel samples respond to deformation and the strain rates and impact momentum of the samples were presented in this chapter. Photomicrographs of impacted steel samples, with shear bands and the properties of shear bands were also presented in this chapter. The appearance of adiabatic shear bands and observed trends during post impact heat treatment were presented.

A general discussion on the findings from the current study was given in chapter 5 and the main conclusions drawn from this work were presented in Chapter 6.

CHAPTER 2.0: LITERATURE REVIEW

(2.1) DEFORMATION AT HIGH STRAIN RATES AND ADIABATIC SHEAR BANDS

Incessant efforts have been put into observing the behavior of materials and their mechanical properties at high strain rates since 1830 when the French military exploded cannon balls to verify the right amount of explosive needed for optimal blast [1]. John Hopkinson [2, 3] did pioneering works on high strain rate testing in 1872 and concluded that stresses of materials are higher for dynamic loadings than for static loading conditions. In 1878, Henri Tresca [4] detailed an experimental program to investigate the heat produced because of plastic deformation.

Since the 1960s, high strain rates of deformation have continued to attract research interest because of their importance as a failure mode in many engineering applications and practices. Foreign object damage, dynamic blanking and cropping, high speed manufacturing or machining, metal working, blast loading, terminal ballistics, structural impacts, explosive forming, earthquakes and crashworthiness underscore the importance of high strain rate testing.

Adiabatic shear band is a mechanism of failure that occurs in materials deformed under high strain rates. “Adiabatic” means there is no heat transfer. The heat produced is retained in the zone where it was formed. Adiabatic shear bands are very thin and consist of extremely sheared material.

In 1944, Zener and Hollomon [5] described a phenomenon of adiabatic heating and the effects of thermal softening and strain hardening leading to strain localization and formation of adiabatic shear bands at high strain rates of deformation. They discovered 32μm wide shear band during a dynamic punching of steel plate with a die. Successive works carried out by researchers have

tried to understand the phenomenon of adiabatic heating of materials during high strain rates deformation.

Studies on high strain rate deformations have been conducted from two main perspectives, the metallurgical approach and the mechanical approach. The mechanical approach is concerned with the properties of the material under high strain rates. The metallurgical approach investigates the reason why the material behaves that way under high strain rate deformations. It has been established that the behavior of materials and their mechanical properties at high strain rates differ considerably from that observed at quasi-static or intermediate strain rates.

Deformation of materials at quasi-static or intermediate strain rates is characterized by slip and twinning mechanisms. However, at high strain rates, plastic deformations are characterized by strain localization along narrow bands. The localization of strain along narrow bands has been found to occur because of adiabatic heating just as described by Zener and Hollomon. The strain localization occurs along narrow bands called adiabatic shear bands.

(2.2) FORMATION OF ADIABATIC SHEAR BANDS

Different researchers on material deformation at high strain rates observed that when materials are subjected to large strains at high strain rates, narrow bands of intense plastic shear, adiabatic shear bands, occur in the microstructure of the material [5, 6, 7, 8, 9, 10, and 11]. They observed that, when the adiabatic shear bands are formed in the material, unexpected failure occurs. Sudden failure of materials due to the formation of adiabatic shear bands stimulated researchers

to find out the mechanisms that led to the formation of shear bands and why they resulted in unexpected failure during subsequent loading.

After years of intense study and analysis on adiabatic shear bands, some researchers came up with explanations of strain localization during high strain rate deformations that lead to the formation of adiabatic shear bands. They explained that during plastic deformation, there is competition between two processes, strain hardening and adiabatic heating in the materials under deformation. Strain hardening is as a result of introduction of new dislocations as well as dislocation barriers that prevent dislocation motion during the deformation processes. The adiabatic heating occurs by the conversion of most of the deformation energy into thermal energy that leads to thermal softening (adiabatic heating). Over 90% of the energy expended in plastic deformation is converted to heat. They found out that at high strain rates of deformation, there is insufficient time for the dissipation of heat from the material to the atmosphere or the surroundings. This led to a localized increase in the temperature of the material. The heat produced is retained in the region or zone where it was created. This leads to stress collapse. Deformation becomes localized in narrow bands leading to the formation of adiabatic shear bands. It has been explained that thermo-mechanical instability occurring in materials under high strain rates of deformation, in which a rapid rise in temperature due to plastic work leads to adiabatic heating and thermal softening, causing a uniform deformation to collapse into narrow bands of intense shear within which material ductility is exhausted, is termed adiabatic shear localization.

In their observation of white bands in steel plates, Zener and Hollomon [5] proposed that the white bands were formed by adiabatic shear, in that the rate at which heat was generated by plastic deformation was greater than the rate at which heat was dissipated to the surroundings.

They therefore concluded that there was a large temperature rise in these bands during the deformation process. They also proposed that the rate of work hardening was lesser than the rate of thermal softening within the white bands. Using the basics of plasticity, at the initial stages of deformation, there is continuous work hardening to large shear strains and the rate of thermal softening due to adiabatic heating is very low as compared to the rate of work hardening. That is the amount of the deformation energy that is converted to heat energy is relatively small. This is indicated by the Isothermal curve below. At this stage, the flow stress increases when strain rate increases. Work hardening is dominant at this stage of the deformation, which is at low strain rates. As the deformation continues, the part of the deformation energy that is converted to heat energy overcomes the rate of work hardening. This leads to thermal softening and the subsequent collapse of stress leading to strain softening. This occurs at the point where the stress reaches a maximum.

When the strain rate is increased, the percentage of the deformation energy converted to heat increases with a small portion of the deformation energy being stored. The distribution of stress, strain and temperature in the material at this stage is not uniform. This is the point of thermo-mechanical instability. At this stage of the deformation, there are irregularities in the values of stress, strain and temperature distribution in the material. At high strain rates, the strain softening (work softening) is dominant leading to extreme localization of deformation in narrow bands.

Since the work of Zener and Hollomon, different material properties and loading conditions have been used by several investigators to predict the properties of adiabatic shear bands and factors that influence its formation. Bassim et al [6, 7, 17, and 20] used direct impact compression bars and torsional Hopkinson bars they developed to create adiabatic shear bands in different materials including AISI 4340 steel, maraging steel, copper, Aluminum, and some metal matrix

composites. They observed that the performance of materials is compromised after adiabatic shear bands are formed in them. The shear bands were found to be harder than the surrounding impacted material. They noted that material fragmentation at high strain rates are preceded by the formation of adiabatic shear bands. A photomicrograph of adiabatic shear band formed in a steel sample deformed at high strain rate by Bassim et al is shown in figure 2.1.

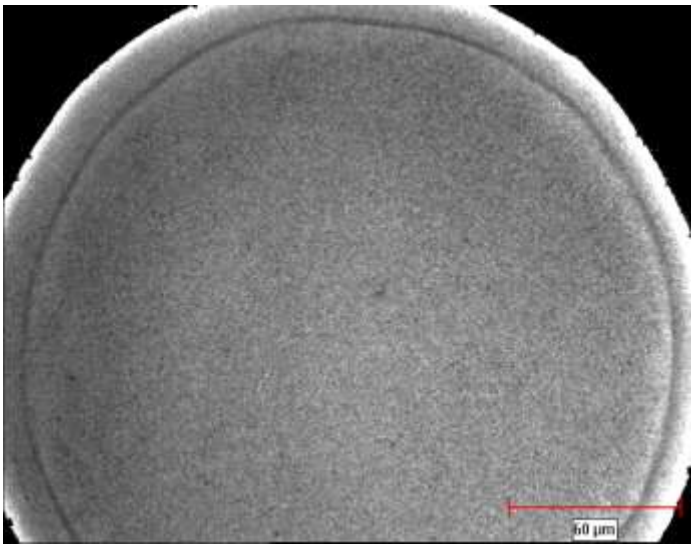

Figure 2.1: Transverse section of an impacted steel sample showing typical circular shape of shear band

Other researchers have studied the formation of adiabatic shear bands in different materials. These researchers selected materials that were susceptible to shear bands and load them at conditions where shear bands can be created in them. The conditions favorable for the formation of shear bands were analyzed and studied. Zurek used dynamic punch-impact test to study adiabatic shear bands instabilities in pearlitic 4340 steel [8]. Zurek reported that at an average strain rate of 18 000 s^{-1} and at an average strain of 0.5, white etching shear bands were formed in the pearlitic steels. He found the shear bands to be harder than the surrounding deformed material. Zurek proposed that the high hardness inside the shear bands is as a result of the fragmentation and spheroidization of cementite and the overall deformation and work hardening of the pearlitic microstructure. The observation of white etching bands by Zurek is in line with the observation made by Zener and Holloman. This is also in line with the observation made by Cho et al in dynamic torsion tests [9]. The formation of adiabatic shear bands is because of part of the deformation energy being converted to thermal energy and retained along narrow bands in the material during deformation. Wittman and Meyers [10] observed white etching adiabatic shear bands in AISI 4340 steel samples by dynamic expansion by means of an explosive charge placed in the longitudinal axis of a hollow AISI 4340 steel cylinder. They conducted SEM investigations on etched surfaces of the AISI 4340 steel samples and reported that alignment of the lamellae along the direction of shear seems to be the event that precedes shear localization. Armstrong et al reported that the initiation and propagation of adiabatic shear bands is as a result of dislocation pile ups which are enhanced by precipitates and inclusions [11]. Erlich et al [13] reported that fragments recovered after the explosion of steel casements are surrounded by shear bands. Raftenberg and Krause [14] reported large numbers of shear bands along the penetration

cavity of steel plates perforated by shaped-charges. Bassim and Odeshi [6] studied the process of deformation at high strain rates and reported that during high strain rate deformation:

(a) there is no plastic deformation in the early stages

(b) then there is a competition between strain hardening and thermal softening at a later stage in the deformation process

(c) in the final stages of the deformation process, thermal softening predominates leading to visco-plastic instability and the formation of adiabatic shear bands

A temperature rise in the materials under high strain rates of deformation is has been reported by most high strain rate researchers. A high rise in temperature of the materials during deformation due to conversion of the deformation energy to heat has been reported by various researchers during the deformation of different materials by different loading conditions at high strain rates. The basics of plastic deformation have been used to explain the relationship between heat produced and the plastic work done during high strain rate deformation. The work done during deformation [15] is given by

$$W = \int_{Lo}^{Lf} PdL \tag{2.1}$$

where P is the applied load, and L is the length of the specimen of initial length Lo and final length Lf. This is also written as

$$W = AoLo \int^{ef} \sigma(e)de \tag{2.2}$$

where Ao and Lo are the original specimen area and length respectively, σ is the engineering stress and e is the engineering strain. If this work is transformed into heat adiabatically, then the increase in temperature, ΔT is given by

$$\Delta T = \frac{1}{\rho Cp} \int^{ef} \sigma(e)de \tag{2.3}$$

where ρ is the density and Cp is the heat capacity of the sample material at constant pressure. Chen et al [16] presented an analytical model for studying the material failure in shear hinges formed during the dynamic plastic response of a circular plate under blunt projectile impact. They obtained analytical solutions for the ballistic perforation performance of a fully clamped circular plate struck by a blunt projectile. They reported that the temperature in the localized shear zone increases sharply from 430^0C to 1527^0C for the plates with $0.7<H/d<0.9$ and subjected to impact velocities of ballistic limits, and then remains as a plateau for the further increase of target thickness. They noted that the maximum temperature of $T=1527^0$C reaches the melting temperature Tm of the Weldox 460 E steel which was being analyzed.

Wittman and Meyers [10] developed a heat flow model in their studies on adiabatic shear bands in AISI 4340 steel samples by high voltage transmission electron microscopy. They developed a finite-difference model to describe the thermal history of the shear bands and reported of a temperature rise of 800^0C. The model was used to calculate temperature rises of up to 1000^0C occurring in the shear bands. Bassim [17] studied the formation of adiabatic shear bands in AISI 4340 steel samples using torsional split Hopkinson bar system. Bassim developed a finite element model during his studies for the formation and evolution of adiabatic shear bands. He reported that during the initial stages of the deformation process the temperature is constant, and then as adiabatic heating causing thermal softening prevails, there is a significant temperature rise of up to 250^0C. He concluded that the expected temperature rise in the shear bands in AISI 4340 is at least 200 ^{0}C depending on the properties and microstructure of the steel. Duffy and Chi [18] performed experiments to study the process of adiabatic shear band initiation and formation in steels. They employed an array of small high-speed infrared detectors, which

provide a plot of temperature as a function of time and position to measure the local temperature in the shear band. They measured temperatures as high as 600 °C within the shear band regions. Dodd and Bai reported temperatures as high as 1200K in steels deformed at high strain rates [19]. Odeshi and Bassim [20] studied the effects of microstructure on the dynamic shear failure of high strength low alloy steels in compression at high strain rates. In their studies, due to the hardened nature of the steels, they anticipated cleavage fracture or brittle fracture of the steel samples into many fragments. However, they observed dimples on the fracture surface and knobbly fracture mode in the quench and hardened steel samples after failure occurred. This indicates that there had been thermal softening leading to melting of the samples along the narrow bands due to adiabatic heating during the deformation. They concluded that the temperature rise inside the shear bands enhances void nucleation and growth.

This rise in temperature occurs before adiabatic shear bands are formed. At a stage in the deformation process, the adiabatic heating wins over the strain hardening process and this result in thermo-mechanical instability that leads to stress collapse and strain localization in narrow bands in the materials.

At the time that some researchers were studying the activities that precede the formation of adiabatic shear bands in different materials, other investigators wanted to find out at what sites or spots in the microstructure of materials do strain localization leading shear bands initiation and propagation occurs. These investigators observed that nucleation sites for strain localization included phase boundaries, precipitates, impurities, inhomogeneities, imperfections and defects within the material under deformation. Bassim and Odeshi [21] analyzed the occurrence of adiabatic shear bands during high strain rate deformation of metals using finite element analysis. They developed a model for the occurrence of adiabatic shear bands in metallic materials. They

reported that adiabatic shear bands initiation sites occur at points of local imperfections in the microstructure of the material. They reported that homogeneous microstructures are less susceptible to the formation of adiabatic shear bands in the range of strain rates provided by the Hopkinson Pressure Bars whereas complex microstructures that produce inclusions, fine precipitates, particles or fibers in metal matrix composites and martensitic lathes are more susceptible to the formation of adiabatic shear bands. Duffy and Chi [22] performed experiments to study the process of adiabatic shear band initiation and formation in low carbon cold-rolled steel, HY-100 and three martensitic AISI 4340 VAR steels of varying hardness. They observed that the critical strain for shear band initiation depends on the magnitude of a preexisting defect. Duffy and Chi reported that the critical strain at which stress collapse occurs depends logarithmically on the size of the initial geometric defects.

Bassim et al [6], in their studies on the shear strain localization and fracture in high strength structural materials reported that reinforcement of aluminum alloys with hard ceramic particles increases the potential of strain localization and occurrence of adiabatic shear bands under high strain rates. They concluded that the presence of hard particles or secondary precipitates in the microstructure of an alloy promotes the occurrence of adiabatic shear bands. Merzer [23] developed a model of shear banding which shows how a wide shear band develops from a narrow imperfection in an elasto-viscoplastic material subjected to dynamic shear strain. In his model, he predicted that the width of the shear band is

a) independent of the properties of the initial imperfection and

b) dependent upon thermal conductivity and strain rate

Feng and Bassim [24] developed a finite element model for the formation of adiabatic shear bands in AISI 4340 steel. They reported that strain localization occurs at where material and

geometrical defects and inhomogeneities exist. These defects and inhomogeneities serve as stress concentrations that result in strain localization during deformation. Bassim [25] in his studies of the formation of adiabatic shear bands in AISI 4340 steel samples using torsional split Hopkinson bar system concluded that adiabatic shear bands initiate at local defects and inhomogeneities in the material under deformation. Multiple nucleation points for shear bands can occur in a single material during deformation leading to the formation of multiple bands [26].

(2.3) TYPES OF ADIABATIC SHEAR BANDS AND THEIR PROPERTIES

There are two main types of adiabatic shear bands. These are deformed and transformed (white etching) shear bands.

Transformed shear bands show white after etching whereas deformed shear bands appear as a dark band. Transformed and deformed bands observed in AISI 4340 steel samples after deforming them in compression using the Hopkinson Pressure Bar by direct impact are shown in figure 2.2 respectively.

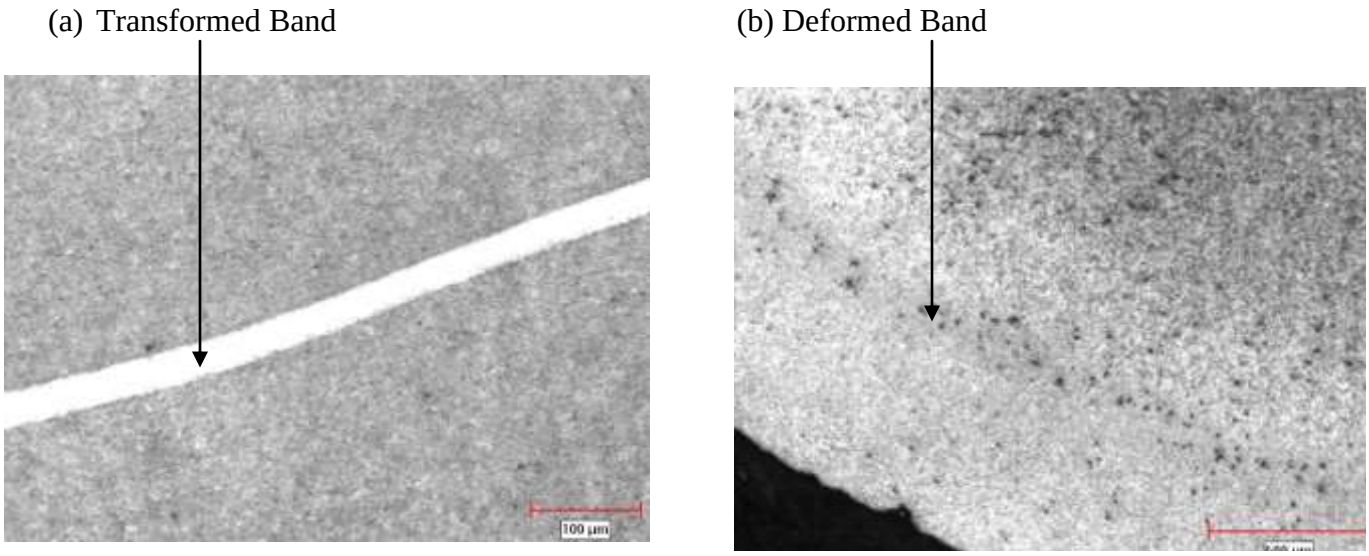

Figure 2.2: Types of shear bands (a) Transformed band (b) Deformed band

Generally, investigators have reported that adiabatic shear bands are harder than the bulk material, brittle and are sites for the initiation and propagation of cracks. The transformed shear bands have been reported as being harder than the deformed bands.

Figure 2.3 shows the hardness distribution of deformed bands and transformed bands formed in AISI 4340 steel samples compared to the hardness of the samples before impact and after impact.

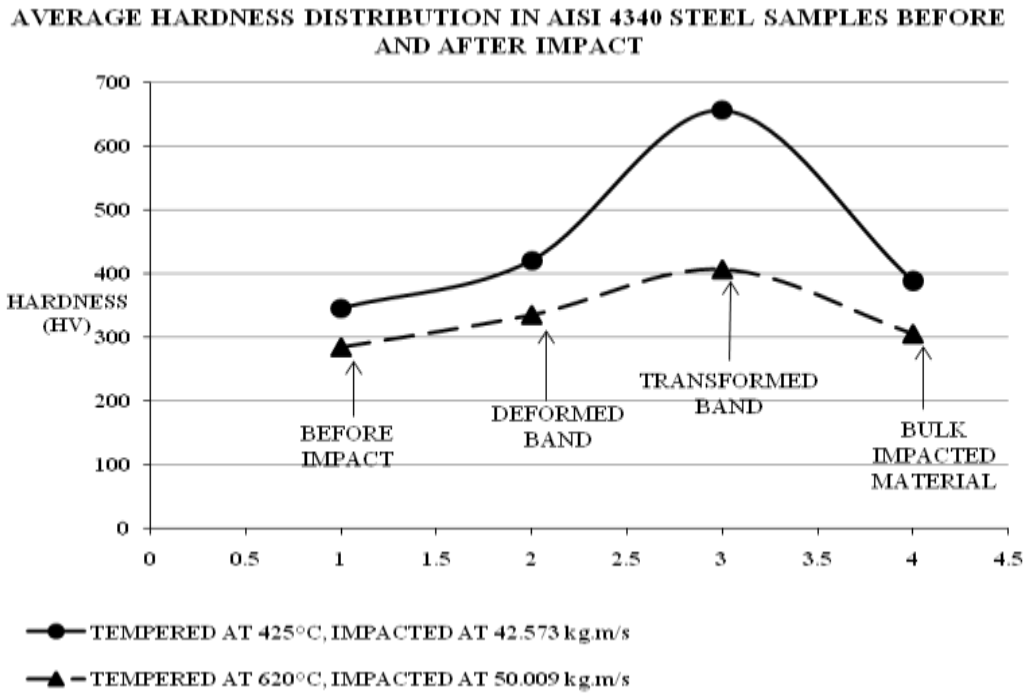

Figure 2.3: Hardness inside and outside ASBs in rolled homogeneous alloy steel after high velocity impact

Factors which affect the type of shear band formed [6, 27] include, the microstructure of the parent material, strain rate, tempering temperature and deformation temperature, temperature attained in the shear bands.

Some researchers showed that the occurrence of either a deformed band or a transformed band depends on the type of material and that some materials are susceptible to deformed bands rather than transformed bands. Various investigators carried out intensive works on different materials to find out what type of material forms what type of band and under what conditions does a particular type of band forms after deformation at high strain rates. Studies show that deformed bands form in low-density materials such as aluminum and copper. Uranium alloys, ferritic and pearlitic steels have been shown to be more susceptible to the formation of deformed bands during deformation.

Shear bands are very narrow and their widths have been reported to depend on the hardness of the material under deformation irrespective of the type of shear band formed in the material. The harder the material under deformation, the narrower the shear bands formed. Elvis Cepus [28] in his thesis on evolution of adiabatic shear bands in high strength steels at high shear strain rates concluded that the size of the adiabatic shear bands in quenched and tempered steels is directly related to the hardness of the material. Narrower adiabatic shear bands are formed in harder steels. Wider adiabatic shear bands are formed in samples tempered at higher temperatures than those tempered at lower temperatures.

(2.3.1) TRANSFORMED ADIABATIC SHEAR BANDS AND THEIR PROPERTIES

Since the discovery of the two different types of shear bands, various investigators have tried to establish the constituents of these shear bands. Many researchers have reported that the transformed shear bands have very fine equiaxed sub-grains that are different from the surrounding matrix.

Zhang et al [29], in their studies on adiabatic shear bands in impact wear using low-alloy steel, reported that the white etching adiabatic shear bands posses nearly equiaxed fine sub grains whereas the neighboring deformed matrix has characteristics of the lathe type. Chen et al [30] reported of highly elongated narrow sub grains extending in the shear direction within the shear band as well as the observation of fine equiaxed cells. Glenn and Leslie [31] were unable to resolve the grain size of the white etching bands because the grain size was thought to be less than 0.1 micrometers that was beyond the resolution limit of the microscope. Wingrove [32], in his studies on the structure of adiabatic shear bands in steel in the hardened and tempered conditions, observed that the white-etching shear bands had

(a) a high dislocation density with cell boundaries;

(b) a microstructure which did not resemble a typical martensite observed in steel , but the diffraction pattern indexed to martensite;

(c) extra appearing spots in the diffraction pattern upon tempering of the white etching zone, an indication of carbide precipitation; and

(d) small precipitates after imaging under dark-field conditions;

Some researchers proposed that a phase transformation from martensite to austenite to untempered martensite occurs in the white etching adiabatic shear bands due to the high temperature rise that occurs in the shear bands during deformation [31]. Other investigators suggested that the white shear bands are highly deformed super-saturated ferrite. Newcomb and Stobbs [33] in their transmission electron microscopy study of the white-etching layer on a railhead indicated that the white layer is of a "martensitic" structure and that it contains carbon in solution. Wingrove [32] reported that the white etching shear bands did not temper in a manner typical of martensite, and did not have the type of structure usually associated with high-carbon martensites. Nevertheless, they had lattice spacing that matches that of martensite. He concluded that the white etching shear bands are martensite though their structures are different from that of normal martensite for the steels used.

However, other researchers disagree with this phase transformation in the shear bands. Zhang et al [29] in their studies on adiabatic shear bands in impact wear using low-alloy steel reported that if phase transformation from tempered martensite to austenite occurs in the narrow bands, then a high percentage of that austenite should remain in the narrow bands when cooled by the surrounding matrix. They however reported in their studies that no apparent austenite was detected in the diffraction patterns of the adiabatic shear bands. Wittman and Meyers et al [10] reported of the absence of austenite in the shear bands since in splat quenching from austenitic phase, the presence of austenite is very common. There was no change in hardness when the sample was super cooled in liquid nitrogen that lends credence to the fact that there was no retained austenite, hence no phase transformation. Transformed shear bands are more brittle and cracks easily propagate through them.

(2.3.2) DEFORMED ADIABATIC SHEAR BANDS

Other investigators did extensive work on deformed shear bands and reported that the deformed bands had much larger sub grains than those in the white etching bands (transformed bands). The deformed shear bands consisted of highly distorted grains when compared to the surrounding matrix because of the large strain in the shear bands [6, 8, 9, and 10]. The deformed bands are regions of intense plastic deformation in the form of flow localization of the original material [27]. The deformed bands appear as dark bands under the optical microscope.

Some of the researchers found that tempering conditions of martensitic steels have an influence on the type of shear band formed [6, 29]. It was proposed that the higher the tempering temperature, the higher the tendency for the occurrence of deformed shear bands rather than transformed bands. Zhang et al [29], in their studies on steels, reported that the microstructure of the dark deformed bands had tempered martensite sub grains. They observed that deformed bands formed readily in steels tempered at higher temperatures.

Other investigators have reported of the formation of both deformed and transformed bands in the microstructure of a single material after deformation under high strain rates [7, 27, and 34]. They observed that the deformed shear bands appear to be leading the transformed bands.

(2.4) FAILURE OF MATERIALS WITH ADIABATIC SHEAR BANDS

After thorough studies on the mechanisms leading to the formation of adiabatic shear bands, the types of shear bands and the properties of shear bands, some investigators began studying the relationship between properties of shear bands and mechanisms of material failure.

Researchers reported that adiabatic shear bands, when formed, are harder than the surrounding impacted material [6 – 10]. Their hard nature makes them susceptible to cracks leading to fracture. Figure 2.4 shows cracks propagating in transformed adiabatic shear bands formed in quench-hardened and tempered steels deformed under high strain rates.

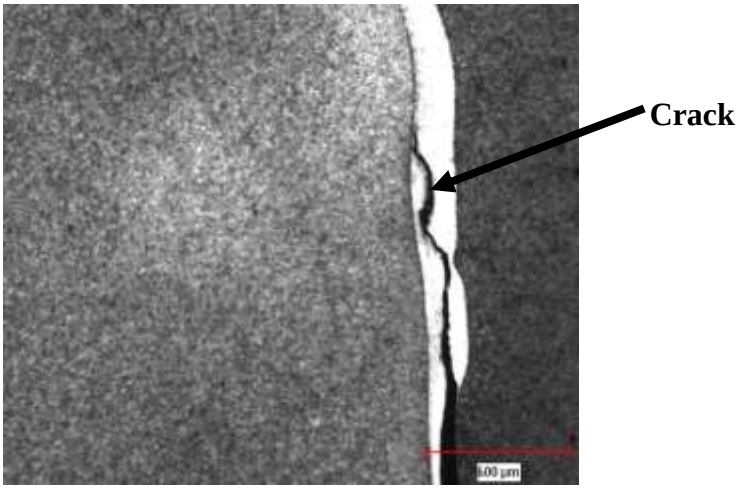

Figure 2.4: Adiabatic shear bands with a crack in quenched and tempered steels impacted at high strain rates

Bassim et al [6] reported that dynamic failure of steels under high strain rates of deformation proceeds in five steps:

(a) Formation of micro-voids inside the shear bands

(b) Coalescence of these micro voids forming void-clusters which are elongated in direction parallel to the shear bands

(c) Initiation of two fine micro-cracks parallel to the shear bands at opposite ends of the void-clusters

(d) Lengthwise growth and interconnection of adjacent micro-cracks

(e) Crack growth and propagation along the shear bands and at some points into the bulk material leading to fracture into two fragments

Mason et al [35], in their calculations for failure on Armco Iron and quenched and tempered 4340 steel, using multiplicity of steady state criterion assumed that failure through adiabatic shear will occur once thermal softening overcomes the rate of strain hardening and modeled this using the following equation,

$$\frac{d\sigma}{d\varepsilon}\Big|_{d\dot{\varepsilon}=0}=\frac{d\sigma}{d\varepsilon}+\sigma\frac{d\sigma}{dT}\frac{1}{\rho Cp}<0 \qquad 2.4$$

where σ is the effective stress, ε, the effective strain, T, the temperature, ρ, the density, and C_p, the specific heat. The rate of work hardening was given by δσ/δε and the rate of thermal softening is σ((δσ/δT)(1/ρ C_p)). When $\delta\sigma/\delta\varepsilon I_{d\dot{\varepsilon}=0} > 0$, there is a stable deformation and when $\delta\sigma/\delta\varepsilon I_{d\dot{\varepsilon}=0} <0$, the deformation is said to be unstable and adiabatic shear will occur. A second condition on the instability during deformation is that the shear strain rates should be high in order for adiabatic shear failure to occur. That is

$$\dot{\boldsymbol{Y}}_{\boldsymbol{P}} > \dot{\boldsymbol{Y}}_{\boldsymbol{crit}} \qquad 2.5$$

$\dot{\boldsymbol{Y}}_{\boldsymbol{P}}$ is the principal shear strain rate and $\dot{\boldsymbol{Y}}_{\boldsymbol{crit}}$ is the minimum critical shear strain rate. Mason et al observed a final separation across the shear region occurring through ductile fracture due to the dimpled fracture surfaces that showed on the failed samples.

(2.5) THE IMPORTANCE OF HIGH STRAIN RATE DEFORMATION TO THE FORMATION OF ADIABATIC SHEAR BANDS

Extensive deformation of materials at high strain rates is a very necessary condition for the development of adiabatic shear bands. Understanding material behavior under large plastic strains during deformation requires measuring the strains and stresses above the tensile necking limit. A compression test and a torsion test are alternative approaches that overcome necking instability that occurs in tension tests. A compression test consists of deforming a cylindrical specimen to produce a thinner cylinder of larger diameter. This test method is suitable when extensive deformation of a material is desired because it is not subjected to the instability of necking that occurs in tension tests. Extensive deformation of materials without fracture is possible in compression tests. Additionally, the specimens for compression tests are comparatively easy to make and it do not entail large volumes of materials. Brittle materials can be tested in compression given that machining of brittle materials for tensile testing is very difficult because they easily break with the least applied force. However, buckling and barreling during compression tests should be avoided. They cause nonuniform stress and strain distribution in test specimens causing difficulty in analyzing results. Unstable lateral material deflection caused by compressive stresses results in buckling. Barreling occurs when a convex surface is produced on the exterior of a cylinder that is deformed in compression. Friction between specimen-bar interfaces causes barreling and it can be reduced by proper lubrication of the interface. Buckling is reduced by selecting specimen geometry with a low length-to-diameter ratio.

Deforming the materials at high strain rates, can induce extensive deformation leading to the formation of adiabatic shear bands. Various materials have been directly impacted at the high

strain rate laboratory at the University of Manitoba based on a modified Hopkinson Pressure bar [6, 7, 17, 26, and 27]. It has been used to study formation of adiabatic shear bands at high strain rates and large strains. The Direct Impact Hopkinson Pressure Bar (DIHPB), developed at the University of Manitoba, can produce strain rates to as high as 10^4/sec. It consists of a projectile, timer, Transmitter, gun barrel, control box and accumulator and firing chamber.

A schematic of the Direct Impact Hopkinson Pressure Bar at the University of Manitoba is shown in figure 2.5.

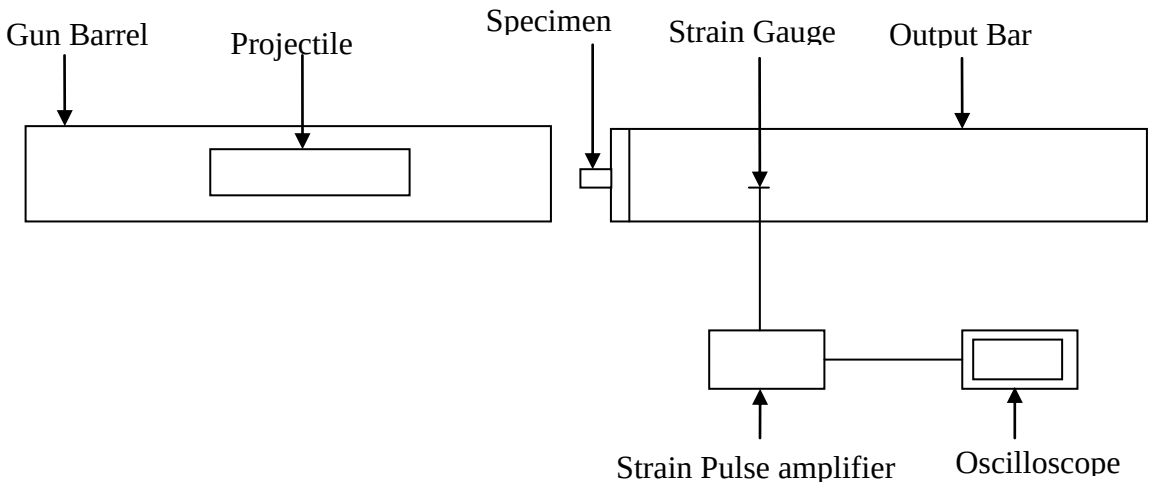

Figure 2.5: A schematic of the Direct Impact Hopkinson Pressure Bar used for high strain rate studies at the University of Manitoba

On the Direct Impact Hopkinson Pressure Bar, it is possible to ensure homogeneous-compression conditions (frictionless compression). A highly viscous gel is applied at the specimen-bar interface as well as the specimen-projector interface to reduce friction. In addition, the specimens are machined to have very smooth surfaces to aid in friction reduction between interfaces. This ensures a uniform reduction in height and allows uniform radial expansion during deformation. This leads to the formation of adiabatic shear bands in the deformed materials due to extensive straining at high strain rates. A schematic of a uniformly deformed and a nonuniformly deformed compression specimen are shown in figure 2.6.

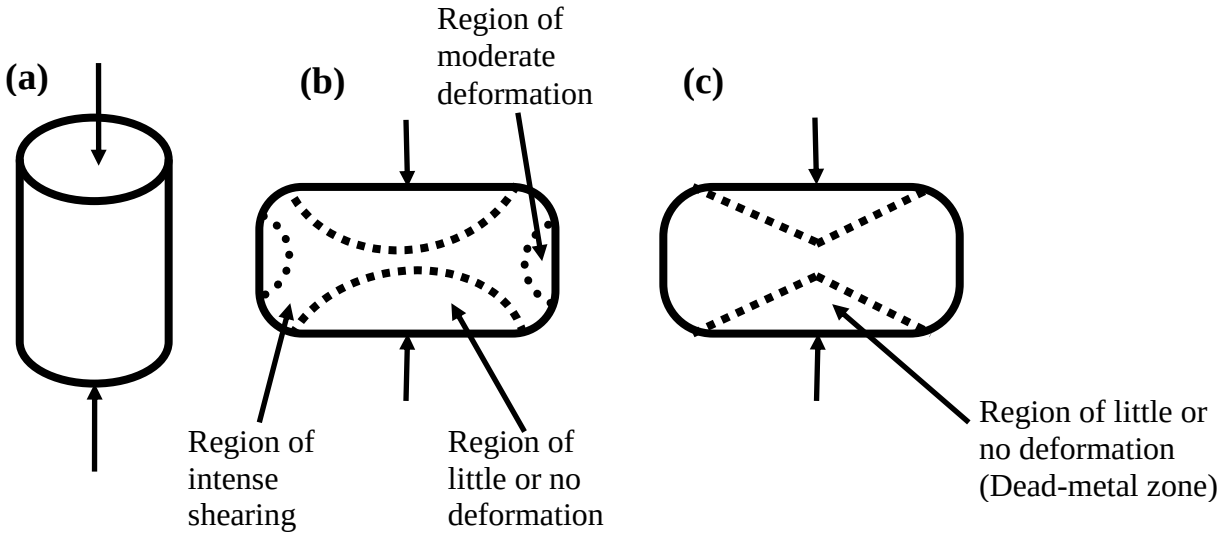

Figure 2.6: A schematic of (a) undeformed compression specimen (b) compression specimen after uniform deformation and (c) nonuniformly deformed compression specimen

(2.6) STABILITY OF ADIABATIC SHEAR BANDS

Almost all the research that has been done on adiabatic shear bands since John Hopkinson's publication in 1872 centered on

(a) the mechanisms of formation of adiabatic shear bands

(b) the types of shear bands formed

(c) appearance and shape of shear bands in the microstructure of the deformed materials

(d) factors that influence adiabatic shear band formations

(e) the failure modes and mechanisms of deformed materials with adiabatic shear bands

Most of these researchers investigated how shear bands are formed and how they lead to failure. These investigators found that once the shear bands are formed, the performance of the material is compromised. The material should be changed or reprocessed and not put in service because it will lead to unexpected failure.

There has been little effort to investigate if these shear bands can be eliminated when they are formed in materials during high strain rate deformations. Until recently, Al-Ameeri et al [26] made an initial effort in addressing the stability of adiabatic shear bands. The idea of the stability of adiabatic shear bands was to determine how permanent or how stable adiabatic shear bands are when they are formed. Can they be reversed so that the material can be put back into service?

Al-Ameeri et al [26] made an initial effort to find out the possibility of eliminating adiabatic shear bands formed in deformed steel samples. She studied the effects of heat treatment on adiabatic shear bands formed in quenched and tempered AISI 4340 steel samples impacted at high strain rates to verify if adiabatic shear bands are stable or if they can be eliminated using heat treatment procedures.

Various researchers reported that the strength and microstructure of materials have an influence on the formation of adiabatic shear bands. Backmann and Finnegan [36] studied the metallurgical effects of some materials at high rates of strain and reported that the microstructure of a material has an influence on the formation of adiabatic shear bands. Bassim et al [6] reported that the occurrence, morphology, width and cracking susceptibility of shear bands are dependent on the strength and microstructure of the material. Nakkalil [27] proposed that the resultant shear bands are sensitive to the original microstructure and the extent of strain localization on the strength and the hardness of the alloy. Since the strength and microstructure of steels are sensitive to heat treatment, there might be the possibility of using heat treatments to influence the microstructure of deformed steels that might in effect influence the contents and morphology of adiabatic shear bands.

To be able to reverse adiabatic shear bands or even attempt to get rid of them from the microstructure of the deformed materials, a thorough understanding of how the shear bands were formed in the material as well as the appearance and constituents of the shear bands is essential. Studies have suggested mechanisms including phase transformations, carbide dissolution, dislocation re-distribution, grain elongation and fragmentation, dynamic recrystallization and dynamic recovery as the mechanisms that lead to the formation of the microstructural evolution associated with shear bands.

Wittman et al [10] reported that the microstructural evolution at high strain rates begin with homogeneous distribution of dislocations rearranging themselves to form dislocation cells , which eventually become elongated sub grains, and finally breakdown into equiaxed microcrystalline structure as strain increases. This leads to thermal softening, plastic flow instability due to stress drop and finally localized deformation along narrow bands. They

reported that the temperature rise in the shear band and the microstructural changes are dependent on the strain. Yazdani et al [37], in their studies on the formation of adiabatic shear bands in copper during torsion at high strain rates, attributed the increase in flow stress and strain with increase in strain rate to the occurrence of strain hardening due to multiplication of dislocations, leading to the formation of dislocation tangles and development of dislocation cells. They concluded that being able to create localized deformation that leads to the formation of adiabatic shear bands are possible only when there is a significant strain within dislocation structures and possible twins. This means that extensive straining and very high density of dislocations go into the formation of adiabatic shear bands.

From the work by Wittman et al [10], and Yazdani et al [37], it can be deduced that there is dislocation distribution, formation of dislocation tangles and cells, elongation of sub grains and break down to equiaxed microcrystalline structure as strain increases that eventually leads to the formation of adiabatic shear bands. This is depicted in the figure 2.7 shown below:

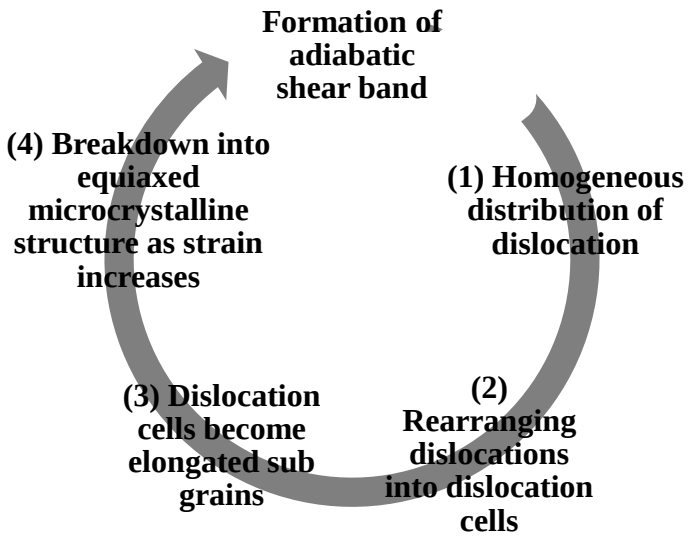

Figure 2.7: A schematic of the sequence of events that lead to the formation of adiabatic shear bands [10, 37]

The studies by Wittman et al (10) and Yazdani et al (37) are similar to the study by Chen et al (38) who proposed that during the formation of adiabatic shear bands the microstructural development occurs in three stages:

(a) Alignment and elongation of grains in shear direction

(b) Partitioning of elongated sub-grains by transverse cell walls under high hydrostatic pressure and shear stress

(c) Fragmentation of lamellae and spheroidization of the cementite in the shear direction

Wittman et al also proposed that the hardening of the shear band region is due to:

a) the diffusion of carbon to dislocation sites due to the temperature rise in the shear bands during deformation as a result of the conversion of plastic work to heat

b) reduction in carbide particle size due to the diffusion of the carbides to dislocation sites

To be able to reverse these activities that might get rid of the shear bands, the strain needs to be decreased, fine crystals need to be coarsened, elongated sub grains need to be resized, dislocation needs to be reduced and homogeneously distributed. This will lead to a reduction in hardness as well as an increase in ductility. Since extensive deformation and millions of dislocations go into the formation of adiabatic shear bands, it may be susceptible to heat treatment. Considering steel as the material, highly strained steel could be relaxed, fine constituents could be coarsened and dislocations could be reduced by heat treatment. From literature, it was found that the shear bands contain very fine particles, millions of dislocations, and are harder than the bulk material. If the fine-grain-sized particles are to be made coarser and hardness reduced to match the bulk material, then annealing heat treatment procedures might be a good procedure to follow.

Annealing is a process heat-treating procedure that is employed to reduce strength or hardness of materials, remove residual stresses, improve toughness, restore ductility, refine grain size and reduce segregation [15, 39, and 40]. There are a variety of annealing heat treatments. However, three processes that can be applied on a low alloy high strength carbon steel like AISI 4340 with a carbon content of 0.37%C to 0.44%C are full, normalizing and recrystallization annealing [39]. In full and normalizing annealing processes, the specimen is heated to elevated temperatures at which the single-phase austenite of uniform composition exists as a stable phase. The sample is held at the elevated temperature for a sufficient amount of time to ensure temperature homogenization and then cooled to room temperature. In full anneal, the sample is cooled slowly in the furnace by decreasing the temperature by 10^0C to 30^0C per hour. This is performed until it reaches a temperature at which all structural changes are completed after which it can be removed from the furnace and cooled to room temperature. This results in the formation of a

coarse microstructure with widely spaced layers. This coarse structure is relatively soft and ductile as compared to the initial structure present before the heating process. In normalize anneal, the structure is cooled in air right after heating to the elevated temperatures and this results in the formation of fine microstructure. It is suggested full annealing may be able to reduce the hardness and coarsen the fine grains in the adiabatic shear bands rather than normalizing annealing processes.

Additionally, from the literature, if cold working (deformation) has strain hardened a material, ductility can be restored by recrystallization procedures [15, 39 and 40]. During plastic deformation, part of the energy being used to deform the material is stored in the material in the form of additional dislocations and increased grain boundary surface area. Adiabatic shear bands contain a high density of dislocations with fine particles. The fine particles lend credence to increased grain boundary surface area. The material will seek to lower its energy when it is heated to a sufficiently high temperature. New crystals nucleate and grow to consume and replace the original structure. The internal energy is reduced by forming new crystals that have not experienced deformation. Strain hardening is lost and ductility is restored. The temperature at which recrystallization occurs varies from one material to the other and depends on the amount of prior deformation. The greater the amount of prior deformation, the greater the stored energy, and the lower the recrystallization temperature [40]. At the recrystallization temperature, atomic diffusion is significant and diffusion plays a major role in recrystallization.

Al-Ameeri [26] impacted quench-hardened and tempered AISI 4340 steel samples by direct impact using the modified Hopkinson pressure bar at the high strain rates studies laboratory at the University of Manitoba. The direct impact was to strain the quench-hardened steel samples extensively to create shear bands in them. She then performed post impact annealing processes

on the deformed samples to investigate how the shear bands respond to heat. She found out that, at lower annealing temperatures, the changes in the shear bands were very little. Complete microstructure and property recovery occurred when she heated an impacted steel sample at 650^0C for 2 hours. SEM investigations of steel samples carried out by Sahar Al-Ameeri after heat treatment at 650^0C showed spheroidized cementite embedded in a ferrite matrix. She observed that soaking the impacted steel samples at 650^0C for 2 hours led to the nucleation of new crystals that have not experienced deformation (strain free crystals) replacing the strained hardened crystals and the longer soaking time leading to coarsening of the fine grains in the shear bands.

CHAPTER 3.0: EXPERIMENTAL PROCEDURE

(3.1) INTRODUCTION

To meet the objectives of the current study required creating adiabatic shear bands in steel samples followed by a post-deformation heat-treatment to determine if they can be eliminated from the deformed samples and under what conditions they would disappear.

Extensive impact at large strain rates and large strains are necessary conditions for the formation of adiabatic shear bands. To facilitate development of adiabatic shear bands in the steel samples required impact at high strain rates. The Direct Impact Hopkinson Pressure Bar (DIHPB), developed at the University of Manitoba, was used to impact the steel samples to generate adiabatic shear bands.

Post-deformation annealing was used to explore the possibility of eliminating the adiabatic shear bands in the steel samples. Heat treatment variables such as temperature and time were used to investigate the influence of temperature on the adiabatic shear bands.

In order to generate adiabatic shear bands in the steel samples used for the current study and to determine if heat treatment can be used to eliminate the shear bands, the experiment was carried out in two main parts.

The first part, Part A, dealt with impact at high strain rates of deformation to generate adiabatic shear bands in the steel samples using the Direct Impact Hopkinson Pressure Bar. The dynamic material behavior of the steel samples under high strain rates and microstructural features favoring the formation of adiabatic shear bands were studied in this part of the experiment. In

this part of the experiment, the objective was to force the formation of adiabatic shear bands in the steel samples.

The second part, Part B, dealt with post-impact annealing of the steel samples to explore how heat treatment can be used to eliminate the adiabatic shear bands and its influence in the impacted steel samples. The effect of temperature and duration of annealing on the structure and properties of adiabatic shear bands in the impacted steel samples were investigated.

(3.2) MATERIAL

AISI 4340 steel was used for this study. AISI 4340 is a low alloy heat treatable steel containing nickel, chromium and molybdenum. It can develop high strength when heat-treated and can retain good fatigue strength. It is applied in aircraft transmission gears, power transmission gears, power shafts and other structural parts. AISI 4340 steel was selected because it can be heat treated to achieve different mechanical and microstructural properties. Samples were cut from a rolled AISI 4340 steel bar and machined to specifications. The machined samples had a diameter of 9.5mm and a length of 10.5mm as shown in figure 3.1. The chemical composition of AISI 4340 steel is given in table 3.1.

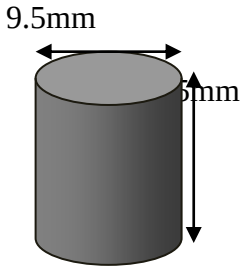

Figure 3.1: Cylindrical sample of AISI 4340 steel used for the study

Table 3.1: Chemical Composition of AISI 4340 steel

CHEMICAL COMPOSITION	MINIMUM (%)	MAXIMUM (%)
Carbon	0.37	0.44
Silicon	0.10	0.35
Manganese	0.55	0.90
Nickel	1.55	2.00
Chromium	0.65	0.95
Molybdenum	0.20	0.35
Phosphorus	0	0.04
Sulphur	0	0.04

The main processes carried out in the first part of the experiment (Part A) were

(a) Austenitization of the steel samples at 855^{O}C followed by rapid quenching in oil,

(b) Samples were grouped into groups five and tempered

(c) A group was tempered at 315 ^{O}C, another group at 425 ^{O}C and another group at 620 ^{O}C all for two hours followed by air cooling,

(d) The two remaining groups were tempered at 315 ^{O}C and 425 ^{O}C respectively for one hour followed by air cooling,

(e) Samples were impacted at large strains and at high strain rates,

(f) Metallographic analysis was used to study selected impacted samples

In the second part of the experiment (Part B):

(a) Austenitization of the steel samples at 855^{O}C followed by rapid quenching in oil,

(b) Samples were grouped into groups of three and tempered,

(c) Two groups were tempered at 315 ^{O}C and 425 ^{O}C respectively for one hour followed by air cooling while the third group was tempered at 620 ^{O}C for two hours followed by air cooling,

(d) The samples in the groups tempered at 315 ^{O}C and 425 ^{O}C respectively for one hour were all impacted at 44 kg.m/s,

(e) The samples in the group tempered at 620^{O}C for two hours were impacted at 50 kg.m/s,

(f) Metallographic analysis was used to study the microstructure of all the impacted samples,

(g) The samples impacted at 44 kg.m/s were annealed at 350 ^{O}C, 450 ^{O}C, and 650 ^{O}C for 30 minutes to 2 hours,

(h) The samples impacted at 50 kg.m/s were annealed at 350 ^{O}C,450 ^{O}C,550 ^{O}C,650 ^{O}C,750 ^{O}C and 850 ^{O}C for 30 minutes to 4 hours,

(i) All annealing processes were followed by metallographic analysis to study the microstructure of the samples.

Details of the experimental procedure are presented in the subsequent sections.

(3.3) DETAILS OF EXPERIMENTAL PROCEDURE

(3.3.1) PRE IMPACT HEAT TREATMENT OF AISI 4340 STEEL SAMPLES

Prior to deformation, the steel samples were heat treated to obtain different strengths and microstructures. This was to determine whether the condition of the steel sample before impact had an influence on the formation of adiabatic shear bands. Additionally, the test conditions and parameters that favor the formation of adiabatic shear bands were to be established. This is to ascertain how repetitive adiabatic shear bands can be generated based on material and test conditions.

Heat treatments of the steel samples were done by austenitize - quench –and- temper procedure. The austenitization was done by first heating the steel samples to the temperature where the face-centered-cubic austenite exists as a single phase. In Fe-C alloys and steels, austenite is the parent phase that transforms to martensite after rapid quenching. The austenitic temperature range for AISI 4340 steel is between 830^{O}C to 860^{O}C.

Thirty-three cylindrical samples of AISI 4340 steel were austenitized at 855^{O}C for one hour in a furnace. The hour holding time of the samples at 855^{O}C was to ensure temperature homogenization and a uniform microstructure in all the samples and avoiding uneven heating and overheating. The samples were wrapped in stainless steel foils, hung on steel wires and placed in a furnace. This was due to the small size of the samples and to decrease oxidization during austenitization. Austenitized steel samples were rapidly quenched in oil to produce a martensitic microstructure. Although the quenching velocity (cooling rate) of oil is much less than water and water is the most efficient quenching media where maximum hardness is required, it causes distortions and tiny cracks in quenched samples. For this reason, water quenching was avoided. The amount of martensite that forms depends only on the lowest temperature that is encountered during the quench and is not a function of time.

During quenching of the steel samples in the current study, the steel wires, on which the samples were hanged, were used to stir the samples in the oil to prevent the formation of air bubbles around the samples. The samples stayed in the oil until cooled before being removed from the oil. The quenched steel samples, now martensitic steel samples, were unwrapped from the steel foils and cleaned.

Due to the brittle nature of martensite, the quenched steel samples were grouped into groups of three with eleven samples in each group and were all tempered. The three groups were tempered at 315 ^{O}C, 425 ^{O}C and 620 ^{O}C respectively for two hours followed by air-cooling. All the samples were wrapped in stainless steel foils before placing them in the furnace. Tempering of martensite is a diffusion-dependent procedure. Diffusion of atoms depends on temperature and time. The two hours tempering duration was to ensure the excess carbon atoms in the martensite move and diffuse from the octahedral sites to form carbides. This result in a less distorted structure and

martensite is replaced by a mixture of ferrite and cementite known as tempered martensite. Tempering allows the carbon atoms to precipitate from the super cooled martensite. During tempering [39,40]

(a) the super saturation of carbon atoms provides the driving force for carbide formation.

(b) the high strain energy provides the driving force for recovery

(c) the high interfacial energy provides the driving force for grain growth and coarsening

(d) retained austenite provides the driving force for transformation to mixtures of ferrite and cementite.

Nine cylindrical samples of AISI 4340 steel were selected from the 315 ^{O}C, 425 ^{O}C and 620 ^{O}C tempered groups. These nine samples were austenitized at 855 ^{O}C for 30 minutes. The samples were wrapped in stainless steel foils, hung on steel wires and placed in a furnace. The nine-austenitized AISI 4340 steel samples were rapidly quenched in oil to give a martensitic microstructure. The samples stayed in the oil until cooled and then removed from the oil. The quenched steel samples were unwrapped from the steel foils and cleaned. The nine quenched steel samples were grouped into two with four samples in one group and five samples in the other group. One group containing four AISI 4340 steel samples was tempered at 315 ^{O}C for one hour followed by air-cooling and the other group was tempered at 425 ^{O}C for one hour followed by air-cooling.

Five groups with two major divisions were obtained. The major divisions were those tempered for two hours at 315 ^{O}C, 425 ^{O}C and 620 ^{O}C and those tempered for one hour at 315 ^{O}C and 425 ^{O}C. Optical micrographs of the tempered steel samples after the heat treatment are shown in figures 3.2 to figures 3.4. Figure 3.2 shows the unimpacted microstructure of a steel sample austenitized at 855 ^{O}C for 1 hour and tempered at 315 ^{O}C for 2 hours. This sample had a hardness

of 358 HV. Figure 3.3 shows the unimpacted microstructure of a steel sample austenitized at 855 ^{O}C for 1 hour and tempered at 425 ^{O}C for 2 hours. This sample had a hardness of 3445 HV. Figure 3.4 shows the unimpacted microstructure of a steel sample austenitized at 855 ^{O}C for 1 hour and tempered at 620 ^{O}C for 2 hours. This sample had a hardness of 284 HV.

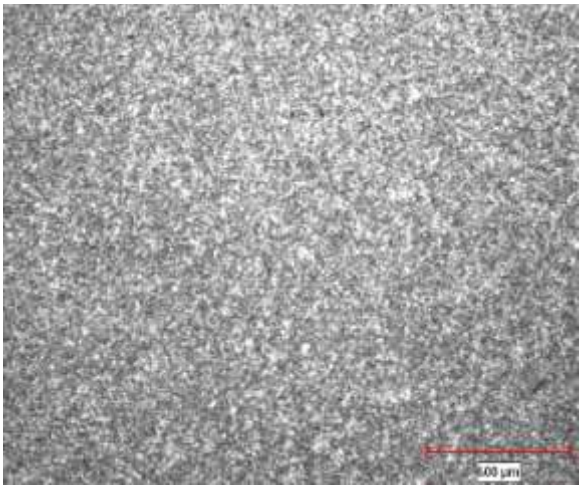

Figure 3.2: Microstructure of a steel sample tempered at 315 ^{O}C for 2 hours

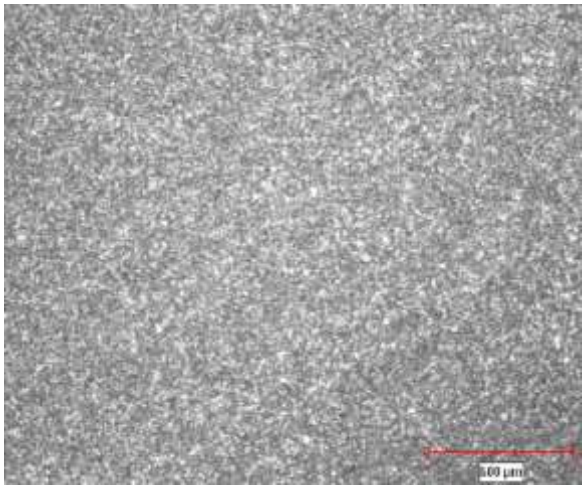

Figure 3.3: Microstructure of a steel sample tempered at 425 ^{O}C for 2 hours

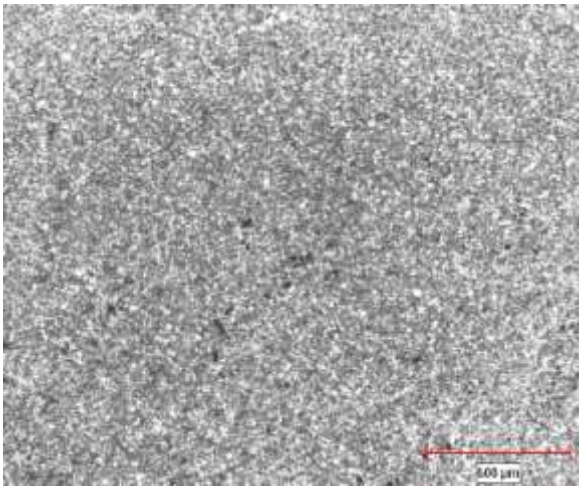

Figure 3.4: Microstructure of a steel sample tempered at 620^{O}C for 2 hours

(3.3.2) IMPACT TEST

To study the influence of heat treatment on adiabatic shear bands, the steel samples needed to be extensively strained at high strain rates to generate shear bands in them. The Direct Impact Hopkinson Pressure Bar (DIHPB) was used to impact the steel samples. Thirty heat-treated samples of AISI 4340 steel were severely strained at high strain rates at room temperature.

Samples tempered for two hours were impacted at pressures ranging between 60 KPa and 260 KPa. Those tempered for one hour were impacted at pressures ranging between 160 KPa and 260 KPa. Summary of impact pressures for each group is presented in table 3.2.

Table 3.2: Summary of Impact Pressures of Samples

Groups Of Samples	Tempering Temperature Of Samples (^{O}C)	Tempering Time Of Samples (Hours)	Impact Pressure (kPa)
1	315	2	60-160
2	315	1	160-260
3	425	2	80-180
4	425	1	180-240
5	620	2	100-260

(3.3.2a) HOPKINSON PRESSURE BAR

Many investigators have used the Hopkinson Pressure Bar, originally developed by Kolsky, to obtain the dynamic compression properties of solid materials. A modified form of the Hopkinson Pressure Bar has been developed at the University of Manitoba that applies large strains and strain rates as high as 10^4/sec in compression. It was used to impact the steel samples in the current study due to its advantages of ensuring homogeneous compression whilst extensively impacting the material at high strain rates. These severe impacts at high strain rates ensure the developments of adiabatic shear bands in the steel samples.

The Direct Impact Hopkinson Pressure Bar (DIHPB) consists of a cylindrical projectile, timer, Transmitter bar, strain gage, hollow gun barrel, control box and accumulator, and firing chamber. The accumulator contains a compressed air that provides pressure that accelerates the cylindrical projectile to strike the sample at high impact velocities. Attached is a pressure gage that is used to set and control the firing pressure. An accumulator pressure button controls the firing pressure. The strain gage is attached on the transmitter bar and is used in conjunction with a differential amplifier and a digital oscilloscope to monitor the strain during the impact test.

The “Control Box” serves as the control center of the Direct Impact Hopkinson Pressure Bar. It has a power switch button that is used for switching the set up on. There is a retract reset button which brings the cylindrical projectile to the start point before firing. The projectile is a solid cylinder machined out of AISI 4340 steel. The projectile is accelerated using an air operated gas gun. A hollow cylinder guides the projectile to strike the sample at high strain rates.

A charge button on the control box initiates pressure charging. A fire button fires the projectile after charging to the required pressure.

Two light beams connected 250mm apart are attached. This is used to calculate the projectile velocity by measuring the time the projectile travels a distance of 250mm. Components of the Direct Impact Hopkinson Pressure Bar (DIHPB) used for the current study is shown in figure 3.5. The left and right views of the DIHPB are shown in figures 3.6 and 3.7.

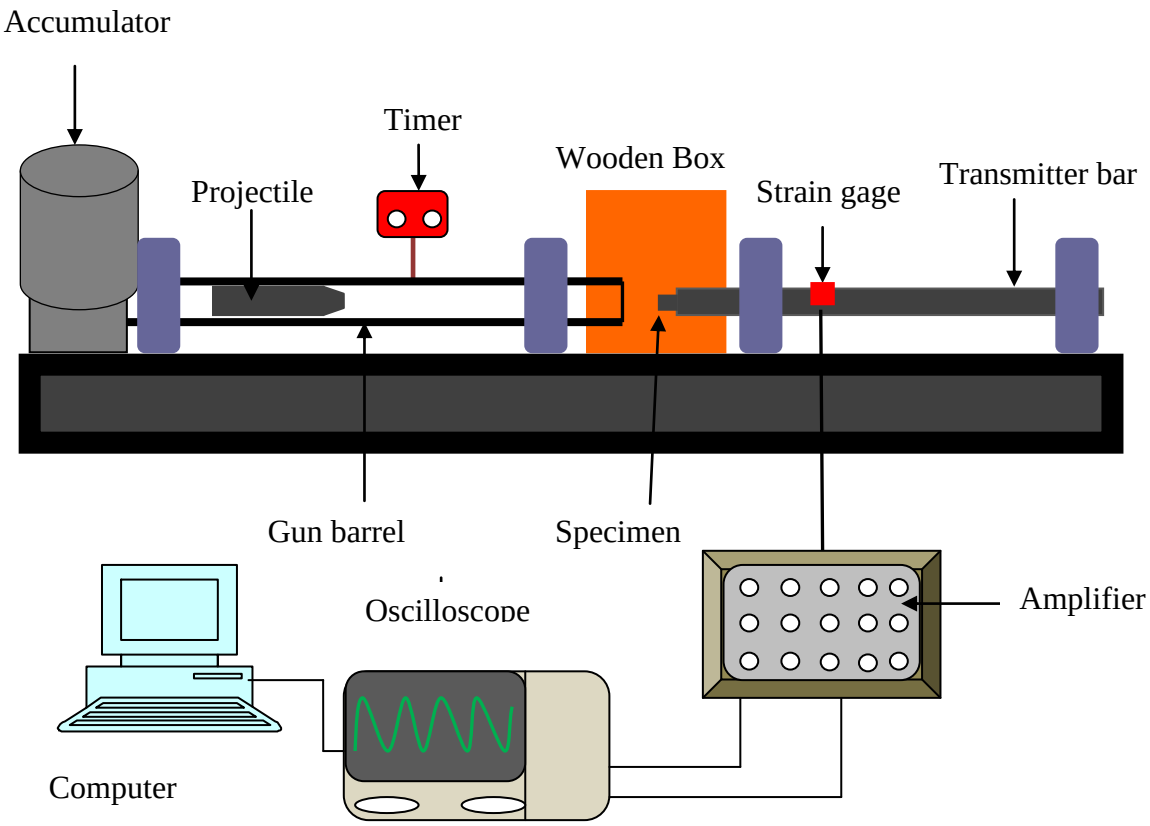

Figure 3.5: Components of the Direct Impact Hopkinson Pressure Bar (DIHPB)

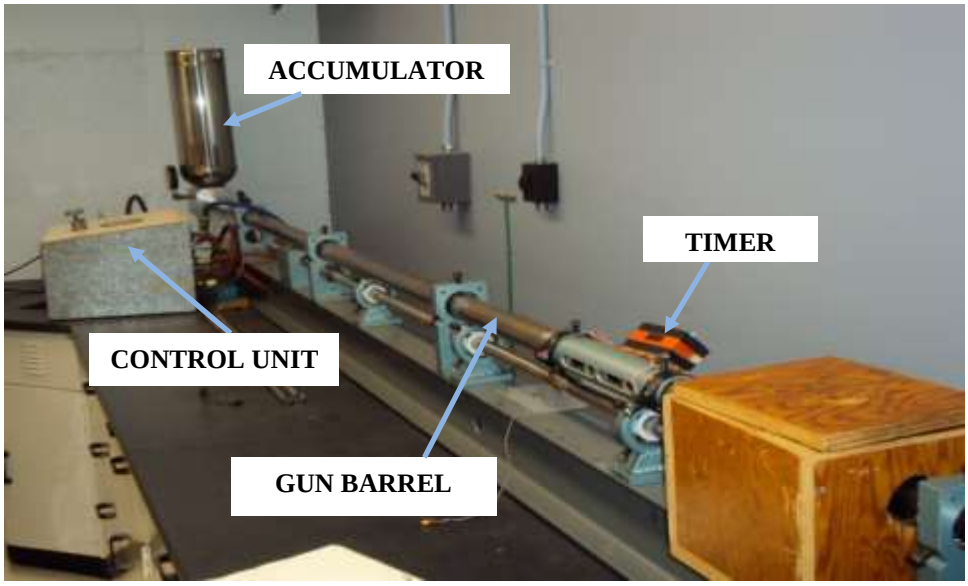

Figure 3.6: Left view of the Direct Impact Hopkinson Pressure Bar (DIHPB)

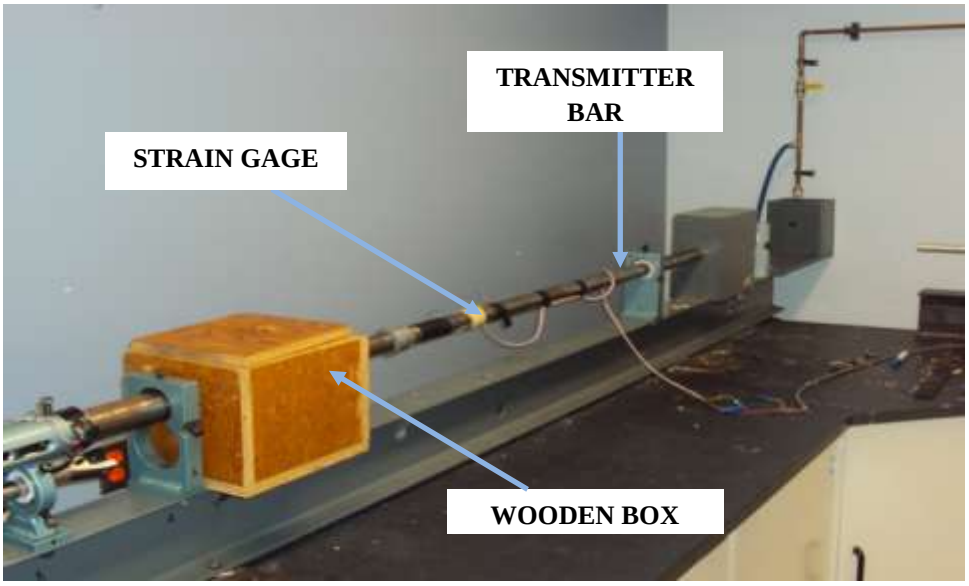

Figure 3.7: Right View of the Direct Impact Hopkinson Pressure Bar (DIHPB)

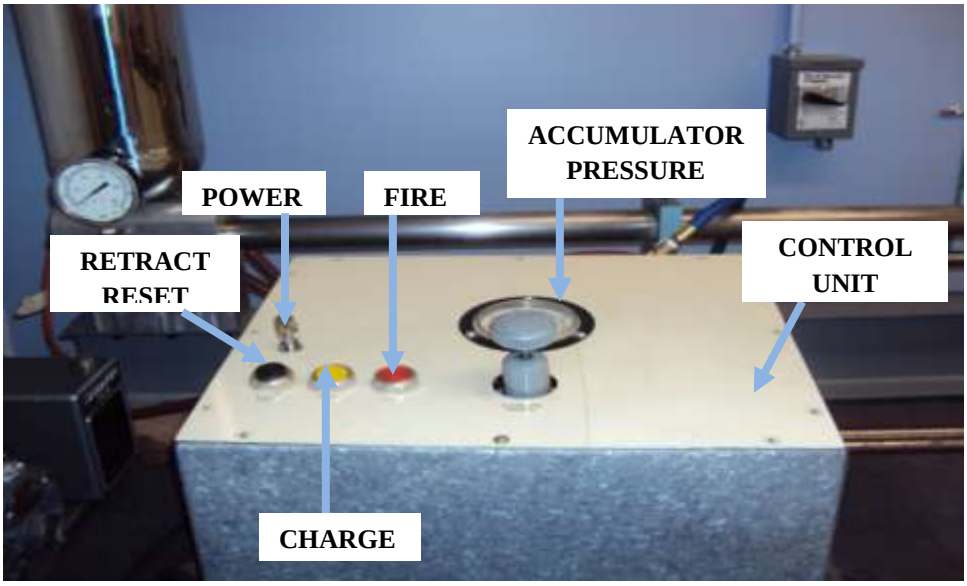

Figure 3.8: The Control Box of the Direct Impact Hopkinson Pressure Bar (DIHPB)

(3.3.2b) IMPACT PROCEDURE

Tempered AISI 4340 steel samples were subjected to high strain rate deformation using the Hopkinson Pressure Bar by direct impact. The samples were attached to the center of the front face of the transmitter bar. This was done by applying a high viscous gel on the flat faces of the steel samples. Friction at the specimen-bar interface prevents spreading of material leading to barreling during deformation. The high viscous gel reduces the friction at the specimen-bar interface and ensures uniform deformation of samples during impact. The gel also helps in keeping the sample stuck at the center of the transmitter bar. A wooden box was fixed around the specimen to reduce noise and prevent flying parts when specimens fracture during deformation.

A high velocity cylindrical projectile made from AISI 4340 steel was used to impact the samples. The hardness value of the projectile was 47 HRC and it had a weight of 18.67 N. An air operated gas gun fires the cylindrical projectile through a hollow barrel .The projectile strikes the specimen attached at the center of the front face of the transmitter bar at a very high impact velocity. This impact generates a compressive pulse (elastic waves) which travels through the specimen and are transmitted into the output bar.

A strain gage and a strain pulse amplifier are attached to the transmitter bar. The generated elastic waves during deformation are captured by the strain gage and a signal is sent to the strain pulse amplifier that amplifies the signals and sends it to an oscilloscope. The strain wave data is stored in the form of voltage and time by the oscilloscope. The firing pressure was varied to obtain different impact momentum during the deformation process. The impact momentum ranged between 31.42 kg.m/s and 50.01 kg.m/s.

Calibration of the transmitted bar with the strain gages shows that, with the current strain gage and bar, the relationship between the measured voltage and the load is

$$P = 0.021796\ V \tag{3.1}$$

where P is the load in Kilo Newton (kN) and V is the corresponding measured voltage in milli Volt (mV).

From the basic characteristics of plastic deformation, a metal is essentially incompressible. Therefore, considering the fact that the volume of a solid remains constant during plastic deformation and assuming a linear variation of displacement with time and constant strain rate, the true stress, σ, and the true strain, ε, at time t during the deformation are given by

$$\sigma_{(t)} = \frac{P(t)}{Ai}\ \frac{Li-(Li-Lf)(t/tf))}{Li} \tag{3.2}$$

$$\varepsilon_{(t)} = \ln\ \frac{Li}{Li-(Li-Lf)(t/tf))} \tag{3.3}$$

where Li is the initial length and Lf is the final length of the steel samples.

The maximum strain in a specimen is directly proportional to the strain rate, έ, and the length of the striker bar, *l*, by the relation

$$\acute{\varepsilon} = \frac{C}{2l}\ \varepsilon \tag{3.4}$$

where C is the longitudinal wave propagation velocity in the transmitter bar.

Dynamic stress strain curves were generated for the steel samples under direct impact using the above equations. The global strain rates for each test were calculated as a function of total strain using the above equation.

(3.3.3) METALLOGRAPHY

Metallography is the study of the microstructure of a material. Basic metallographic steps include sectioning and cutting, mounting, grinding, polishing, etching, microscopic analysis and hardness testing. The purpose of the metallographic analysis was to verify which sample had shear bands formed in its microstructure and to document on the properties of the shear bands.

Selected impacted samples were mounted, ground, polished and etched to reveal the microstructure of the samples. Microscopic analysis was then performed on all the samples using the Zeiss Optical Microscope with the Clemex Vision Analyzer. This was done to investigate the occurrence of adiabatic shear bands as well as changes in the microstructure of the impacted samples.

(3.3.3a) MOUNTING, GRINDING, POLISHING AND ETCHING

To reveal the microstructure of the impacted steel samples under the microscope, the steel samples were ground, polished and etched. The grinding and polishing removes unwanted particles from the surface of the impacted steels.

Due to the small size of the cylindrical steel samples used for this experiment, they were mounted for easier handling during grinding and polishing. The mounting also protects the specimen edge and maintains the integrity of the surface features of the steel samples. To mount the cylindrical steel samples, a high pressure and temperature in a mould were used to fuse black granular Bakelite phenol of specific gravity 1.4 gm/cm^3 into a solid mass around the impacted steel samples. The high temperature and pressure in the mould compacts and melts the black

Bakelite powder around the steel samples. The shrinkage of the black Bakelite powder in compression is 0.006. This forms a cylindrical plastic mount around the steel samples. The mould temperature and pressure used for this experiment were 130 ^{O}C and 4.2 MPa respectively.

Mounted steel samples were ground using emery papers. Grinding was required to planarize the specimen and was accomplished by decreasing the particle size or the abrasive grit sequentially to obtain surface finishes that were ready for polishing. Polishing was done on a 6-micron diamond wheel and a 1-micron diamond wheel until a mirror surface was obtained. The main purpose of the polishing was to remove the damage produced during grinding. The polishing also ensured that the specimens were flat and that all secondary phases or inclusions are retained.

The polished specimens were then etched. Etching optically enhances microstructural features such as phase features and grain size. A 2% Nital solution consisting of 100 ml Ethanol and 1-20 ml Nitric acid was the etchant used for etching the specimens. Cotton buds were dipped in the 2% Nital solution and swiped on the mirror surface of the steel specimen for thirty seconds. The etched steel specimens were then rinsed in water. Alcohol was used to rinse the steel specimens after rinsing in water to prevent the acid from damaging the lens of the optical microscope. Etched steel samples were then dried and studied under the optical microscope for the occurrence of adiabatic shear bands. Figure 3.9 shows an impacted steel sample mounted in Bakelite.

Figure 3.9: Impacted AISI 4340 Steel Samples Mounted in Bakelite

(3.3.3b) MICRO-HARDNESS TESTING

Buehler micromet micro hardness testing machine was used to measure the micro-hardness of the steel samples by the Vickers hardness test (HV).

A regular quadrangular pyramid diamond indenter with a face-to-face angle (the apex angle between opposite faces) of 136^{O} was used to form indents inside and outside the shear bands in the steel specimens.

A test force of 300 gram-force that corresponds to 2.942 N was applied during each test. After an equilibrium condition is reached and further penetration ceases, the force remained applied for 15 seconds. The test force was applied to form indents in the shear bands and in the bulk materials of the impacted specimen outside the shear bands.

When the indenter was removed, two small parallel lines guided by microscopic lens were used to measure the two diagonals of the indent made by the quadrangular pyramid diamonds. The micromet micro hardness testing system calculates the hardness value that corresponds to the measured diagonals of the quadrangular pyramid diamond indenter.

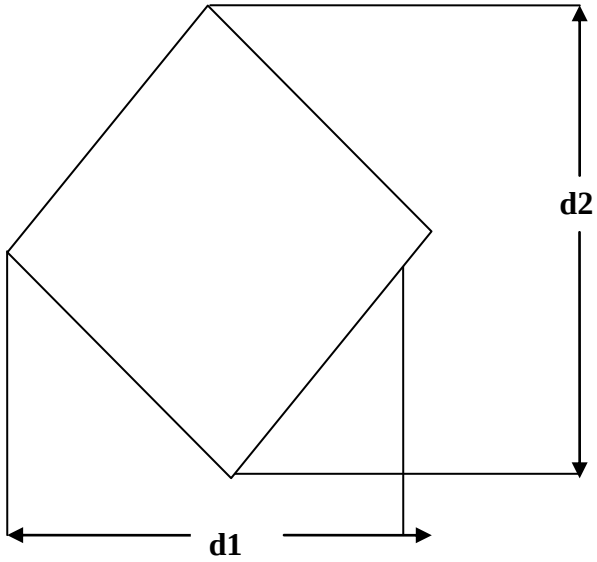

Figure 3.10: Schematic of the indent made by the diamond indenter

The Vickers hardness number is related to the applied force and the surface area of the measured unrecovered indentation produced by the diamond indenter. The micromet micro hardness-testing machine calculates the Vickers hardness based on the equation below

$$HV = k\left(\frac{F}{S}\right) = 0.102\left(\frac{F}{S}\right) = 0.102\left((2F\sin\text{ø}/2)/d^2\right) = 0.1891(F/d^2) \qquad 3.5$$

where

HV = Vickers hardness

k = Constant ($k=1/g_n=1/9.806650=0.102$)

F = Test Force (N)

S = surface area of indentation (mm^2)

d = Average length of two diagonals (mm), $d= (d_1 + d_2)/2$

ø = Face-to –face apex angle of diamond indenter (136^O)

g_n = Standard acceleration due to gravity

Indents were made inside the shear bands and an average value for the hardness inside the shear bands was calculated. To compare the increase in hardness in the shear bands to the bulk impacted material, indents were made outside the shear bands and the average hardness was calculated for the bulk material. Seven to ten readings were taken from each of the hardness inside the shear bands and the hardness of the surrounding materials and averaged.

The Vickers hardness testing procedure was used because the deformation produced by the diamond indenter is negligible on the hard AISI 4340 steel samples. The indentations are geometrically similar irrespective of the size and the test was easier since the samples surfaces were well polished. Detailed results of the hardness of the shear bands and the hardness of the surrounding impacted materials are presented in chapter 4. Figure 3.11 shows how the indents were made inside and outside the shear bands using a regular quadrangular pyramid diamond indenter.

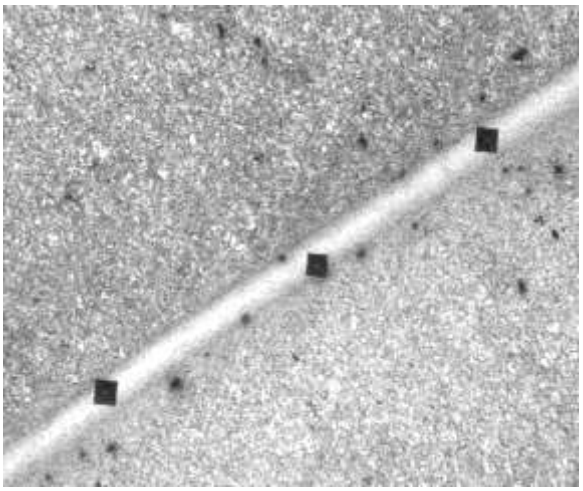

Figure 3.11: Optical micrograph showing indents formed in the shear bands

(3.3.3c) THICKNESS MEASUREMENTS OF THE SHEAR BANDS

The thicknesses of the shear bands were measured. These were done after mounting the samples on the optical microscope. When a sample has a shear band, the shear band appears as a white band or a black band after etching. Under the optical microscope, after the selection of a proper magnification, the thicknesses of the shear bands were measured using the Clemex Vision analyzer. The thickness of the shear bands were measured across the entire length of the shear band. About fifteen to twenty readings were taken from each shear band and averaged. Detailed results of the width of the shear bands are presented in chapter 4. Figure 3.12 shows variations in the width of the shear bands.

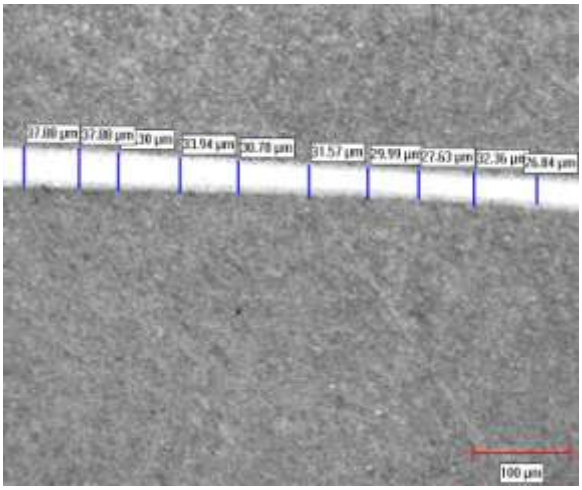

Figure 3.12: Optical micrograph showing how the thickness of a shear band varies

(3.3.4) POST IMPACT ANNEALING PROCESSES

Adiabatic shear bands contain very fine particles and are harder than the bulk material. Reversing this structure would be to coarsen these fine particles and reduce the hardness. Annealing is a process heat-treating operation that is used to reduce strength or hardness, refine grain size, remove residual stresses, improve toughness, restore ductility, and reduce segregation. Annealing heat treatment procedures was used to reverse the adiabatic shear bands and its properties to suit that of the bulk material.

It was documented from the first part of this study that when AISI 4340 steel samples were austenitized at $855^{O}C$ for 30 minutes, tempered at 315 OC or 425 OC for one hour, and impacted at 44.43 kg.m/s, clearly defined transformed bands are formed. In addition, it was found that when AISI 4340 steel samples were austenitized at $855^{O}C$ for 30 minutes, tempered at $620^{O}C$ for two hours, and impacted at 50.01 kg.m/s, clearly defined transformed bands are also formed. To perform heat treatment procedures on the shear bands, it required producing clearly defined shear bands before performing annealing heat treatments on them. Only transformed bands were used for the current study.

Fifteen cylindrical samples of AISI 4340 steel samples were austenitized at $855^{O}C$ for 30 minutes. This was to ensure that only the face centered cubic austenitic single phase existed in all the steel samples. The 30 minutes was to ensure temperature homogenization and prevent uneven microstructure from occurring. All the fifteen samples were wrapped in stainless steel foils and were hung on stainless steel wires before placing them in the furnace. The stainless steel foils reduced oxidation of the AISI 4340 steel samples at the austenitization temperature of $855^{O}C$.

After soaking at 855^{O}C for 30 minutes, the samples were removed and quickly quenched in oil to produce a martensitic microstructure. The stainless steel wires were used to stir the oil during quenching to prevent air bubbles from forming on the surfaces of the steel samples to ensure a very efficient martensitic transformation. The samples were removed from the oil and cleaned.

The quenched steel samples were grouped into groups of three and tempered to produce a tempered martensite structure. The first group was tempered at 315 ^{O}C for 1 hour followed by air-cooling. The second group was tempered at 425 ^{O}C for one hour followed by air-cooling. The third group was tempered at 620 ^{O}C for two hours followed by air-cooling. All the samples were wrapped in stainless steel foils before placing them in the furnace.

The samples that were tempered at 315 ^{O}C for one hour and 425 ^{O}C for one hour were all impacted at 44.43 kg.m/s. The other samples that were tempered at 620 ^{O}C for two hours were all impacted at 50.01 kg.m/s. The entire impact tests were done directly using the Hopkinson Pressure Bar.

Samples were cut into two transversely after the impact tests to obtain more samples for the annealing processes. All the impacted samples were mounted in black Bakelite powder under heat and pressure. They were then ground, polished, etched and studied under the Zeiss Optical microscope. The thickness of the shear bands were each measured. The thicknesses of the shear bands were measured across the entire length of the shear bands. About fifteen to twenty readings were taken from each shear band and averaged. The hardness of the shear bands and the hardness of the surrounding material were all measured using the Buehler micromet micro hardness testing machine. Seven to ten readings were taken from each of the hardness inside the shear bands and the hardness of the surrounding materials and averaged.

After measuring the thicknesses and the hardness of the shear bands and the surrounding material, the samples were broken off from the Bakelite. They were cleaned and wrapped in stainless steel foils for annealing.

The first group, consisting of AISI 4340 steel samples tempered at 315 ^{O}C for one hour and impacted at 44.43 kg.m/s , were annealed at 350 ^{O}C, 450 ^{O}C and 650 ^{O}C from 30 minutes to 2 hours. The second group, consisting of AISI 4340 steel samples tempered at 425 ^{O}C for one hour, and impacted at 44.43 kg.m/s were annealed at 350 ^{O}C, 450 ^{O}C and 650 ^{O}C from 30 minutes to 2 hours. Samples in the third group, consisting of AISI 4340 steel tempered at 620 ^{O}C for two hours and impacted at 50.01kg.m/s, were annealed at 350 ^{O}C, 450 ^{O}C, 550 ^{O}C, 650 ^{O}C, 750 ^{O}C, and 850 ^{O}C from 30 minutes to 4 hours. After heating, the samples were all cooled in air.

The impacted samples were held at these temperatures for the various times ranging between 30 minutes and 4 hours. Soaking the AISI 4340 steel samples at the higher temperatures were done for shorter times whilst soaking at the lower temperatures were done for longer times. This provided information on how different temperatures and times affect the properties of the shear bands and the surrounding material.

After each time and temperature process, the samples were mounted, ground, polished and etched and then studied under the optical microscope. The thickness of the shear bands was measured for each sample after each annealing process. Fifteen to twenty measurements were taken for the thicknesses and averaged. The hardness of the shear bands and the hardness of the surrounding material were also measured after each annealing process. A test force of 300grams that corresponds to 2.942 N was applied for 15 seconds to form indents in the shear bands and in

the bulk materials of the impacted specimen outside the shear bands. Seven to ten hardness measurements were taken for both the shear bands and the surrounding material and averaged.

In the next chapter, the results obtained from all parts of this investigation are presented and analyzed.

CHAPTER 4.0: EXPERIMENTAL RESULTS AND OBSERVATIONS

The fingerprint of extensive deformation at large strains and high strain rates is the formation of adiabatic shear bands. The samples were directly impacted using the Direct Impact Hopkinson Pressure Bar (DIHPB) to ensure severe deformation at large strains and high strain rates to generate adiabatic shear bands. The results below show that impact momentum and strain rates affect the shear bands but the initial condition of the steel samples also has a significant effect on how and the type of shear band formed. The stress response graphs are indicative of the behavior of the samples and their respond to deformation.

(4.1) DYNAMIC BEHAVIOR OF AISI 4340 STEEL SAMPLES UNDER IMPACT

(4.1.1) EFFECTS OF THE DIFFERENT TEMPERING TIME AND TEMPERATURE ON THE DYNAMIC BEHAVIOR OF THE STEEL SAMPLES DURING THE IMPACT TEST

Five different groups of AISI 4340 steel were subjected to dynamic mechanical loading in compression at high strain rates using the direct impact Hopkinson Pressure Bar system. The five major groups were

During the dynamic impact loading, it was observed that the steel samples tempered at $315^{O}C$ and $425^{O}C$ for one hour could be deformed at higher impact momentums and higher strain rates without failing or fracturing as compared to their counterparts that were tempered at $315^{O}C$ and $425^{O}C$ for two hours. It was also observed that the steel samples tempered at $620^{O}C$ for two hours could be deformed at higher impact momentums and strain rates without failing and

fracturing as compared to the other samples tempered at 315^{O}C and 425^{O}C for two hours. This can be attributed to embrittlement occurring at these tempering temperatures.

During the dynamic impact tests, the impact momentums of the steel samples in the 315 ^{O}C group tempered for two hours ranged from 31.4 kg.m/s to 40.7 kg m/s. The sample that was impacted at 40.7 kg.m/s failed by breaking into two halves along a 45^{O} angle to the longitudinal axis of the sample. However, it was observed that the samples in the 315 ^{O}C group tempered for one hour showed higher impact toughness than those in the 315 ^{O}C group tempered for two hours. The samples in the 315 ^{O}C group tempered for one hour did not fail at this same impact momentum of 40.7 kg.m/s during the impact tests. The samples in the 315 ^{O}C group tempered for one hour were impacted to as high as 50.0 kg.m/s without failing. The impact momentum of the 315 ^{O}C group tempered for one hour ranged between 40.7 kg.m/s to 50.0 kg.m/s. None of the samples in this group failed within the impact momentums at which they were tested.

The impact momentums of the samples in the 425 ^{O}C group tempered for two hours were from 33.3 kg.m/s to 42.6 kg.m/s. The sample in this group impacted at 42.6 kg.m/s fractured along a 45^{O} angle to the longitudinal axis of the sample. The fractured sample showed that the material had disintegrated into two parts. However, total fragmentation of the sample did not occur because of high temperature fusion of the two halves together. This suggests a significant rise in temperature along the path of shear strain localization. The sample from the 425 ^{O}C group, tempered for two hours and impacted at 42.6 kg.m/s that broke into two, had an average nominal strain 0.4024.

Samples in the 425 ^{O}C group tempered for one hour exhibited higher impact toughness than the samples in the 425 ^{O}C group tempered for two hours. Samples in the 425 ^{O}C group tempered for one hour were impacted to as high as 46.3 kg.m/s without failing. However, when a sample in

this group was impacted at 48.2 kg.m/s it failed. The impact momentum of the samples in this group tempered at 425 ^{O}C for one hour ranged from 42.6 kg.m/s to 48.2 kg.m/s at which the sample failure occurred.

The samples tempered at 315 ^{O}C and at 425 ^{O}C for one hour, all showed higher impact toughness than those tempered at 315 ^{O}C and at 425 ^{O}C for two hours. They absorbed much of the impact energy without failing at impact momentums at which those tempered at 315 ^{O}C and 425 ^{O}C for two hours were failing.

The impact momentums of the 620 ^{O}C group tempered for two hours ranged between 35.1 kg.m/s to 50.0 kg.m/s. None of the samples in this group fractured during the impact tests. The Tables 4.1 and 4.2 show the test conditions during impact and the calculated impact momentums and strain rates of the steel samples after impact respectively. All the samples highlighted yellow fractured during the impact.

Table 4.1: Geometry Of Samples Before Impact

SAMPLE	TEMPERING TEMPERATURE AND TIME	L_O (mm)	D_O (mm)	AREA $(mm)^2$	L_F (mm)
1	315^OC –2 HRS	10.52	9.5	70.88	10.03
2	315^OC –2 HRS	10.55	9.49	70.73	9.50
3	315^OC –2 HRS	10.55	9.5	70.88	9.36
4	315^OC –2 HRS	10.53	9.5	70.88	9.06
5	315^OC –2 HRS	10.53	9.52	71.18	8.83
6	315^OC –2 HRS	10.52	9.51	71.03	7.34
1	315^OC – 1 HR	10.51	9.49	70.70	8.51
2	315^OC – 1 HR	10.56	9.51	71.03	8.33
3	315^OC – 1 HR	10.56	9.50	70.88	7.72
4	315^OC – 1 HR	10.57	9.50	70.88	7.35
1	425^OC –2 HRS	10.51	9.50	70.88	9.42
2	425^OC –2 HRS	10.60	9.49	70.73	9.02
3	425^OC –2 HRS	10.56	9.50	70.88	8.64
4	425^OC –2 HRS	10.53	9.49	70.73	8.46
5	425^OC –2 HRS	10.56	9.49	70.73	8.18
6	425^OC 2 HRS	10.56	9.50	70.88	6.79
7	425^OC –2 HRS	10.54	9.49	70.73	6.30
1	425^OC –1 HR	10.57	9.49	70.73	7.89
2	425^OC –1 HR	10.51	9.49	70.66	7.54
3	425^OC –1 HR	10.53	9.51	71.03	7.29
4	425^OC 1 HR	10.51	9.49	70.73	5.76
1	620^OC –2 HRS	10.53	9.50	70.88	8.52
2	620^OC –2 HRS	10.54	9.49	70.73	8.00
3	620^OC –2 HRS	10.55	9.50	70.88	7.69
4	620^OC –2 HRS	10.54	9.47	70.44	7.32
5	620^OC –2 HRS	10.54	9.49	70.73	6.99
6	620^OC –2 HRS	10.53	9.50	70.88	6.80
7	620^OC –2 HRS	10.53	9.49	70.73	6.07
8	620^OC –2 HRS	10.54	9.52	71.18	6.04

Table 4.2: Momentum and Strain Rates of Impacted Samples

SAMPLE	TEMPERING TEMPERATURE AND TIME	PRESSURE	VELOCITY (m/s)	MOMENTUM (kg.m/s)	L_O-L_F (mm)	NOMINAL STRAIN	STRAIN RATE (S^{-1})
1	315^{O}C –2 HRS	60	16.2	31.4	0.5	0.05	439
2	315^{O}C –2 HRS	80	17.1	33.3	1.1	0.10	938
3	315^{O}C –2 HRS	100	18.1	35.1	1.2	0.11	1066
4	315^{O}C –2 HRS	120	19.1	36.1	1.5	0.14	1321
5	315^{O}C –2 HRS	140	20.0	38.9	1.7	0.16	1530
6	315^{O}C –2 HRS	160	20.1	40.7	3.2	0.30	2864
1	315^{O}C – 1 HR	160	20.1	40.7	2.0	0.19	1801
2	315^{O}C – 1 HR	180	211	42.6	2.2	0.21	1998
3	315^{O}C – 1 HR	220	23.8	46.3	2.8	0.27	2547
4	315^{O}C – 1 HR	260	25.8	50.0	3.2	0.30	2879
1	425^{O}C –2 HRS	80	17.1	33.3	1.1	0.11	983
2	425^{O}C –2 HRS	100	18.1	35.1	1.6	0.15	1414
3	425^{O}C –2 HRS	120	19.1	36.1	1.9	0.18	1717
4	425^{O}C –2 HRS	140	20.0	38.9	2.1	0.19	1864
5	425^{O}C –2 HRS	160	20.1	40.7	2.4	0.23	2138
6	425^{O}C 2 HRS	180	21.1	42.6	3.8	0.36	3376
7	425^{O}C –2 HRS	180	21.1	42.6	4.2	0.40	3809
1	425^{O}C –1 HR	180	21.1	42.6	2.7	0.26	2421
2	425^{O}C –1 HR	200	22.9	44.4	2.9	0.28	2675
3	425^{O}C –1 HR	220	23.8	46.3	3.2	0.31	2912
4	425^{O}C 1 HR	240	24.8	48.2	4.8	0.45	4278
1	620^{O}C –2 HRS	100	18.1	35.1	2.0	0.19	1804
2	620^{O}C –2 HRS	120	19.1	36.1	2.5	0.24	2281
3	620^{O}C –2 HRS	140	20.0	38.9	2.9	0.27	2567
4	620^{O}C –2 HRS	160	20.1	40.7	3.2	0.31	2890
5	620^{O}C –2 HRS	180	21.1	42.6	3.6	0.34	3190
6	620^{O}C –2 HRS	200	22.9	44.4	3.7	0.35	3354
7	620^{O}C –2 HRS	240	24.8	48.2	4.5	0.42	4010
8	620^{O}C –2 HRS	260	25.8	50.0	4.5	0.43	4042

(4.1.2) DYNAMIC STRESS RESISTANT GRAPHS FOR IMPACTED AISI 4340 STEEL SAMPLES TEMPERED FOR TWO HOURS

The signal from the strain gage on the transmitter bar was captured by the oscilloscope as a voltage and time data. Strain gage amplifiers were employed to magnify the signals from the strain gage. A typical graph showing the voltage and time data captured by the oscilloscope is shown in figure 4.1. This shows how the material responds to deformation during impact.

The oscilloscope data was converted to load-time data using static calibrations. Stress resistance graphs for all the impacted samples were estimated using the data recorded by the oscilloscope during the impact tests using the equations 4.1 and 4.2.

$$\sigma_{(t)} = \frac{P(t)}{Ai} \frac{Li - (Li - Lf)(t/tf))}{Li} \qquad 4.1$$

$$\varepsilon_{(t)} = In \frac{Li}{Li - (Li - Lf)(t/tf))} \qquad 4.2$$

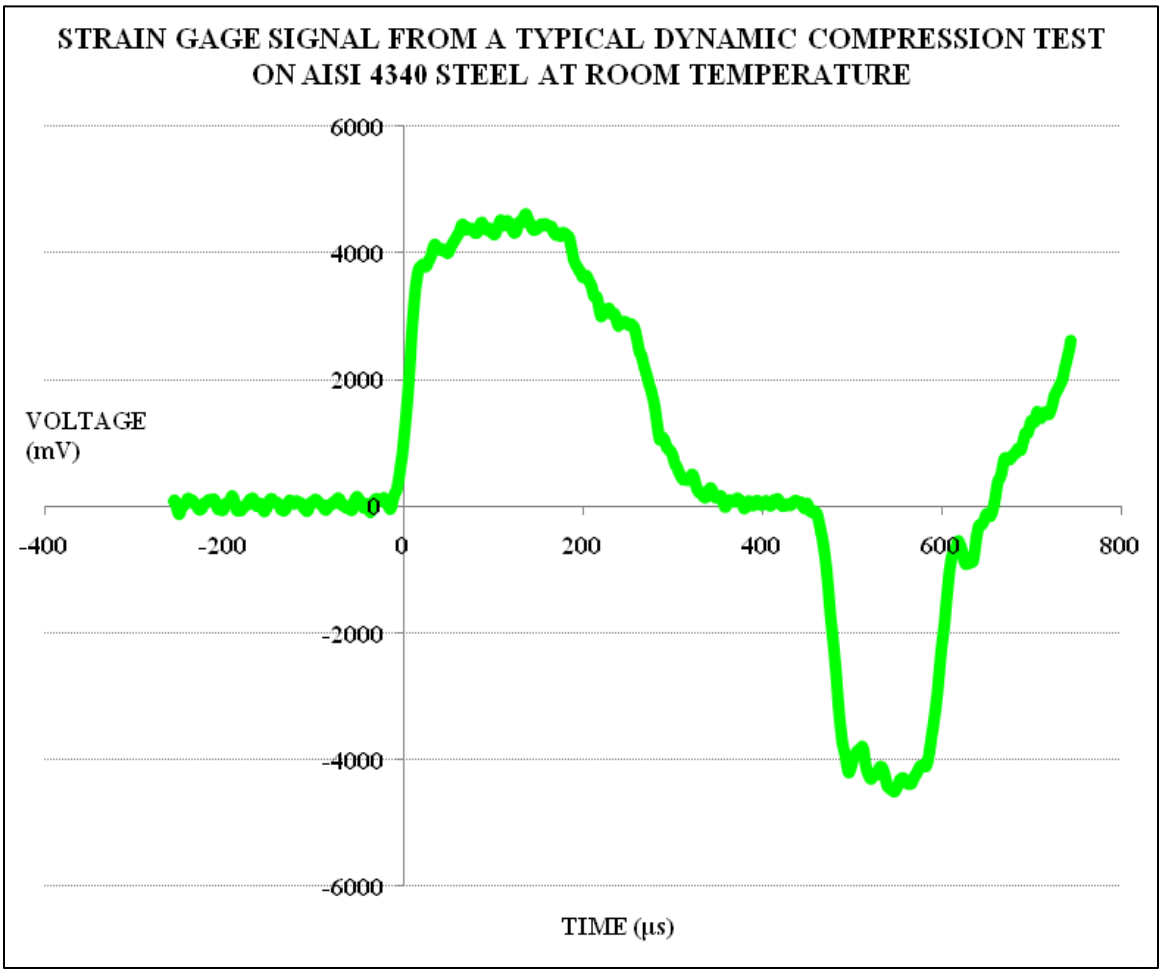

Figure 4.1: A typical strain gage signal from the dynamic compression test on AISI 4340 steel sample at room temperature

(4.1.2a) TRUE STRESS – TRUE STRAIN GRAPHS FOR AISI 4340 STEEL SAMPLES TEMPERED AT 315^{O}C FOR TWO HOURS

Dynamic stress strain curves for the materials in compression at high strain rates were estimated. The graphs for the samples tempered at 315^{O}C for two hours and impacted at momentums ranging from 31.4 kg.m/s to 38.855 kg.m/s are shown in figure 4.2.

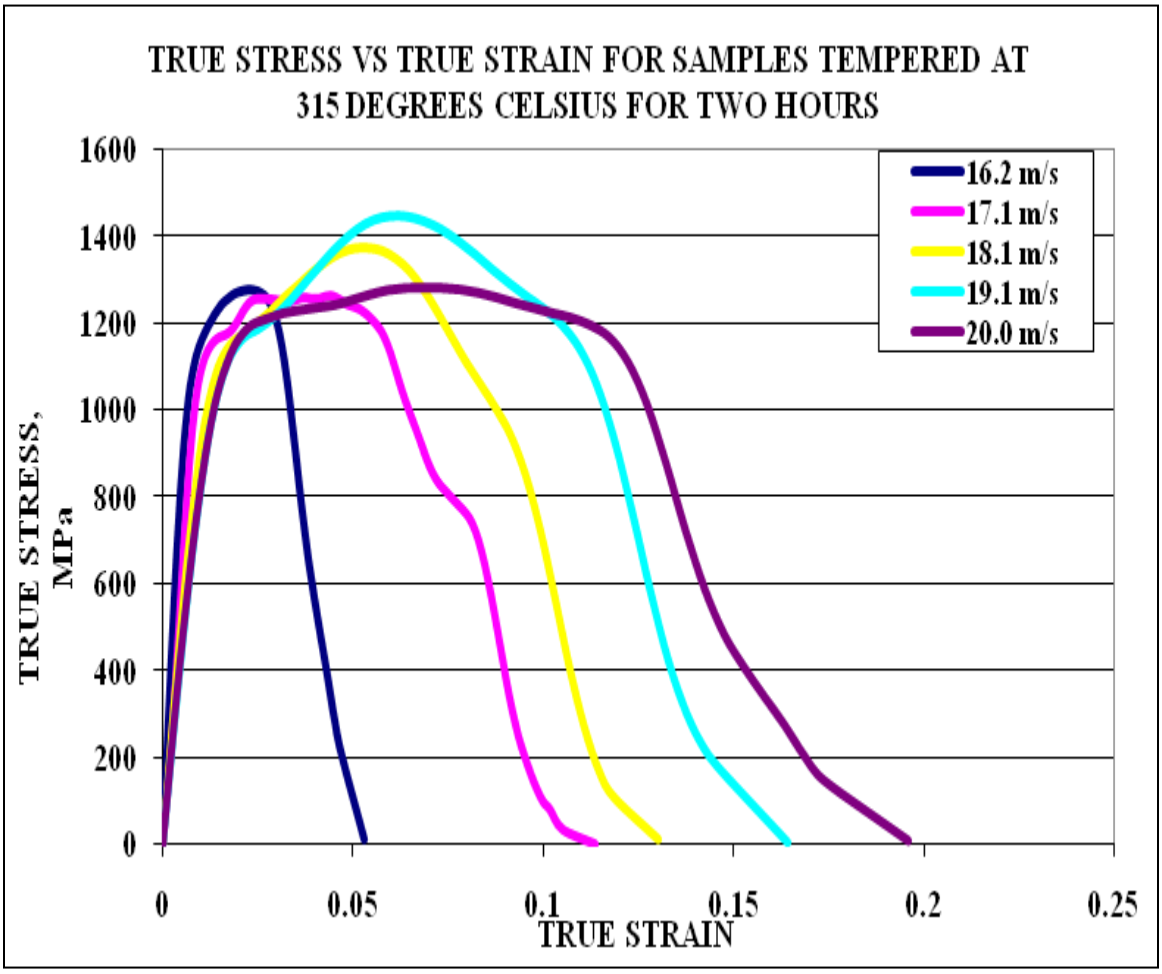

Figure 4.2: True stress strain graph for quenched-hardened AISI 4340 Steel samples tempered at 315^{O}C for 2 hours

The true flow stress, for each impact momentum increases as the true strain increases from the initial stages of the deformation, thus there is a proportional increase in flow stress with strain at the initial stages of the deformation. The flow stress continues to increase as strain increases until it reaches a maximum. After reaching a maximum, the flow stress decreases continuously as strain increases. In summary, flow stress increases initially with strain, reaches a maximum and decreases with subsequent increase in strain. This trend for the flow stress is prevalent in all the impacted samples irrespective of the impact momentum or the strain rates.

Under the dynamic impact loading, the steel samples in this group showed higher strengths and lower total strains when compared to all the samples in the other groups. Within the impact momentums of 31.4 kg.m/s to 39.0 kg.m/s, the maximum value of the flow stresses or the true stress responses ranged from 1263.7 MPa to 1444.5 MPa. It was observed that higher impact momentums leads to higher maximum flow stresses during the impact tests. There is an increase in strain as the impact momentum increases for each of the samples.

The strain rates calculated for this group of steel during the impact tests ranged from 440 S^{-1} to 1531 S^{-1}. The higher the strain rate, the higher the flow stresses. In addition, a higher impact momentum leads to higher strain during the deformation process. The sample that failed in this group achieved a strain rate of 2864 S^{-1}. High impact velocities lead to high amounts of deformations, hence high strain rates. The area covered by the true-stress-strain graph can be approximated as the amount of deformation. This shows that the deformation energy and the amount of deformation increases as the strain rate increases.

Very low true strains were obtained for the steel samples in this group as compared to the other groups as shown in tables 4.1 and 4.2. This is attributed to the relatively brittle nature of the

samples in this group due to the effect of tempered martensite embrittlement. The true strains ranged from 0.053 to 0.196. The shear strain to fracture for the sample that failed was measured to be 0.360.

The graph for the sample deformed at 16.2 m/s looks a little different from the remaining graphs. There is a proportional increase and decrease in flow stresses with strains both at the initial stages and at the final stages of the deformation respectively. However, the other graphs have a very smooth increase in stress as strain increases. They reach a maximum and then decrease continuously. At a point during the continual decrease in flow stress, there is a very sharp increase in strain, which is observed as a bump on the graphs. Thus an abrupt drop or discontinues drop in the flow stress is seen on this graph.

Thermal softening as a result of the conversion of impact energy to thermal energy dominates the latter stages of the deformation leading to observed drop in flow stress at high strain values. This is the point of stress collapse, which is due to the rapid thermal softening effect of adiabatic heating leading to strain localization. Thus, the point of stress collapse indicates the occurrence of localized adiabatic shearing. This is illustrated in figure 4.3, which compares the sample impacted at 16.2 m/s to the sample impacted at 17.1 m/s.

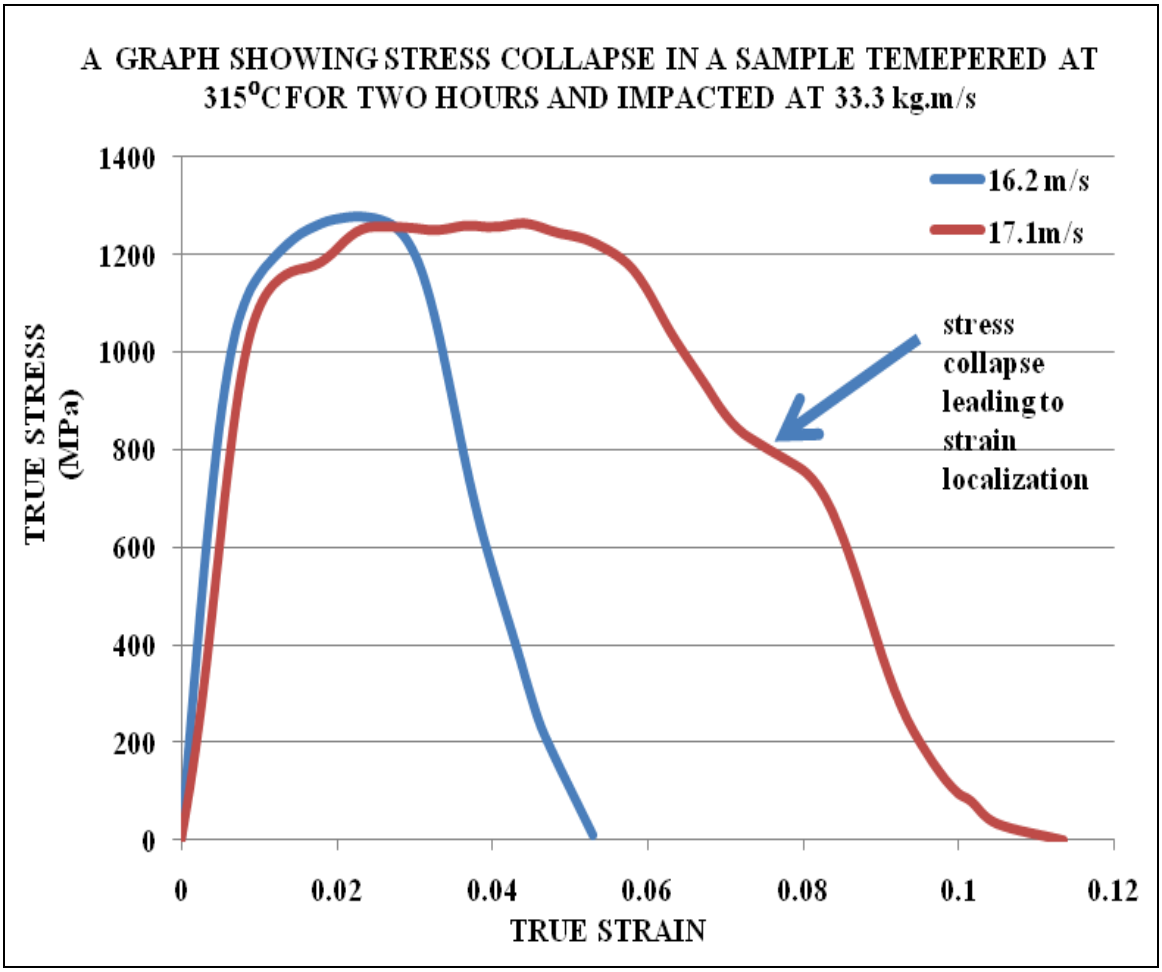

Figure 4.3: Stress Collapse in a Quench-hardened Steel Sample Tempered at 315^{0}C for2 hours

(4.1.2b)TRUE STRESS – TRUE STRAIN GRAPHS FOR AISI 4340 STEEL SAMPLES TEMPERED AT 425^{O}C FOR TWO HOURS

Typical stress-strain curves obtained from high strain-rate compression tests on the AISI 4340 steel samples in the 425 ^{O}C group tempered for 2 hours are shown in figure 4.4. The impact velocities of the samples these graphs were from 17.1 m/s to 21.0 m/s.

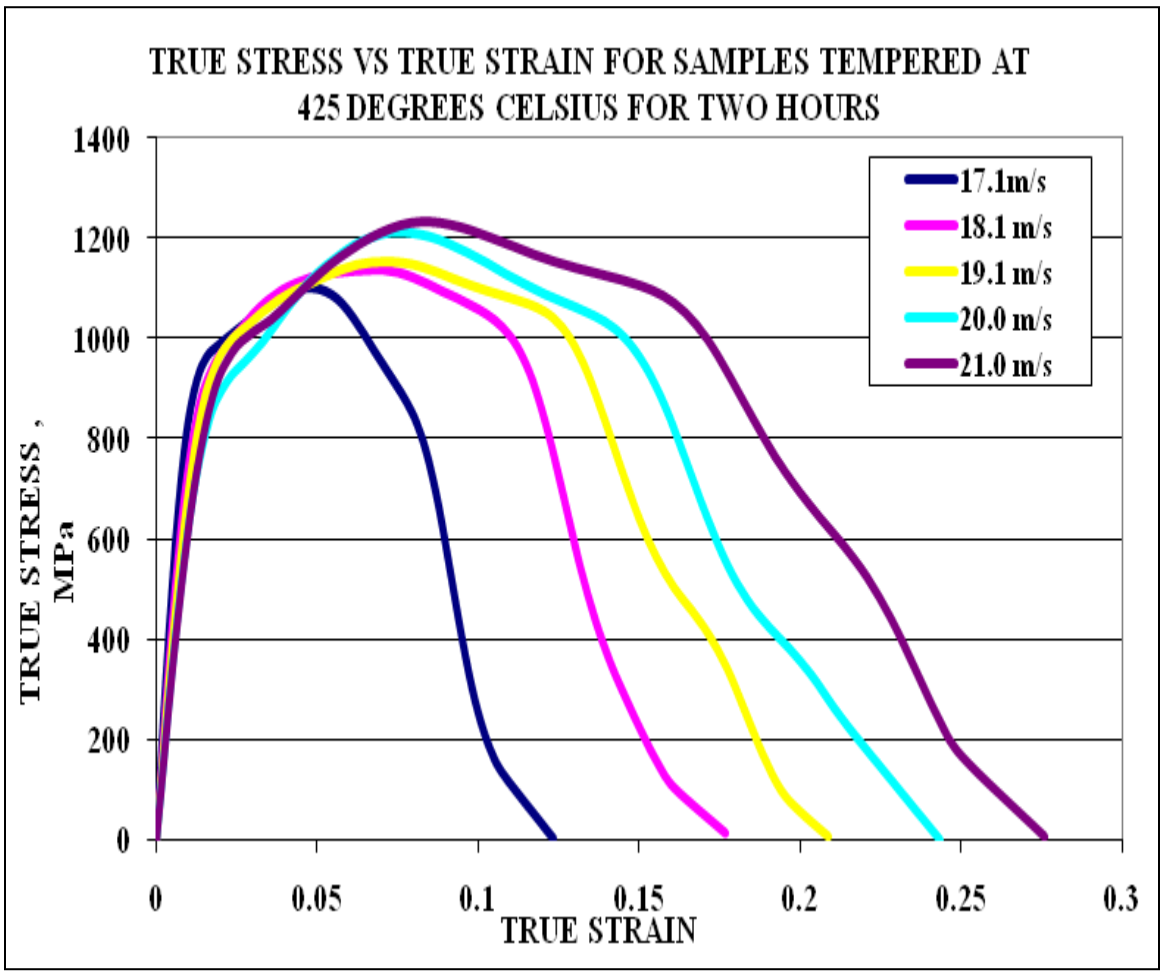

Figure 4.4: The True stress strain graph for quenched-hardened AISI 4340 Steel samples tempered at 425^{O}C for 2 hours

The true flow stress increases initially with true strain, reaches a maximum and decreases with subsequent increase in strain. The maximum flow stresses attained in this group were smaller than the highest flow stresses attained in the previous group. The strength of steel depends on the microstructure and the heat treatment. Heat treatment parameters such as temperature and time alter the mechanical properties of the steel samples. High tempering temperatures for quenched-hardened and tempered steel leads to reduction in strength and hardness, and an improvement in ductility and toughness. Comparatively, higher flow stresses were obtained in the previous group of steel samples tempered at 315^{O}C for two hours than in the steel samples tempered at 425^{O}C for two hours. Maximum flow stresses attained for the steel samples tempered at 425^{O}C for two hours were from 1102.8 MPa to 1233 MPa whilst 1263.7 MPa to 1444.5 MPa were the flow stresses attained in the steel samples tempered at 315^{O}C for two hours. This can be attributed to the different microstructures of the steel samples in each group due to the different tempering conditions.

The higher tempering temperature leads to an improvement in ductility and a decrease in strength for the steel samples. This can be seen in the fact that when a sample from this group was impacted at 40.7 kg.m/s, the sample did not fail. However when a steel sample from the previous group, which was tempered at 315^{O}C for two hours, was impacted at this same impact momentum of 40.7 kg.m/s, it failed and fractured into two halves. This shows the higher toughness of the samples in this group due to the higher tempering temperature than the AISI 4340 steel samples tempered at 315^{O}C.

Higher true strains were obtained in the steel samples tempered at 425^{O}C than those tempered at 315^{O}C. The true strains ranged from 0.123 to 0.276. The shear strains to fracture for two samples that failed in this group were 0.441 and 0.515. At the same impact momentums, the strain rates

of the samples in this group were higher than the strain rates of the previous group. The strain rates calculated for this group were from 983 S^{-1} to 2139 S^{-1}. The two steel samples that failed in this group had strain rates of 3376 S^{-1} and 3810 S^{-1}. The maximum strain in a specimen is directly proportional to the strain rate, $\dot{\varepsilon}$, and the length of the striker bar, l. The strain rate increases when strain increases. The higher strains attained during the deformation of the samples in this group led to the higher strain rates due to the better ductility of the steel samples in this group. The higher tempering temperature makes the steel samples more ductile, hence higher strains can be achieved during the deformation process. The point of stress collapse, which is indicative of the occurrence of adiabatic shearing, can be seen on the graphs of the samples impacted at higher momentums.

(4.1.2c) TRUE STRESS - TRUE STRAIN GRAPHS FOR AISI 4340 STEEL SAMPLES TEMPERED AT 620^{O}C FOR TWO HOURS

The true stress-strain curves for the AISI 4340 steel samples tempered at 620^{O}C for two hours are shown in figure 4.5.

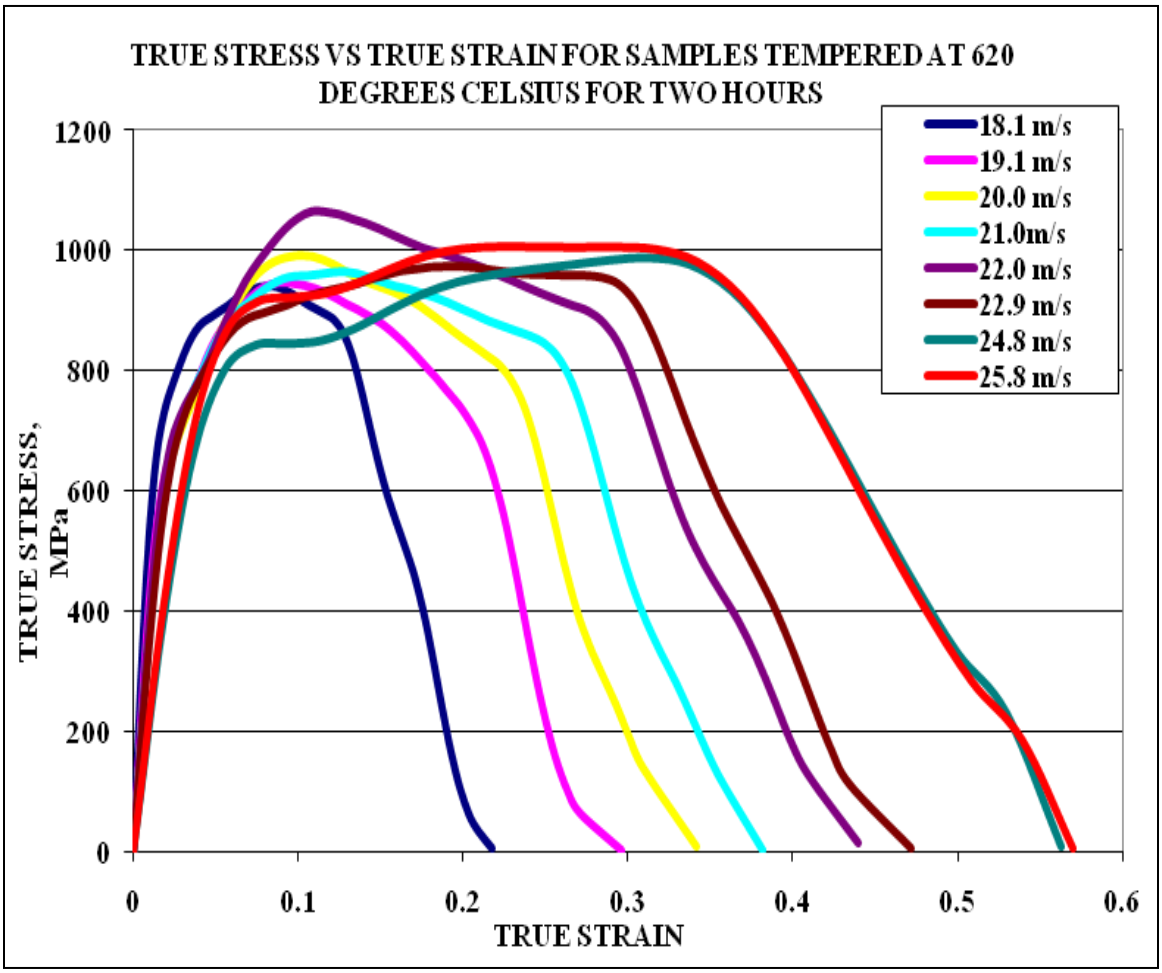

Figure 4.5: The True stress-strain graphs for quenched-hardened AISI 4340 Steel samples tempered at 620^{O}C for 2 hours

The true flow stress graphs of this group are similar to the graphs of all the other groups. The flow stress increases initially with strain, reaches a maximum and decreases with subsequent increase in strain.

However, under the dynamic impact loading, the AISI 4340 steel samples tempered at $620^{O}C$ for two hours showed lower strengths and higher total strains as compared to the AISI 4340 steel samples tempered at $315^{O}C$ and $425^{O}C$ for two hours. The maximum flow stresses for the steel samples in this group were from 941.0 MPa to 1066.1 MPa, which were lower as compared to that of the other groups. Comparatively very high true strains were obtained under the dynamic impact loading conditions for the samples in this group compared with that of all the other groups. The true strains of the samples in this group during the dynamic impact test ranged from 0.218 to 0.5702. The higher tempering temperature made this sample more ductile than all the other groups since they were tempered at lower temperatures as compared to this group. However, during the tempering, tradeoffs were made on the strength of the material to compensate for the increase in ductility and toughness.

The maximum strain in a specimen is directly proportional to the strain rate, $\dot{\varepsilon}$. Due to the more ductile nature of the steel samples in this group the strain rates calculated were higher. The samples were also deformed at higher strain rates without failing. The strain rates in this group varied from 1805 S^{-1} to 4043 S^{-1}. This shows that the steel samples in this group had better toughness properties as compared to the samples in the other groups tempered at $315^{O}C$ and $425^{O}C$.

Shear strain localization leading to the occurrence of adiabatic shear bands, which show as stress collapse, can be seen on the graphs of the samples impacted at higher momentums. They show as

discontinues drops in the flow stresses on the graphs signifying strain localization. The extent to which the steel samples in the $620^{O}C$ group tempered for two hours were deformed without fracture indicates how ductile the samples were as compared to all the other groups.

(4.1.3) OBSERVED TRENDS IN DYNAMIC BEHAVIOR OF STEEL DURING IMPACT

(4.1.3A) FLOW STRESS COMPARISON FOR THE STEEL SAMPLES TEMPERED FOR TWO HOURS

Figure 4.6 shows the stress responses of AISI 4340 steel samples from the three different tempering groups under the same impact momentum.

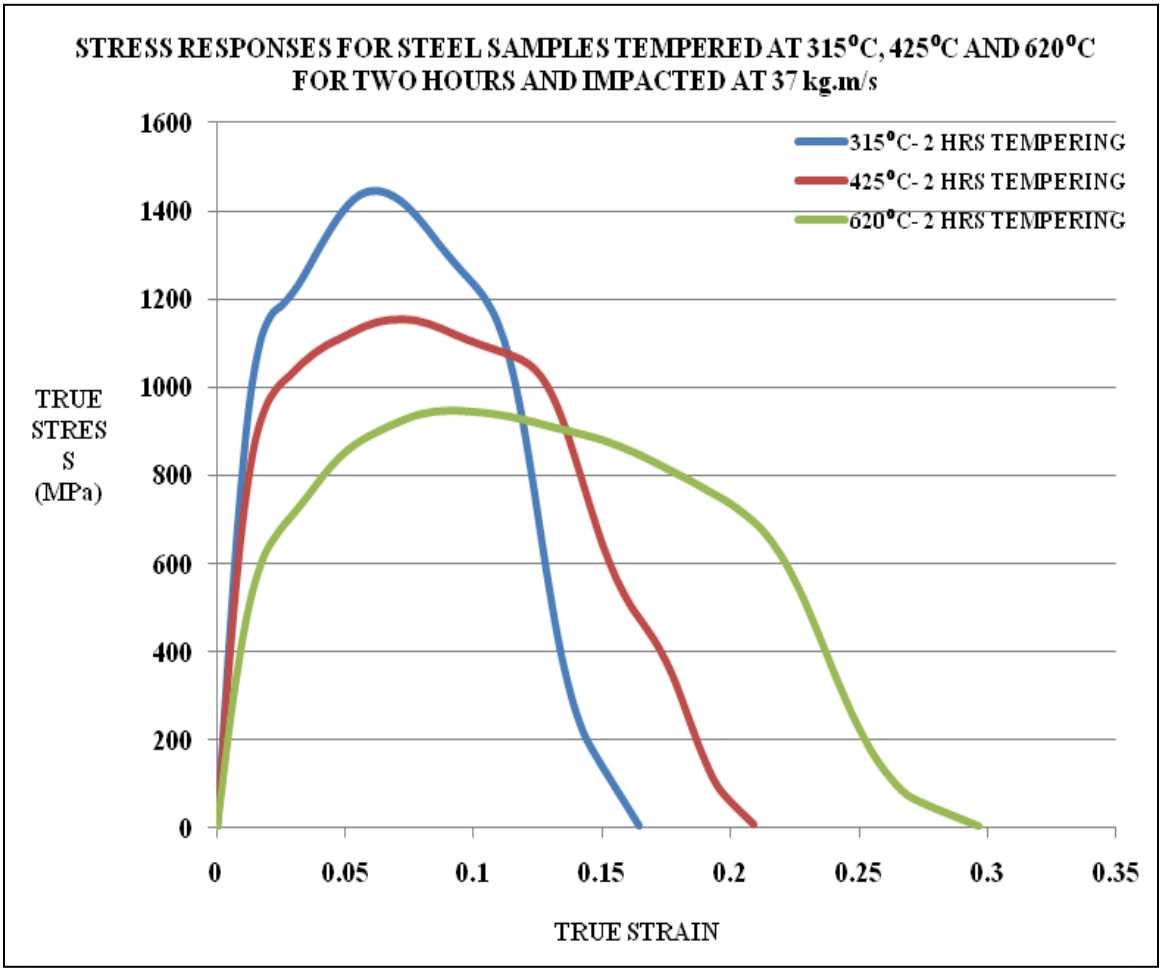

Figure 4.6: Variations In Stress Response Graphs Of Quenched-Hardened AISI 4340 Steel Samples Tempered At 315 ^{O}C, 425 ^{O}C, And 620 ^{O}C For 2 Hours

The dynamic mechanical behavior of steels depends on the metallurgical variables, the test methods and the nature of the applied stresses. The shape and magnitude of the stress-strain curve of a metal depends on

a) Its composition
b) Heat treatment
c) Prior history of plastic deformation and strain rate and
d) Temperature and state of stress imposed during the testing

Different heat treatment variables were used in processing the steel samples used for this study. The heat treatment variables determined largely the mechanical behavior of the samples. Under the dynamic impact loading, it was observed that the steel samples tempered at $315^{O}C$ for two hours had the highest strength and lowest total strains than those tempered at $425^{O}C$ and $620^{O}C$ for two hours. The steel samples tempered at $620^{O}C$ for two hours were more ductile and had the highest strains during impact than the steels in the groups under the same impact momentums. However, it has the lowest strength compared to the other steels tempered at $315^{O}C$ and $425^{O}C$ for two hours.

Toughness of a material may be considered as the total area under the stress-strain curves. This area is an indication of the amount of work per unit volume that can be done on the material without causing it to rupture. The total area under the stress-strain curves were greater for the steels in the $620^{O}C$ group tempered for two hours than the other groups under the same impact momentums. This shows that more energy was absorbed during the impact by the steels in this group tempered for two hours than those tempered at $315^{O}C$ and $425^{O}C$ for two hours.

(4.1.3B) EFFECTS OF IMPACT MOMENTUM ON STRAIN RATE

Figure 4.7 shows the effect of impact momentum on strain rates for the various steel samples tempered at 315^{O}C and 425^{O}C for two hours and the steel samples tempered at 315^{O}C and 425^{O}C for one hour. Figure 4.8 shows the effect of impact momentum on strain rates for steel samples tempered at 315^{O}C, 425^{O}C and 620 ^{O}C respectively for two hours.

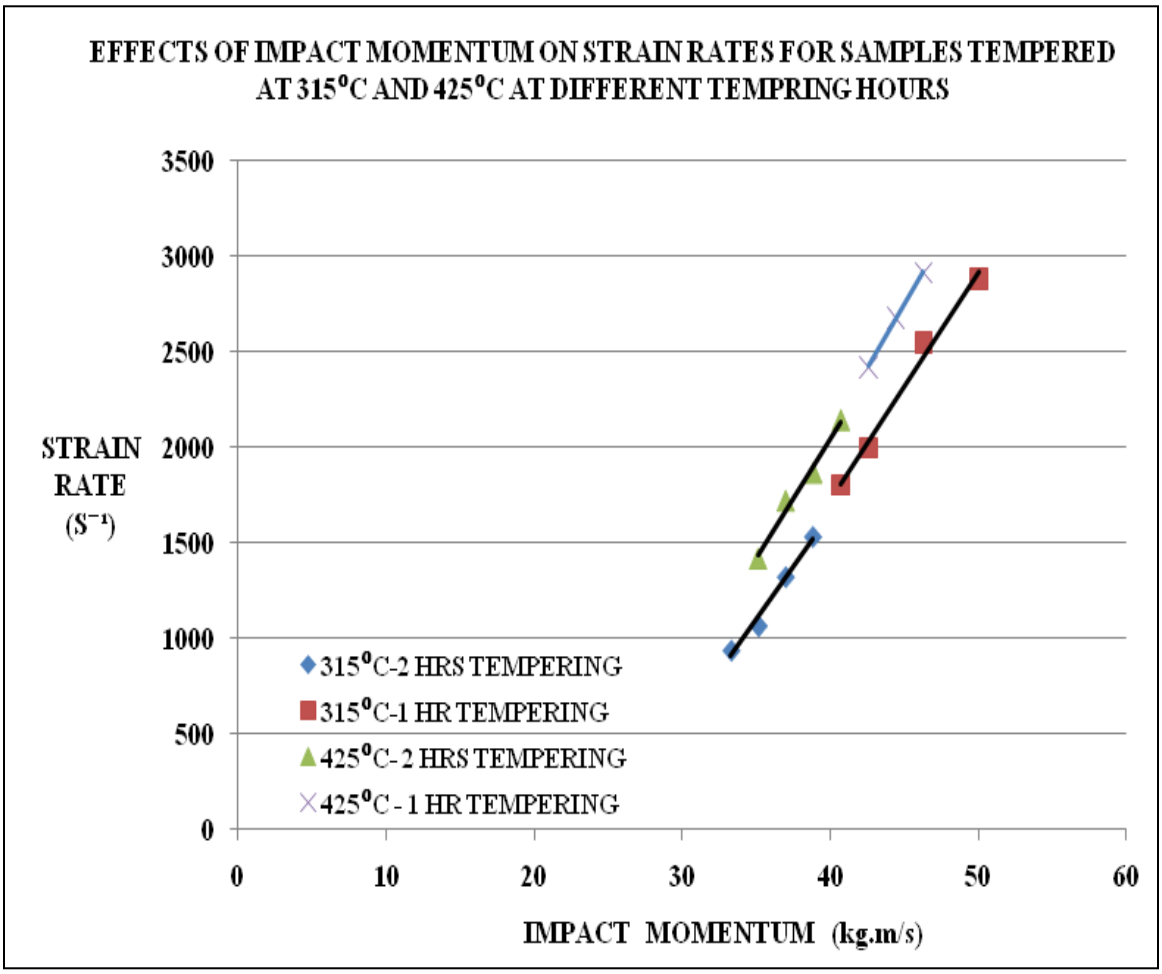

Figure 4.7: Effect of Impact Momentum on Strain Rates for Steel Samples Tempered at 315^{O}C and 425^{O}C

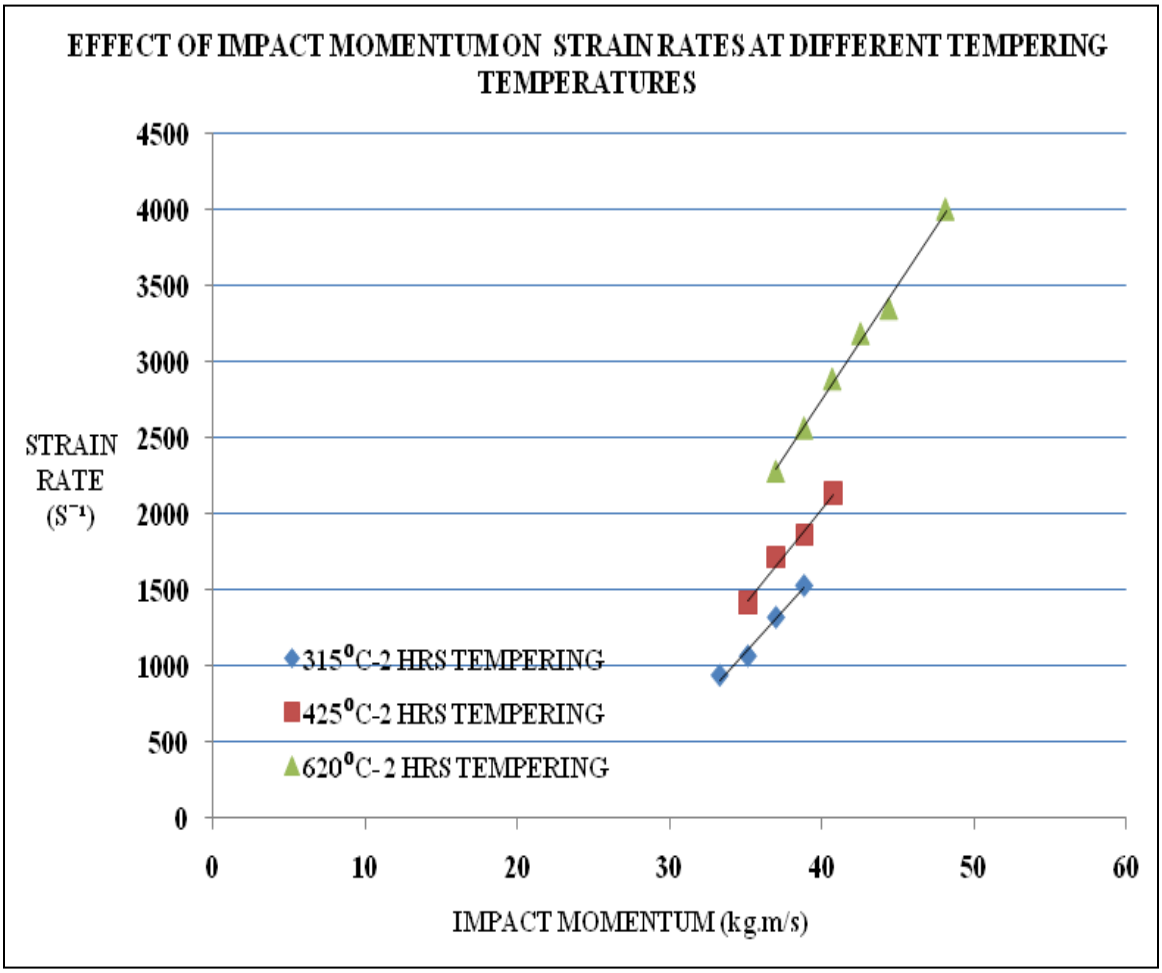

Figure 4.8: Effect of Impact Momentum on Strain Rates At Different Tempering Temperatures

Irrespective of the heat treatment conditions of the various steel samples, the graphs show that the higher the firing pressure of the gun, the higher the impact momentum, and the higher the strain rates generated in the samples. This was seen in all the impacted samples at the different tempering temperatures and times. Strain rate is directly related to the maximum strain in the

sample during the deformation. Higher strains are generated at higher impact momentums, hence the high strain rates.

However, at the same impact momentum, the higher the tempering temperature, the higher the strain rate generated in the sample. At an impact momentum of 38.9 kg.m/s, the strain rate for the sample tempered at 315 ^{O}C for two hours is 1531 S^{-1}, the sample tempered at 425 ^{O}C for two hours is 1864 S^{-1} and the sample tempered at 620 ^{O}C for two hours is 2568 S^{-1}. The increase in the strain rates for the various steel samples at their respective tempering temperatures can be attributed to the higher ductility associated with higher tempering temperatures of the steel samples. Higher tempering temperatures lead to improvement in toughness and ductility of steel. Ductile materials achieve higher strains than less ductile materials at the same impact momentum, hence higher strain rates. This can be seen in figure 4.9.

Figures 4.10 and 4.11 illustrate how impact momentum affects total engineering strain at the different tempering temperatures. It is seen that the higher the tempering temperature, the higher the engineering strain at the same impact momentum.

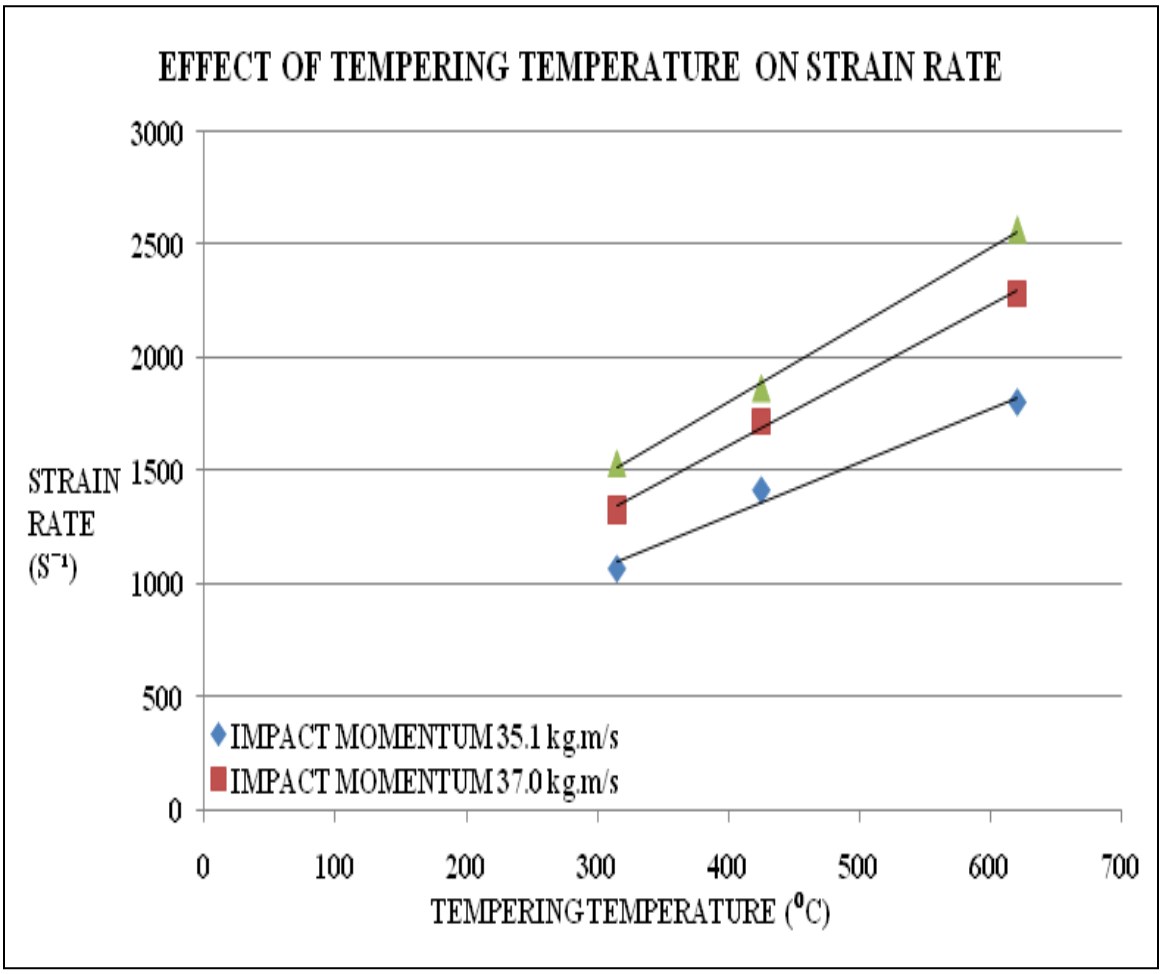

Figure 4.9: Effect of Tempering Temperature on Strain Rates

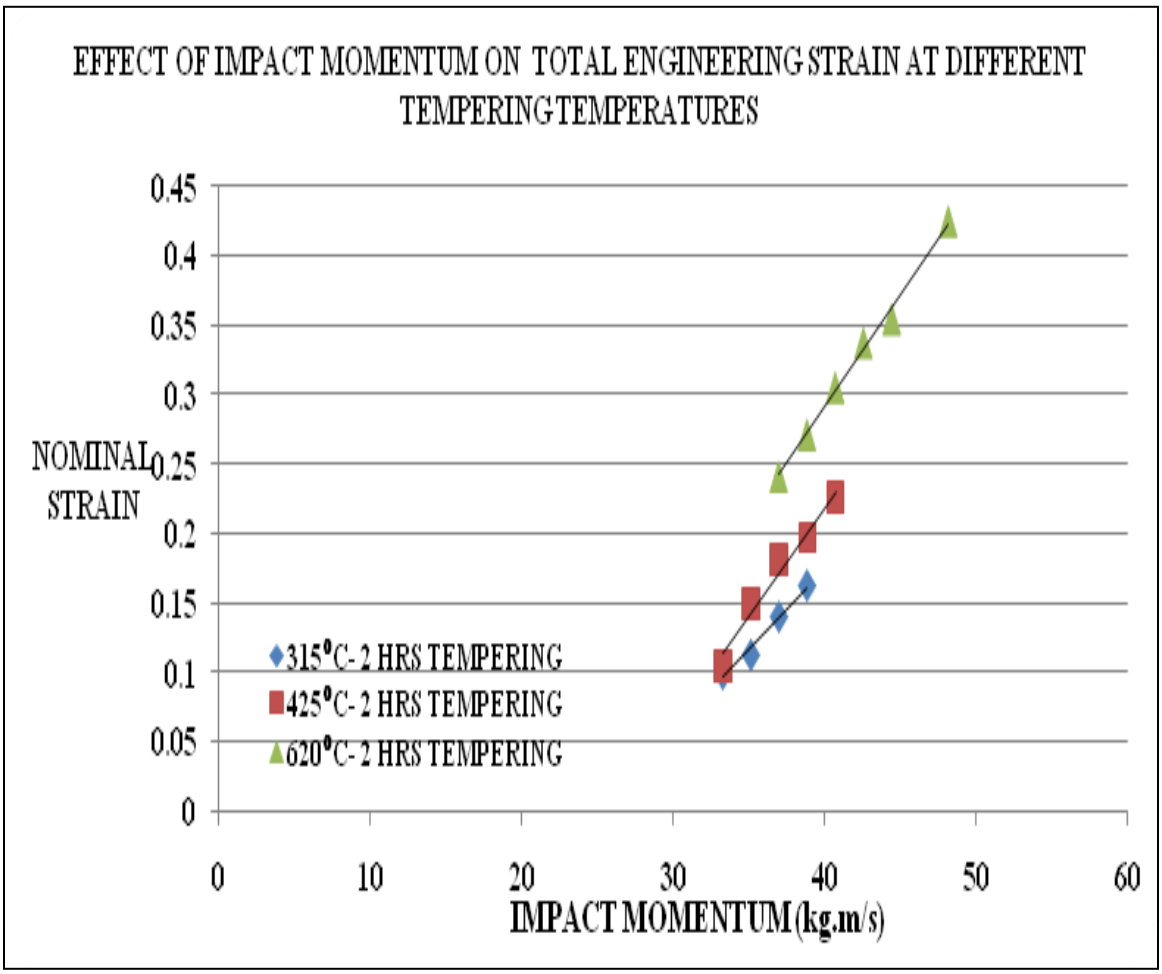

Figure 4.10: Effect of Impact Momentum on Total Engineering Strain

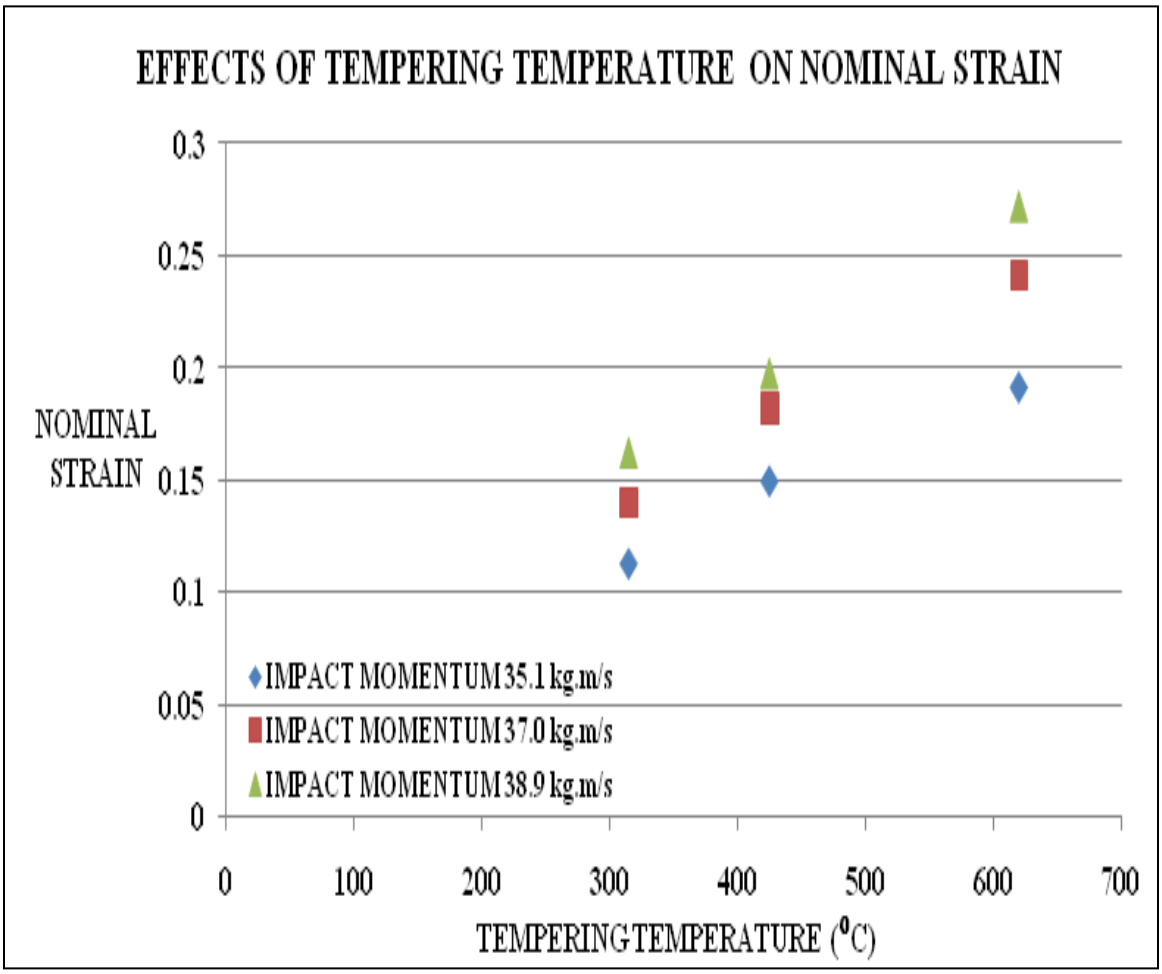

Figure 4.11: Effect of Tempering Temperature on Total Engineering Strain

(4.2) RESULTS OF METALLOGRAPHIC ANALYSIS ON THE AISI 4340 STEEL SAMPLES AFTER DEFORMATION

Selected impacted steel samples were mounted, ground, polished and etched to reveal the microstructure of the samples. Microscopic analysis was then performed on all the etched samples using the Zeiss Optical Microscope with the Clemex Vision Analyzer.

Metallographic analysis on the impacted steel samples showed the formation of both deformed and transformed shear bands. The transformed shear bands formed appeared as white narrow bands close to the edges of the impacted samples. However, the deformed shear bands appeared as dark narrow bands in the impacted samples. Whether a deformed band or a transformed band were formed depended on many factors such as strain rates generated in the samples during the deformation, the microstructure, tempering temperature, tempering time and hardness of the material. In some of the impacted steel samples, cracks were observed in the transformed shear bands. However, there were no cracks in any of the deformed shear bands formed in the impacted steel samples used for this study.

It was observed that the tempering time affects the formation of the adiabatic shear bands in the steel samples during the deformation. The distinctiveness and the clarity of the adiabatic shear bands were affected by the length of time that the samples were soaked at the tempering temperatures. In general, it was observed that very well developed, clear adiabatic shear bands were formed in the impacted steel samples tempered for one hour than those formed in the samples tempered for two hours at both $315^{O}C$ and $425^{O}C$. The shear bands that were formed in the impacted samples tempered at $315^{O}C$ and $425^{O}C$ for two hours were more diffused. The shear bands were not clearly formed and were dim as compared to those tempered at $315^{O}C$ and $425^{O}C$ for one hour.

Most of the deformed bands formed were found to propagate across almost the entire circumference of the impacted samples. They propagated along circular paths close to the edges and along the entire circumference of the impacted samples. However, none of the transformed shear bands formed propagated across the entire circumference of the impacted samples. Thus, the lengths of the deformed shear bands formed in the impacted steel samples were longer than the transformed shear bands.

During polishing of impacted samples, clearly formed shear bands could be seen as shinning curves or arcs close to the edges on the surfaces of very well polished steel samples even before etching to reveal the microstructure. When the polished samples were etched, the adiabatic shear bands appeared as circular propagating paths on the transverse sections around the edges of the samples at low magnifications. A clearly distinct circular propagating deformed adiabatic shear band formed close to the edge of a steel sample impacted at 46.3 kg.m/s is shown in figure 4.12.

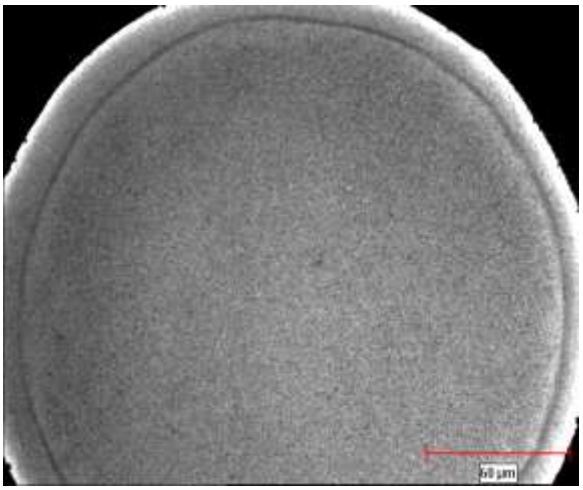

Figure 4.12: A deformed adiabatic shear band formed in an impacted sample

At very high magnifications on the optical microscope, transformed shear bands were surrounded by narrow bands of intensely sheared regions as shown in figure 4.13. Their appearances were comparable to the surrounding impacted materials but showed severe shearing. They served as borders between the narrow white shear bands, which were beyond the resolution of the optical microscope, and the neighboring impacted materials. The material and shear flow pattern during the deformation as a result of the intense heating can be seen in the narrow boundary bands.

Figure 4.13 shows the narrow boundaries between a transformed adiabatic shear band and the surrounding bulk material in a sample tempered at $315^{O}C$ for one hour and impacted at 44.4 kg.m/s. The surrounding narrow bands are seen as boundaries between the transformed shear band and the surrounding bulk material at high magnifications on the optical microscope. However, this is not seen at low magnifications since they all appear very white and bright.

Figure 4.14 show the shear flow pattern of material around a transformed shear band in a steel sample tempered at $315^{O}C$ for one hour and impacted at high strain rates.

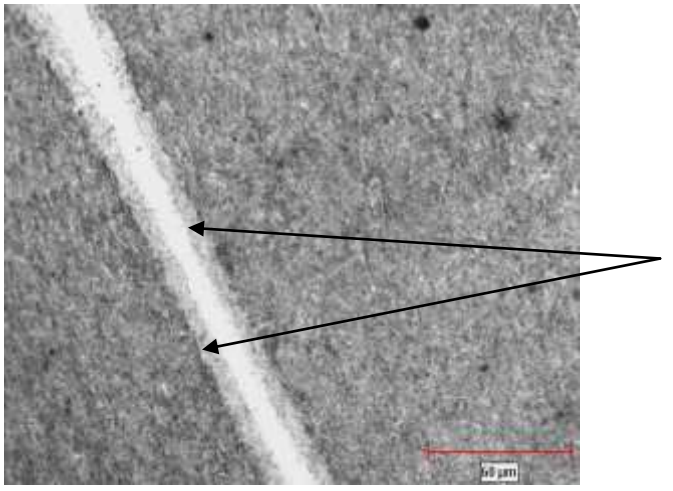

Figure 4.13: Upper and lower boundaries of a transformed shear band

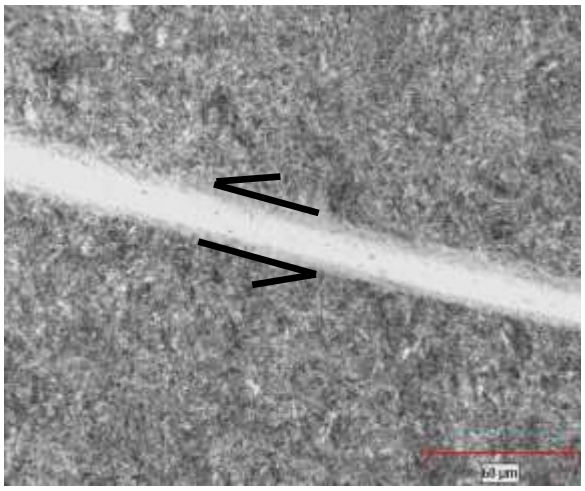

Figure 4.14: Shear flow pattern of material around a transformed shear band

(4.2.1) ADIABATIC SHEAR BANDS IN AISI 4340 STEEL SAMPLES TEMPERED AT 315^{O}C

Both deformed and transformed adiabatic shear bands were observed in the impacted steel samples of this group. However, more transformed shear bands were produced than the deformed shear bands. The transformed bands were narrower compared to the deformed bands.

(4.2.1a) ADIABATIC SHEAR BANDS IN SAMPLES AUSTENITIZED AT 855^{O}C FOR 1 HOUR, TEMPERED AT 315^{O}C FOR 2 HOURS AND IMPACTED AT HIGH STRAIN RATES

The optical micrographs for the adiabatic shear bands formed in the steel samples tempered at 315^{O}C for two hours are presented in figures 4.15 and 4.16.

Figure 4.15 shows a transformed band formed in a sample tempered at 315 ^{O}C for two hours and impacted at 37.0 kg.m/s. The transformed shear band was formed close to the edge of the sample and it ended in a deformed shear band. The transformed shear band had a width of 58 μm and a hardness of 545HV. The deformed shear band was 80 μm in width.

Figure 4.16 shows a steel sample tempered at 315 ^{O}C for two hours and impacted at 38.9 kg.m/s. A transformed shear band of width 53 μm with a hardness of 581HV was formed. The shear bands formed in the samples tempered at 315^{O}C for two hours were diffused, dim and not properly developed.

Figure 4.17 shows an unimpacted steel sample tempered at 315 ^{O}C for two hours. The hardness of the sample after tempering was 358 HV.

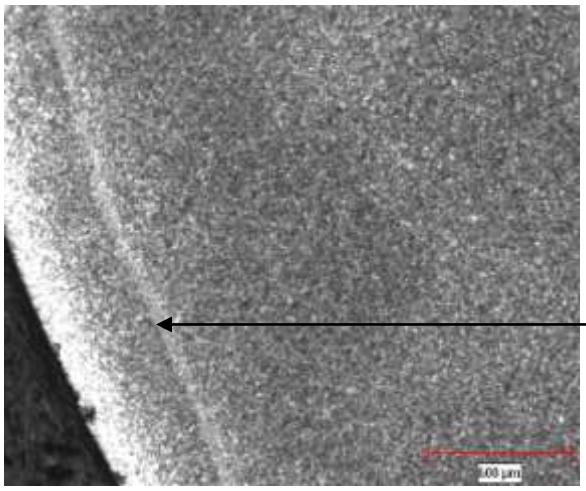

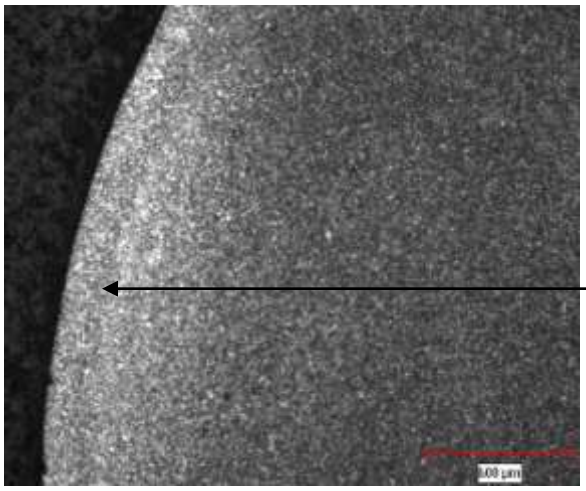

Figure 4.15: Shear bands in a sample tempered at 315^{O}C for 2 hours and impacted at 37.0 kg.m/s

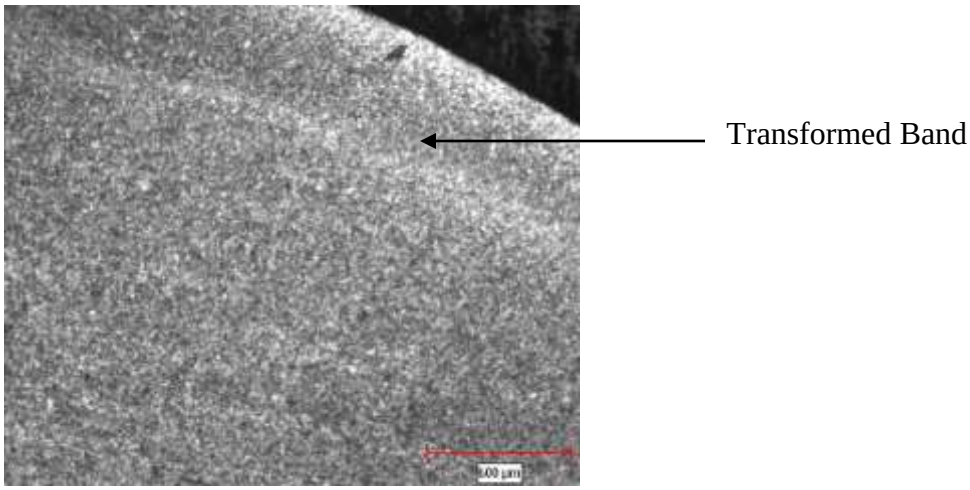

Figure 4.16: Shear band in a sample tempered at 315^{O}C for 2 hours and impacted at 38.9 kg.m/s

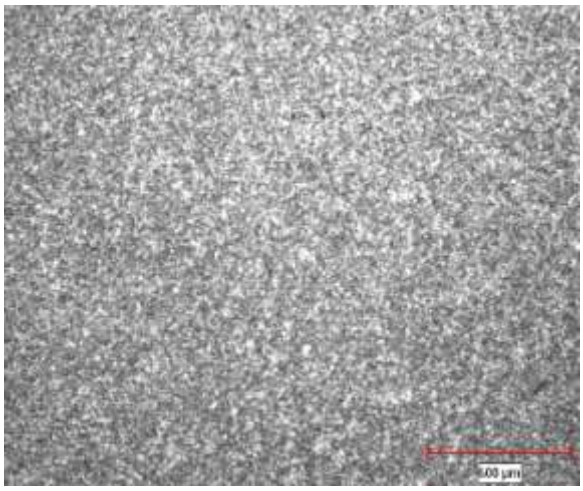

Figure 4.17: Unimpacted sample after tempering at 315^{O}C for two hours

(4.2.1b) ADIABATIC SHEAR BANDS IN STEEL SAMPLES AUSTENITIZED AT 855^{O}C FOR 30 MINUTES, TEMPERED AT 315^{O}C FOR 1 HOUR AND IMPACTED AT HIGH STRAIN RATES

The optical micrographs below are the adiabatic shear bands formed in the steel samples tempered at 315^{O}C for one hour. Figure 4.18 shows a transformed adiabatic shear band formed in a steel sample tempered at 315^{O}C for one hour and impacted at 42.6 kg.m/s. The width of the shear band was 125 μm. This transformed band ended in a deformed band of width 189 μm.

Figure 4.19 shows a transformed adiabatic shear band formed in a steel sample tempered at 315^{O}C for one hour and impacted at 46.3 kg.m/s. The transformed band ended in a deformed band and with cracks propagating through it. The transformed band had a width of 37 μm and a hardness of 620 HV. Figure 4.20 shows a crack propagating in the transformed shear band depicting the susceptibility of adiabatic shear bands to the propagation of cracks.

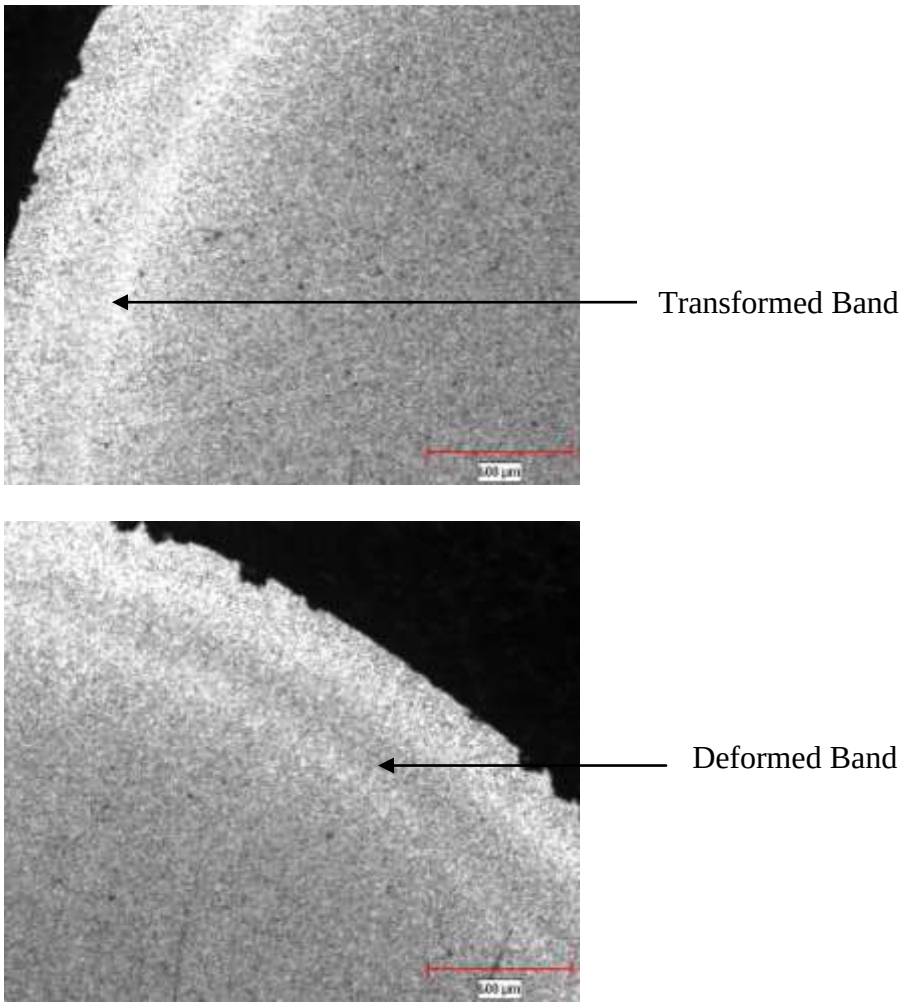

Figure 4.18: Shear bands in a sample tempered at 315^{O}C for 1 hour and impacted at 42.6 kg.m/s

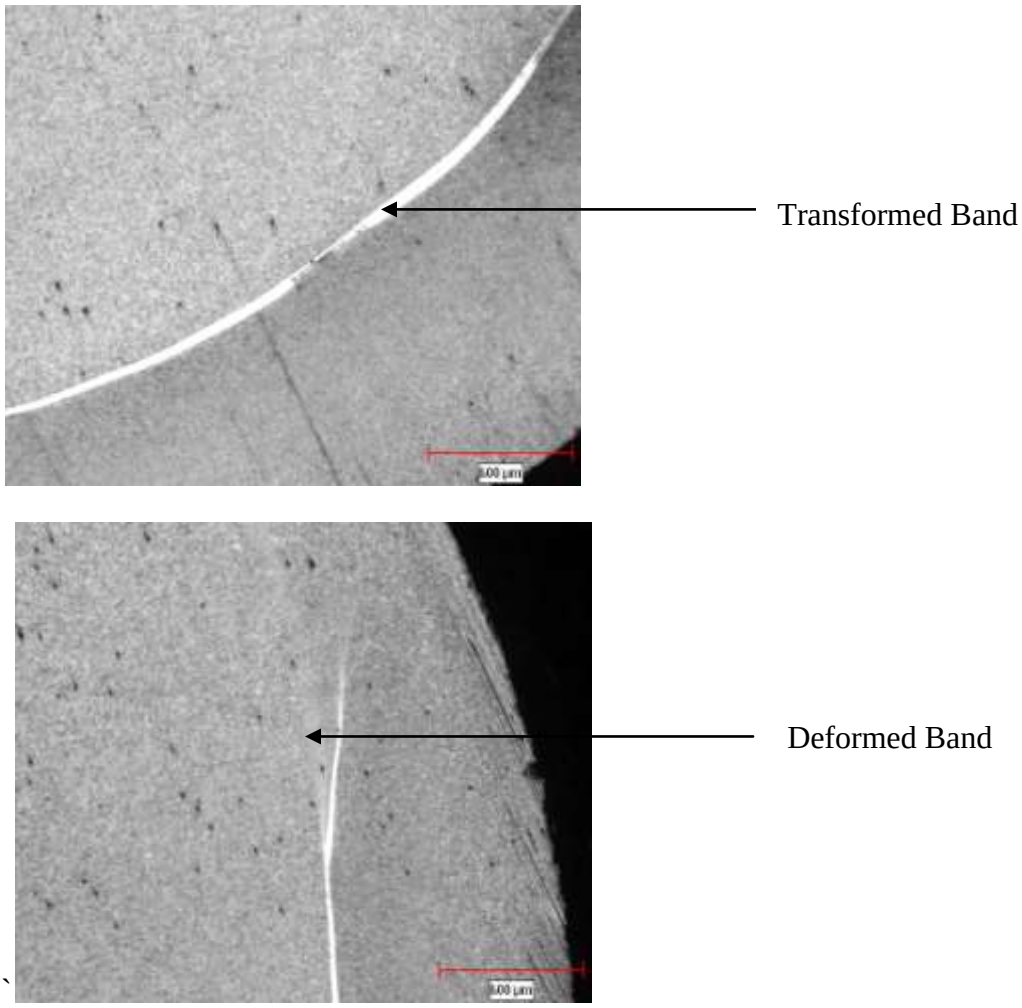

Figure 4.19: Shear bands in a sample tempered at 315^{O}C for 1 hour and impacted at 46.3 kg.m/s

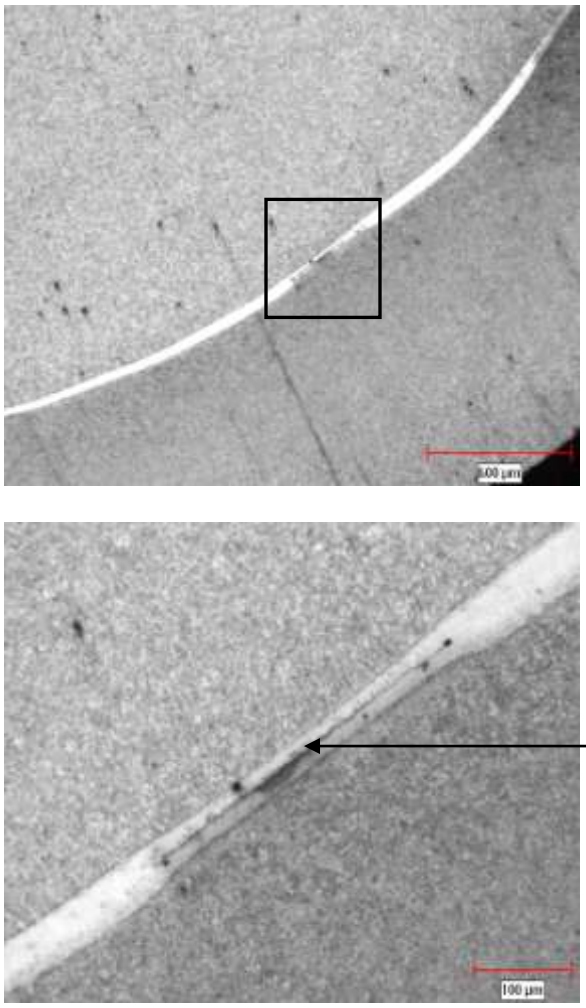

Figure 4.20: A Crack propagating in a transformed shear band

(4.2.1C) THE HARDNESS AND THICKNESS DISTRIBUTION OF THE SHEAR BANDS FORMED IN STEEL SAMPLES TEMPERED AT 315^{O}C AND DEFORMED AT HIGH STRAIN RATES

A Buehler micromet micro hardness-testing machine was used to measure the micro-hardness of the steel samples by the Vickers hardness test (HV). The thicknesses of the shear bands were also measured. A graph showing the variations in the thickness of the deformed bands and the transformed bands at the different tempering times are presented in figure 4.21.

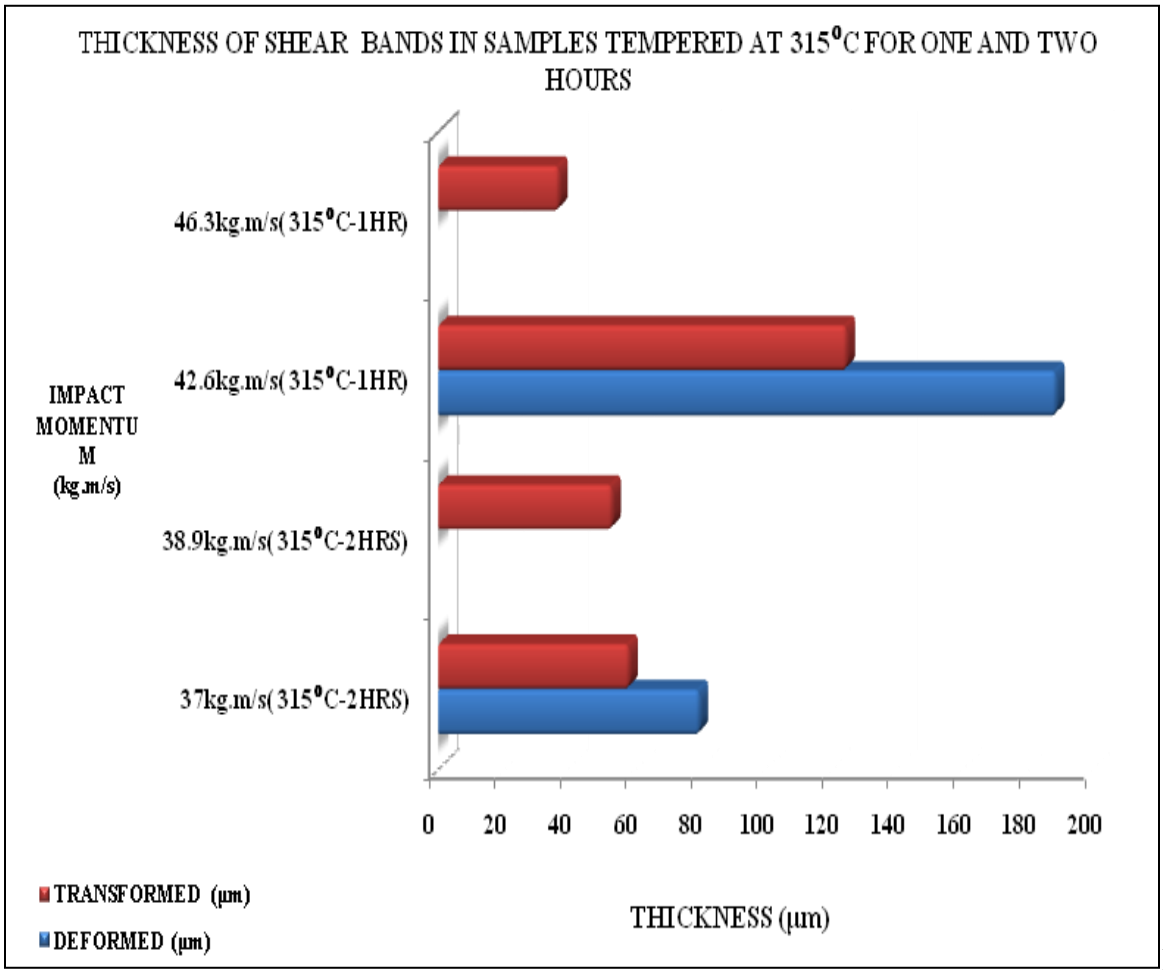

Figure 4.21: A Comparison of the Thickness of Deformed Bands and Transformed Bands formed in Samples Tempered at 315^{O}C

At the same impact momentum values, the deformed shear bands formed were thicker than the transformed shear bands. In addition, the lengths of the deformed bands were always longer than the lengths of the transformed bands.

With the steel samples tempered at $315^{O}C$ more transformed shear bands were formed in the impacted samples than deformed shear bands. Clear and distinct transformed bands were formed in the samples tempered at $315^{O}C$ for one hour than those formed in the samples tempered at $315^{O}C$ for two hours.

The hardness of the shear bands compared to the nearby materials as well as the differences in the hardness of the deformed bands and the transformed bands are presented in figure 4.22.

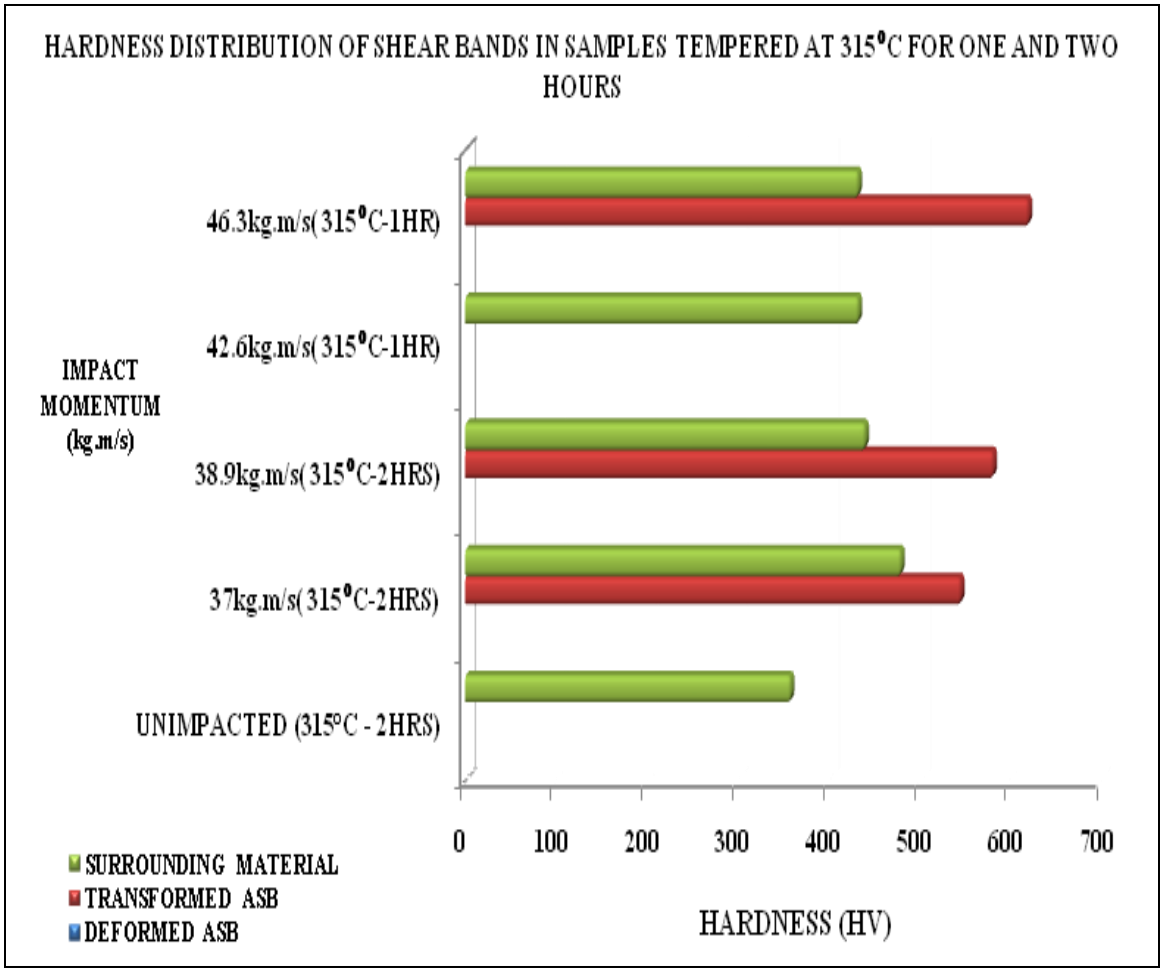

Figure 4.22: A Comparison of the Hardness of the Surrounding Material and the Shear Bands formed in Samples Tempered at 315^{O}C

The increase in hardness of deformed samples was due to increased dislocation densities, dislocation-dislocation interactions and dislocation pinning in the deformed samples as shown by figure 4.22. The initial average hardness of the unimpacted AISI 4340 steel sample in this group, which was tempered at 315^{O}C for two hours, was 358 HV. After impact at 37.0 kg.m/s, the average hardness of the surrounding material increased from 358 HV to 480 HV. This represents

approximately 34% increase in average hardness of the material as compared to the average hardness of the initial unimpacted sample.

It was observed that the average hardness of the transformed shear bands formed in the impacted samples was higher compared to the neighboring material in the impacted sample and the initial unimpacted sample. The difference in hardness can be attributed to the fine carbides and high dislocation densities in the shear bands. The average hardness of the transformed band in the sample impacted at 37.0 kg.m/s was 546 HV, which represents approximately a 52% increase in hardness as compared to the hardness of the initial unimpacted sample. In addition, this also represents a 14% increase in hardness compared to the hardness of the material surrounding the shear band in the impacted sample. The sample impacted at 38.9 kg.m/s had a 62% increase in hardness compared to the hardness of the initial unimpacted sample. In addition, there was a 32% increase in the hardness compared to the hardness of the material surrounding the shear band in the impacted sample.

It was also observed that the average hardness of the transformed bands increases as the impact momentum increases irrespective of the tempering time. The hardness of the transformed bands in the samples impacted at 37.0kg.m/s, 38.9 kg.m/s and 46.3 kg.m/s are 546 HV, 581 HV and 620 HV respectively.

Tables 4.3 to 4.6 are summaries of the microscopic analysis done on the steel samples that were tempered at $315^{O}C$ for one hour and those tempered for two hours. Tables 4.3 and 4.5 show the widths of the shear bands while tables 4.4 and 4.6 show the hardness variations in the shear bands and the surrounding materials.

Table 4.3: Widths of adiabatic shear bands in samples tempered at 315 ^{O}C for 2 hours

IMPACT MOMENTUM (kg.m/s)	DEFORMED BAND (μm)	TRANSFORMED BAND (μm)
37.0	80	58
38.9		53
40.7	SAMPLE FRACTURED	

Table 4.4: Hardness of adiabatic shear bands in samples tempered at 315 ^{O}C for 2 hours

IMPACT MOMENTUM (kg.m/s)	DEFORMED BAND (HV)	TRANSFORMED BAND (HV)	SURROUNDING MATERIAL (HV)
UNIMPACTED SAMPLE	358		
37.0		546	479
38.9		581	440
40.7	SAMPLE FRACTURED		

Table 4.5: Widths of adiabatic shear bands in samples tempered at 315 ^{O}C for 1 hour

IMPACT MOMENTUM (kg.m/s)	DEFORMED BAND (μm)	TRANSFORMED BAND (μm)
42.6	189	125
46.3		37

Table 4.6: Hardness of adiabatic shear bands in samples tempered at 315 ^{O}C for 1 hour

IMPACT MOMENTUM (kg.m/s)	DEFORMED BAND (HV)	TRANSFORMED BAND (HV)	SURROUNDING MATERIAL (HV)
46.3		620	433

(4.2.2) ADIABATIC SHEAR BANDS IN AISI 4340 STEEL SAMPLES TEMPERED AT 425^{O}C

Both deformed and transformed adiabatic shear bands were observed in the impacted samples of this group. The transformed shear bands appeared as white narrow bands in the etched samples whilst the deformed bands appeared as dark narrow bands. Cracks were observed in the transformed bands formed in the sample that fractured during impact. The shear bands in the samples that were tempered for two hours were diffused, dim and not clearly formed compared to the shear bands in the samples that were tempered for one hour.

(4.2.2a) ADIABATIC SHEAR BANDS IN SAMPLES AUSTENITIZED AT 855^{O}C FOR 1 HOUR, TEMPERED AT 425^{O}C FOR 2 HOURS AND IMPACTED AT HIGH STRAIN RATES

The optical micrographs for the adiabatic shear bands formed in the steel samples tempered at 425^{O}C for two hours are presented in figures 4.23 to 4.26. Figure 4.23 shows a deformed shear band formed in a steel sample tempered at 425^{O}C for two hours and impacted at 37.0 kg.m/s. The width of the deformed band was 165μm and it had a hardness of 414 HV.

Figure 4.24 shows a transformed shear band formed in a steel sample tempered at 425^{O}C for two hours and impacted at 38.9 kg.m/s. The width of the transformed shear band was 66 μm and it had a hardness of 508 HV.

Figure 4.25 shows a transformed shear band formed in a steel sample tempered at 425^{O}C for two hours and impacted at 40.7 kg.m/s. The width of the transformed shear band was 68μm.

Figure 4.26 shows a transformed shear band formed in a steel sample tempered at 425^{O}C for two hours and impacted at 42.6 kg.m/s. This sample broke after impact and cracks propagated in the transformed shear band. The width of the transformed shear band was 109 µm and it had a hardness of 656 HV. The transformed shear band ended in a deformed shear band with a width of 158 µm and a hardness of 420 HV. Figure 4.27 shows the transformed shear band of this sample with a crack propagating through it. Figure 4.28 shows an unimpacted sample tempered at 425^{O}C for two hours and it had a hardness of 345 HV.

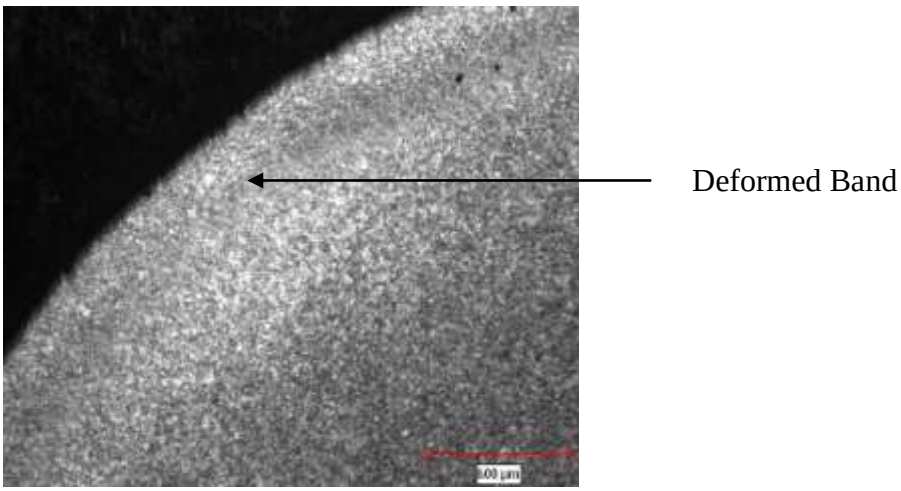

Figure 4.23: Shear band in a sample tempered at 425^{O}C for 2 hours and impacted at 37.0 kg.m/s

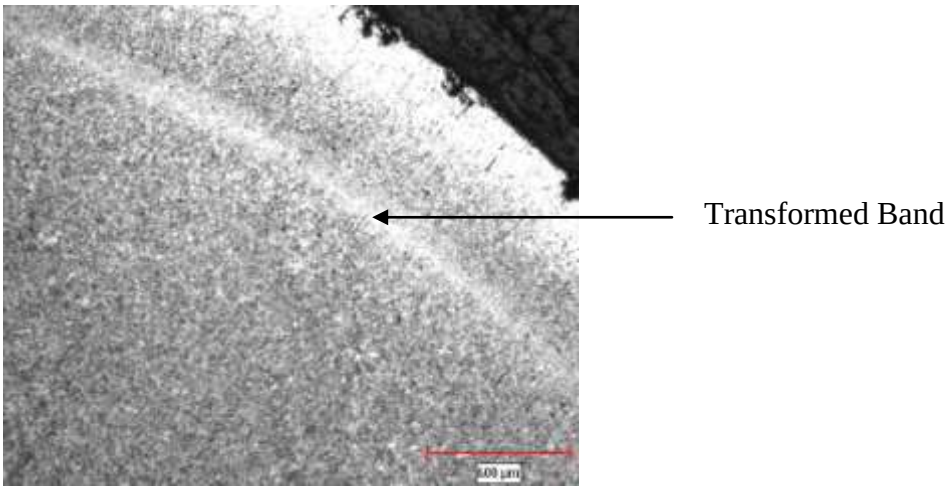

Figure 4.24: Shear band in a sample tempered at 425OC for 2 hours and impacted at 38.9 kg.m/**s**

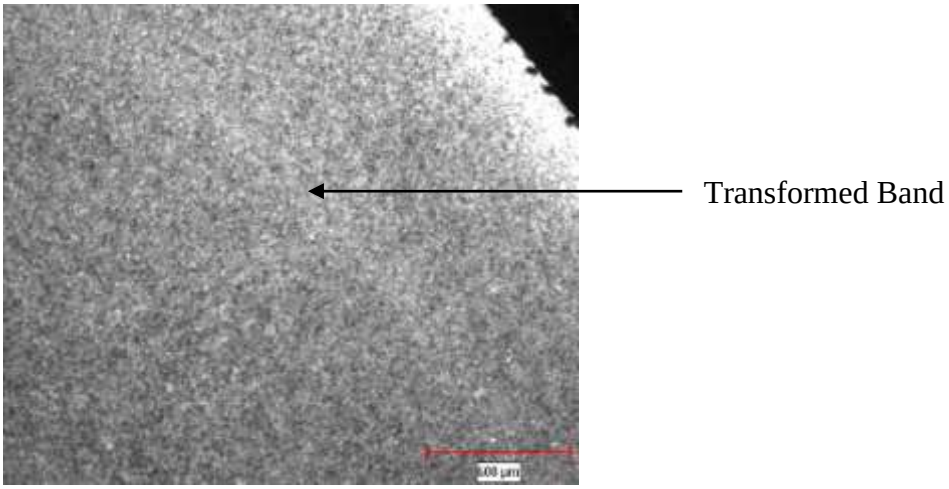

Figure 4.25: Shear band in a sample tempered at 425^{O}C for 2 hours and impacted at 40.7 kg.m/s

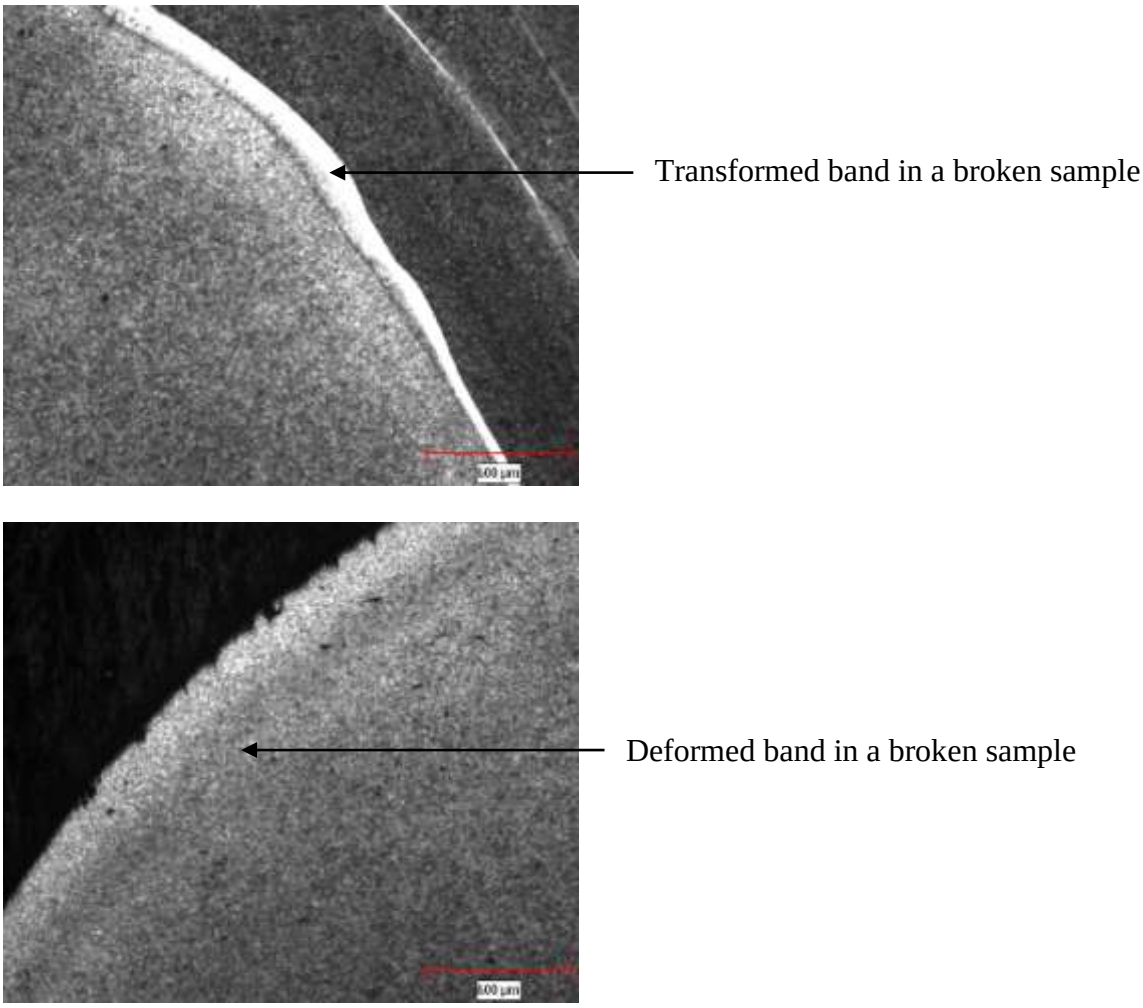

Figure 4.26: Shear bands in a sample tempered at 425^{O}C for 2 hours and impacted at 42.6kg.m/s

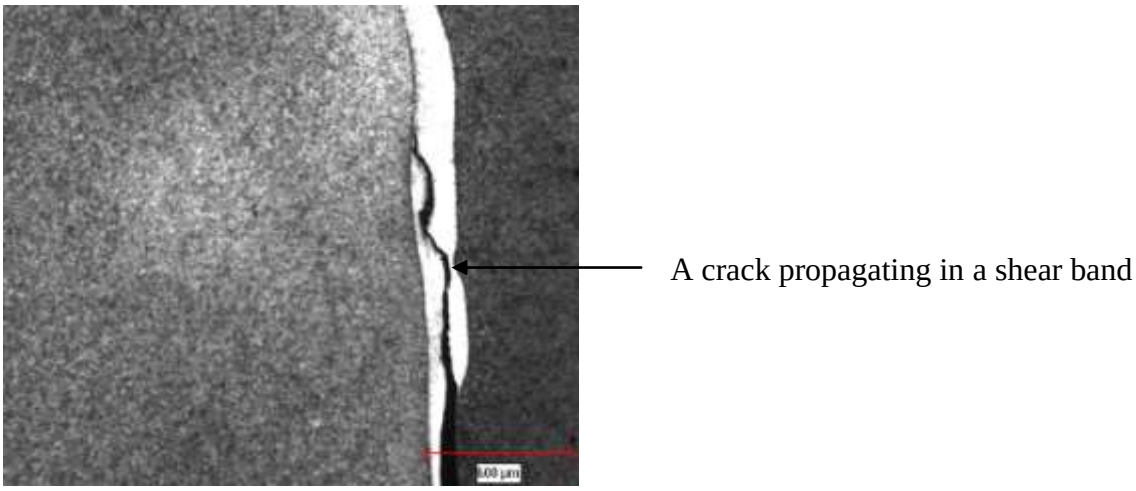

Figure 4.27: A Crack propagating in a transformed shear band

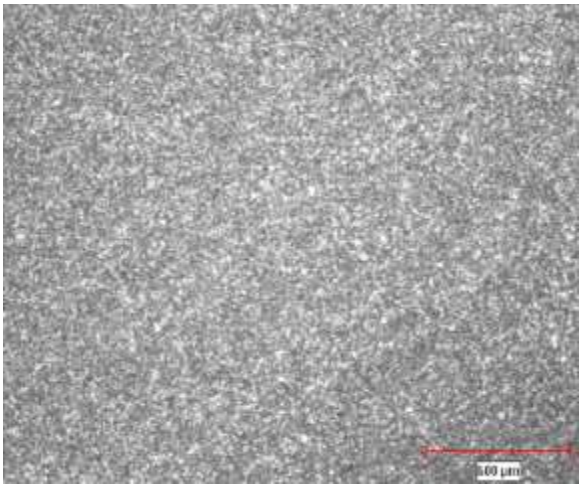

Figure 4.28: Unimpacted sample after tempering at $425^{O}C$ for 2 hours

(4.2.2B) ADIABATIC SHEAR BANDS IN SAMPLES AUSTENITIZED AT 855^{O}C FOR 30 MINUTES, TEMPERED AT 425^{O}C FOR 1 HOUR AND IMPACTED AT HIGH STRAIN RATES

The optical micrographs for the adiabatic shear bands formed in the steel samples tempered at 425^{O}C for one hour are presented in figures 4.29 to 4.30. Figure 4.29 shows a transformed band ending in a deformed band formed in a steel sample tempered at 425^{O}C for one hour and impacted at 44.4 kg.m/s. The transformed shear band had a width of 37 μm and a hardness of 483 HV. The deformed band also had a width of 148 μm and a hardness of 406 HV.

Figure 4.30 shows a steel sample tempered at 425^{O}C for one hour that formed both a deformed band and a transformed band after impact at 46.3 kg.m/s. The width of the deformed band was 232 μm and it had a hardness of 421 HV. The transformed band had a width of 205 μm.

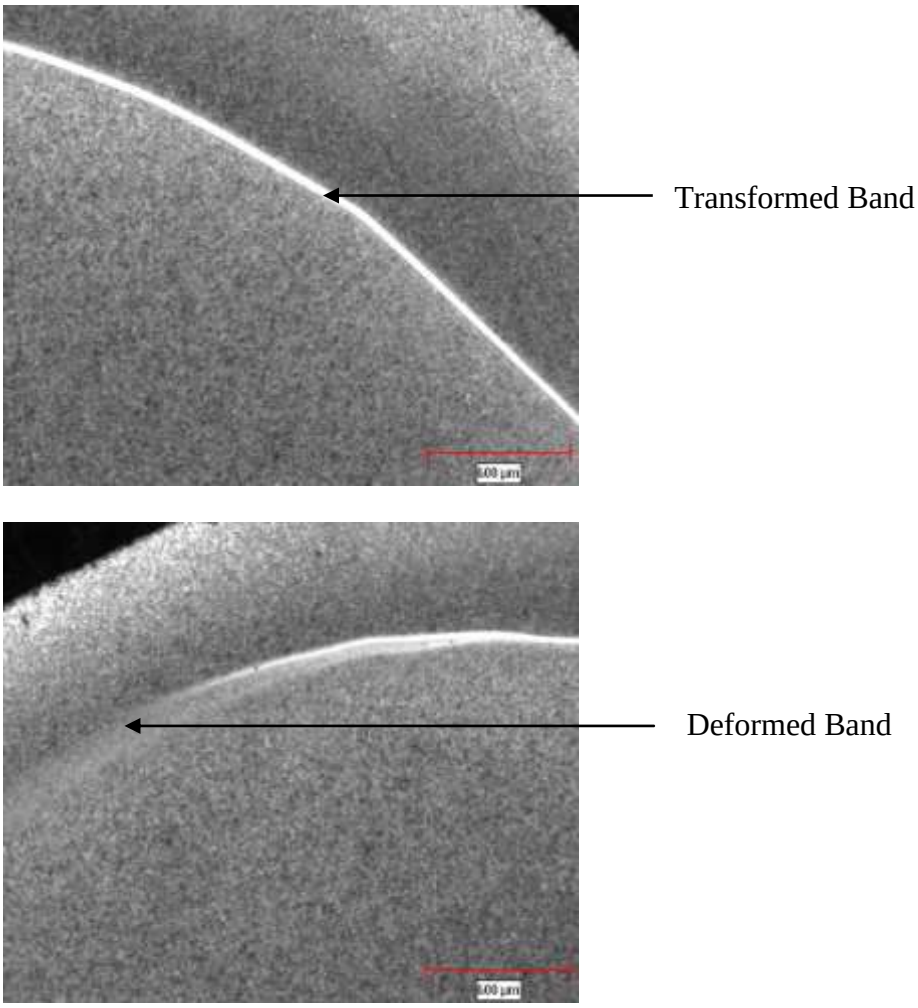

Figure 4.29: Shear band in a sample tempered at 425^{O}C for 1 hour and impacted at 44.4 kg.m/s

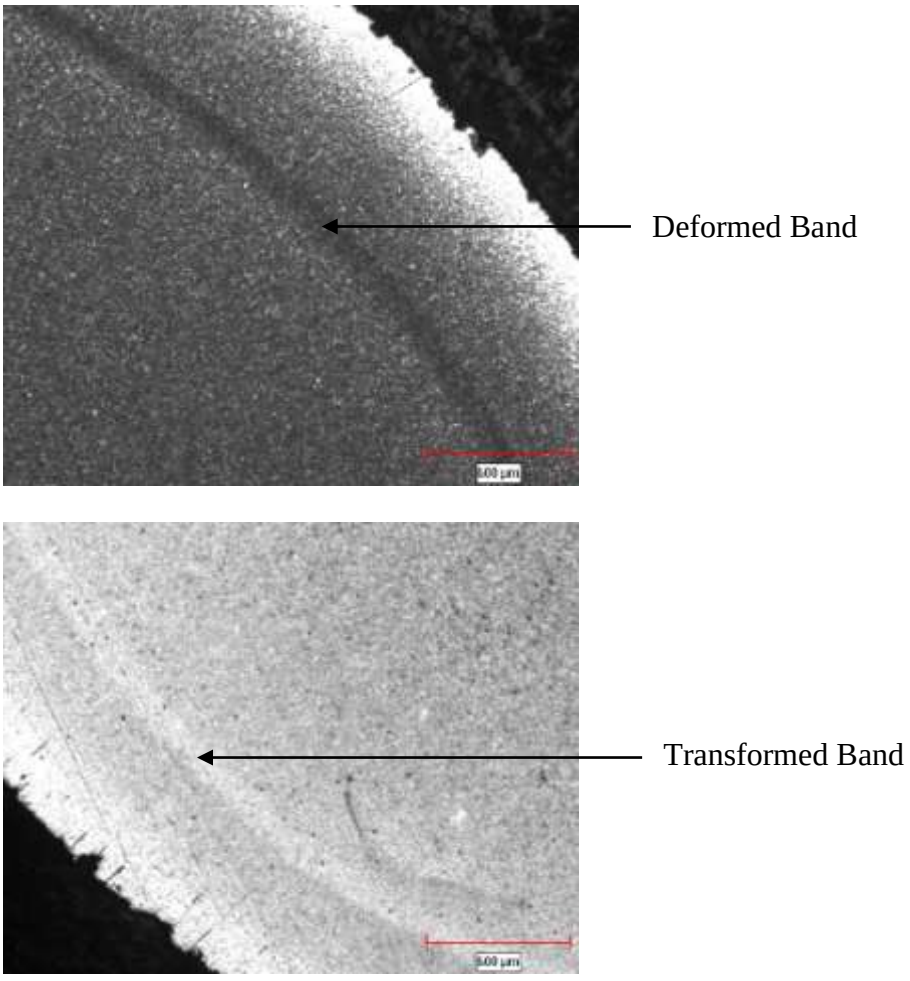

Figure 4.30: Shear bands in a sample tempered at 425^{O}C for 1 hour and impacted at 46.3kg.m/s

(4.2.2C) THE HARDNESS AND WIDTH DISTRIBUTION OF THE SHEAR BANDS FORMED IN STEEL SAMPLES TEMPERED AT 425^{O}C AND IMPACTED AT HIGH STRAIN RATES

A Buehler micromet micro hardness-testing machine was used to measure the micro-hardness of the steel samples by the Vickers hardness test (HV). The widths of the shear bands were also measured. A graph showing the variation in the width of the deformed bands and the transformed bands for samples tempered at 425^{O}C at one and two hours respectively is presented in figure 4.31.

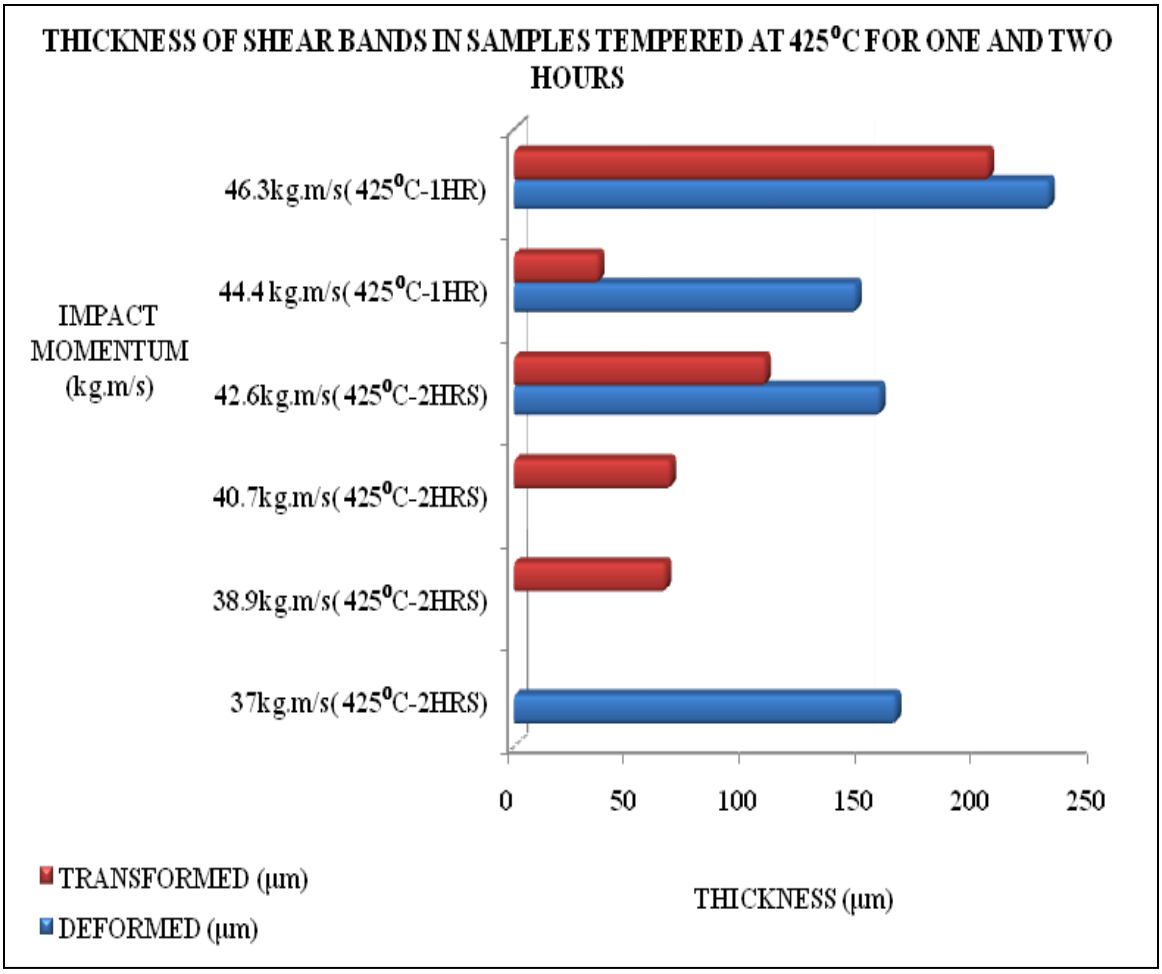

Figure 4.31: A Comparison of the Thickness of Deformed Bands and Transformed Bands formed in Samples Tempered at 425^{O}C

More clear and distinct adiabatic shear bands were formed in the samples tempered at 425^{O}C for one hour than those formed in the samples tempered at 425^{O}C for two hours. Deformed adiabatic shear bands formed in the impacted steel samples were always thicker than the transformed shear bands formed at the same impact momentum. In some steel samples, only deformed shear bands or transformed shear bands were formed after impact. However, other samples had both

deformed and transformed bands formed in them with the transformed bands always ending in deformed bands.

The hardness of the shear bands compared to the surrounding materials as well as the variations in the hardness of the deformed bands and the transformed bands are presented in figure 4.32.

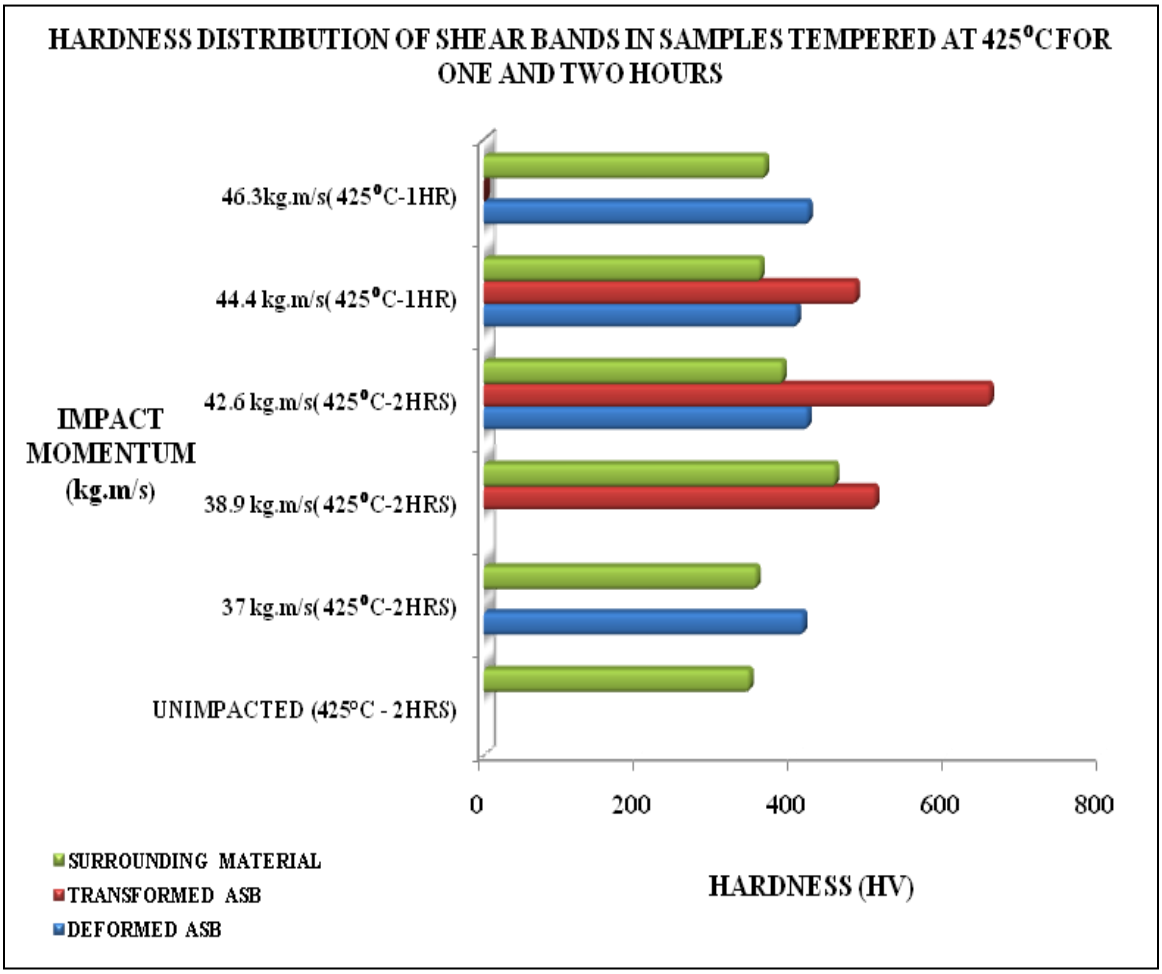

Figure 4.32: A Comparison of the Hardness of the Surrounding Material and the Shear Bands formed in Samples Tempered at 425^{O}C

The average hardness of the transformed adiabatic shear bands formed in the impacted steel samples at the same impact momentums was always harder than the average hardness of the deformed adiabatic shear bands and the surrounding material.

The average hardness of the unimpacted AISI 4340 steel sample tempered at $425^{O}C$ for two hours was 345HV. After impacting the sample at 37.0 kg.m/s, the hardness of the deformed band formed was 414 HV, which represents approximately 20% increase in hardness compared to the unimpacted sample. In addition, the hardness of the deformed bands increased by 17% as compared to the l neighboring material of the shear band.

At an impact momentum of 38.9 kg.m/s, the hardness of the transformed shear band increased by 47% compared to the hardness of the unimpacted material. In addition, the hardness of the transformed band increased by 12% compared to the material surrounding the shear band. In general, the hardness of the shear bands was always higher than that of the surrounding material.

Tables 4.7 to 4.10 are summaries of the microscopic analysis done on the steel samples that were tempered at $425^{O}C$ for one hour and those tempered for two hours. Tables 4.7 and 4.9 show the widths of the shear bands while tables 4.8 and 4.10 show the hardness variations in the shear bands and the surrounding materials.

Table 4.7: Widths of adiabatic shear bands in samples tempered at 425 ^{O}C for 2 hours

IMPACT MOMENTUM (kg.m/s)	DEFORMED BAND (μm)	TRANSFORMED BAND (μm)
37.0	165	
38.9		66
40.7		68
42.6	158	109

Table 4.8: Hardness of adiabatic shear bands in samples tempered at 425 ^{O}C for 2 hours

IMPACT MOMENTUM (kg.m/s)	DEFORMED BAND (HV)	TRANSFORMED BAND (HV)	SURROUNDING MATERIAL (HV)
UNIMPACTED SAMPLE	345		
37.0	414		354
38.9		508	456
42.6	420 SAMPLE FRACTURED	656	388

Table 4.9: Widths of adiabatic shear bands in samples tempered at 425 ^{O}C for 1 hour

IMPACT MOMENTUM (kg.m/s)	DEFORMED BAND (μm)	TRANSFORMED BAND (μm)
44.4	148	37
46.3	232	205

Table 4.10: Hardness of adiabatic shear bands in samples tempered at 425 ^{O}C for 1 hour

IMPACT MOMENTUM (kg.m/s)	SAMPLES TEMPERED AT 425 ^{O}C FOR ONE HOUR		
	DEFORMED BAND (HV)	TRANSFORMED BAND (HV)	SURROUNDING MATERIAL (HV)
44.4	406	483	359
46.3	421		365

(4.2.3) ADIABATIC SHEAR BANDS IN SAMPLES AUSTENITIZED AT 855^{O}C FOR ONE HOUR, TEMPERED AT 620^{O}C FOR 2 HOURS AND IMPACTED AT HIGH STRAIN RATES

Most of the adiabatic shear bands formed in the impacted steel samples in this group were of the deformed shear band type. Nevertheless, at a very high strain rate, a clearly distinct transformed adiabatic shear band developed. This transformed shear band was distinct and clear; and it ended in a deformed band.

The optical micrographs of the adiabatic shear bands formed in the steel samples tempered at 620^{O}C for two hours are presented in figures 4.33 to 4.37. Figure 4.33 shows a deformed shear band formed in a steel sample tempered at 620^{O}C for two hours and impacted at 42.6 kg.m/s. The deformed band had a width of 119 μm and a hardness of 353 HV.

Figure 4.34 shows a deformed band formed in a sample tempered at 620^{O}C for two hours and impacted at 44.4 kg.m/s. The shear band had a width of 202 μm and a hardness of 340 HV.

Figure 4.35 shows a deformed band that had a width of 237 μm formed in a sample tempered at 620^{O}C for two hours and impacted at 48.2 kg.m/s.

Figure 4.36 shows a transformed band in a steel sample tempered at 620^{O}C for two hours and impacted at 50.0 kg.m/s. The width of the transformed band was 32 μm and the hardness was 405 HV. This transformed band ended in a deformed band as shown in figure 4.37. The width of the deformed band was 143 μm and it had a hardness of 334 HV. Figure 4.38 shows the unimpacted steel sample tempered at 620^{O}C for two hours with a hardness of 284 HV.

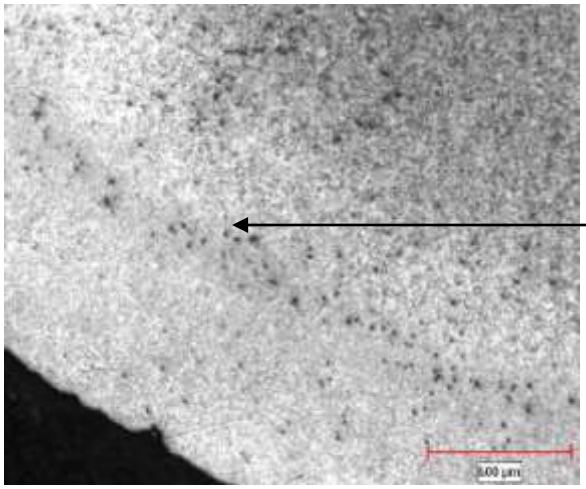

Figure 4.33: Shear band in a sample tempered at 620^{O}C for 2 hours and impacted at 42.6kg.m/s

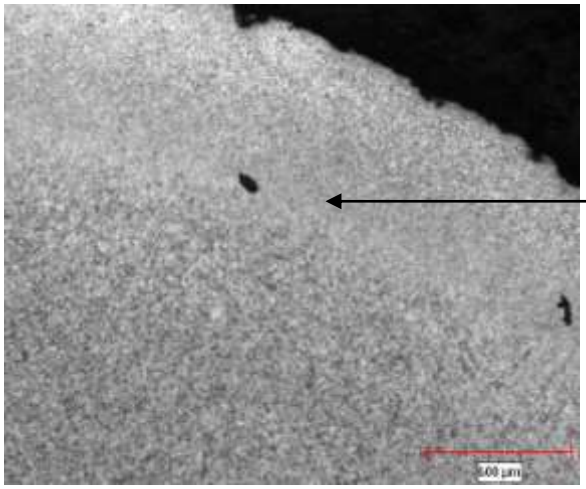

Figure 4.34: Shear band in a sample tempered at 620^{O}C for 2 hours and impacted at 44.4kg.m/s

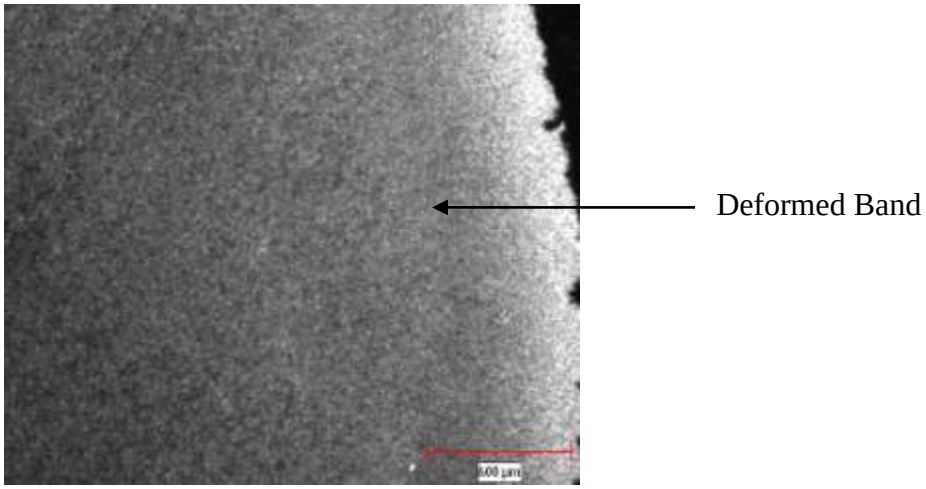

Figure 4.35: Shear band in a sample tempered at 620^{O}C for 2 hours and impacted at 48.2 kg.m/s

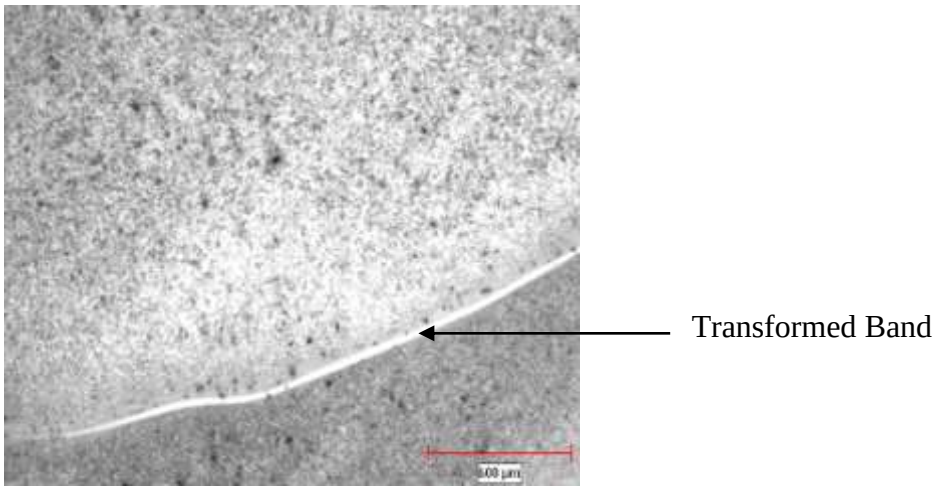

Figure 4.36: Shear band in a sample tempered at 620^{O}C for 2 hours and impacted at 50.0 kg.m/s

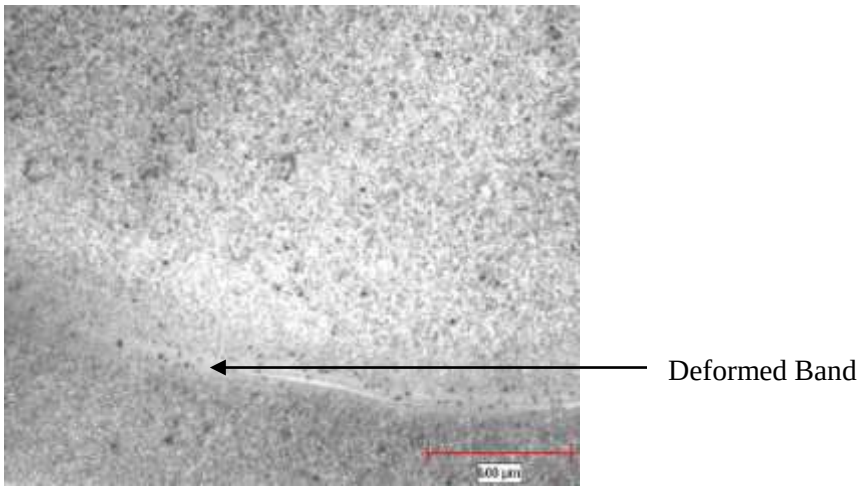

Figure 4.37: Shear band in a sample tempered at 620^{O}C for 2 hours and impacted at 50.0 kg.m/s

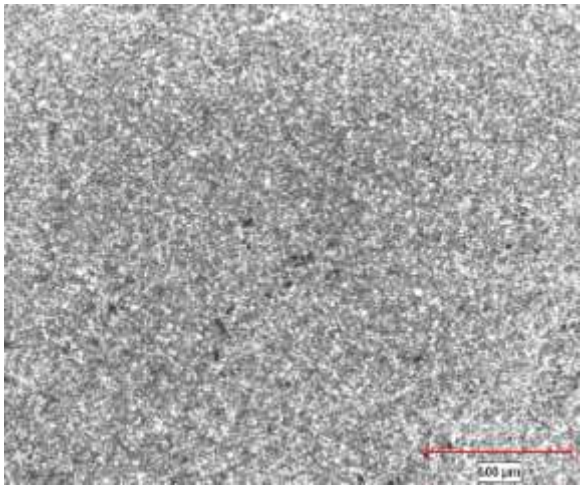

Figure 4.38: Unimpacted sample after tempering at 620^{O}C for two hours

(4.2.3a) THE HARDNESS AND THICKNESS DISTRIBUTION OF THE SHEAR BANDS FORMED IN SAMPLES TEMPERED AT 620^{O}C AND IMPACTED AT HIGH STRAIN RATES

A Buehler micromet micro hardness-testing machine was used to measure the micro-hardness of the steel samples by the Vickers hardness test (HV). The widths of the shear bands were measured. Figure 4.39 shows the variations in the width of shear bands formed in samples tempered at 620^{O}C for two hours.

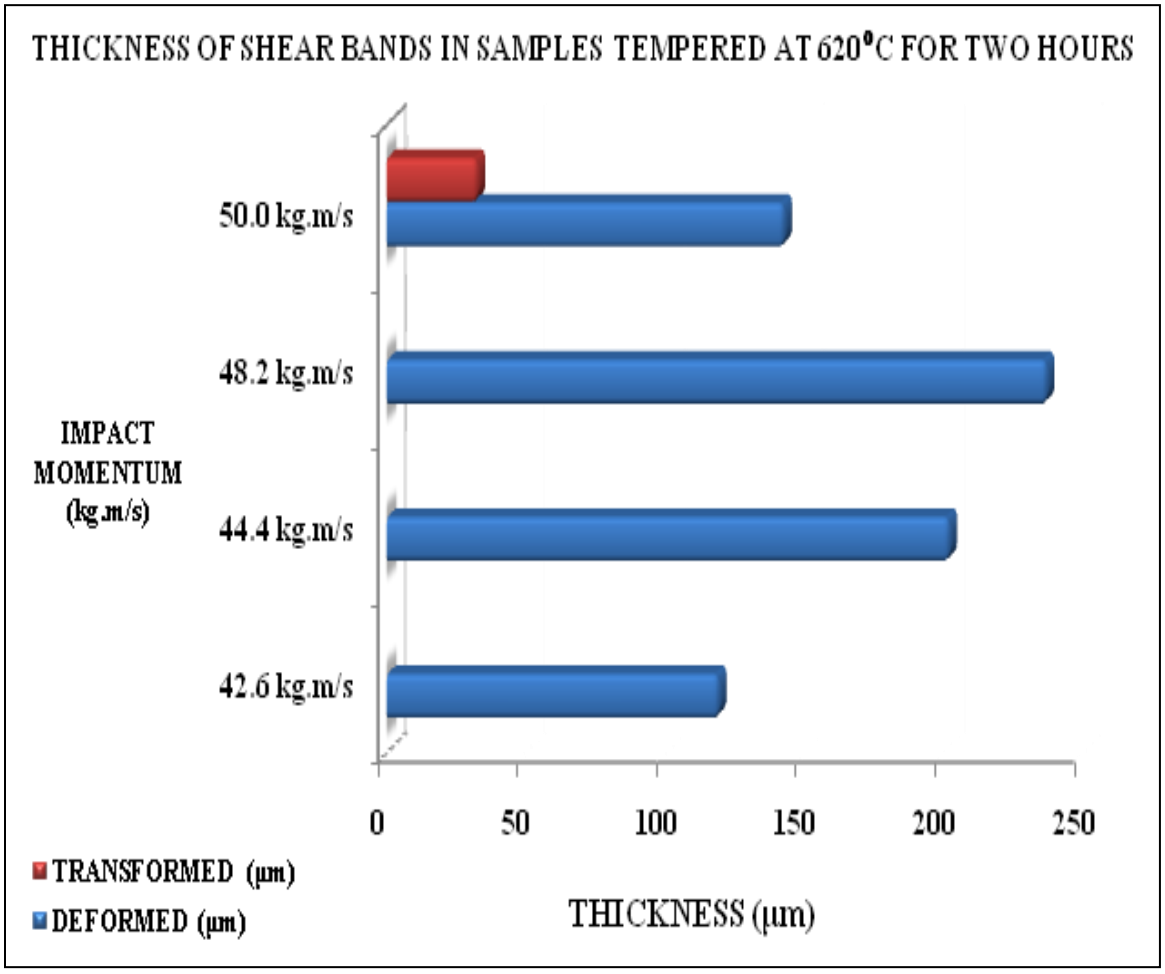

Figure 4.39: A Comparison of the Thickness of Deformed Bands and Transformed Bands formed in Samples Tempered at 620^{O}C for 2 hours

Most of the adiabatic shear bands formed in the impacted samples in this group were deformed shear bands. The deformed shear band formed is thicker than the transformed shear band in the impacted sample that had both bands formed. The graph shows that as the impact momentum increases, the thickness of the deformed shear bands increases.

The hardness of the shear bands compared to the surrounding materials as well as the variations in the hardness of the deformed bands and the transformed bands are presented in a figure 4.40.

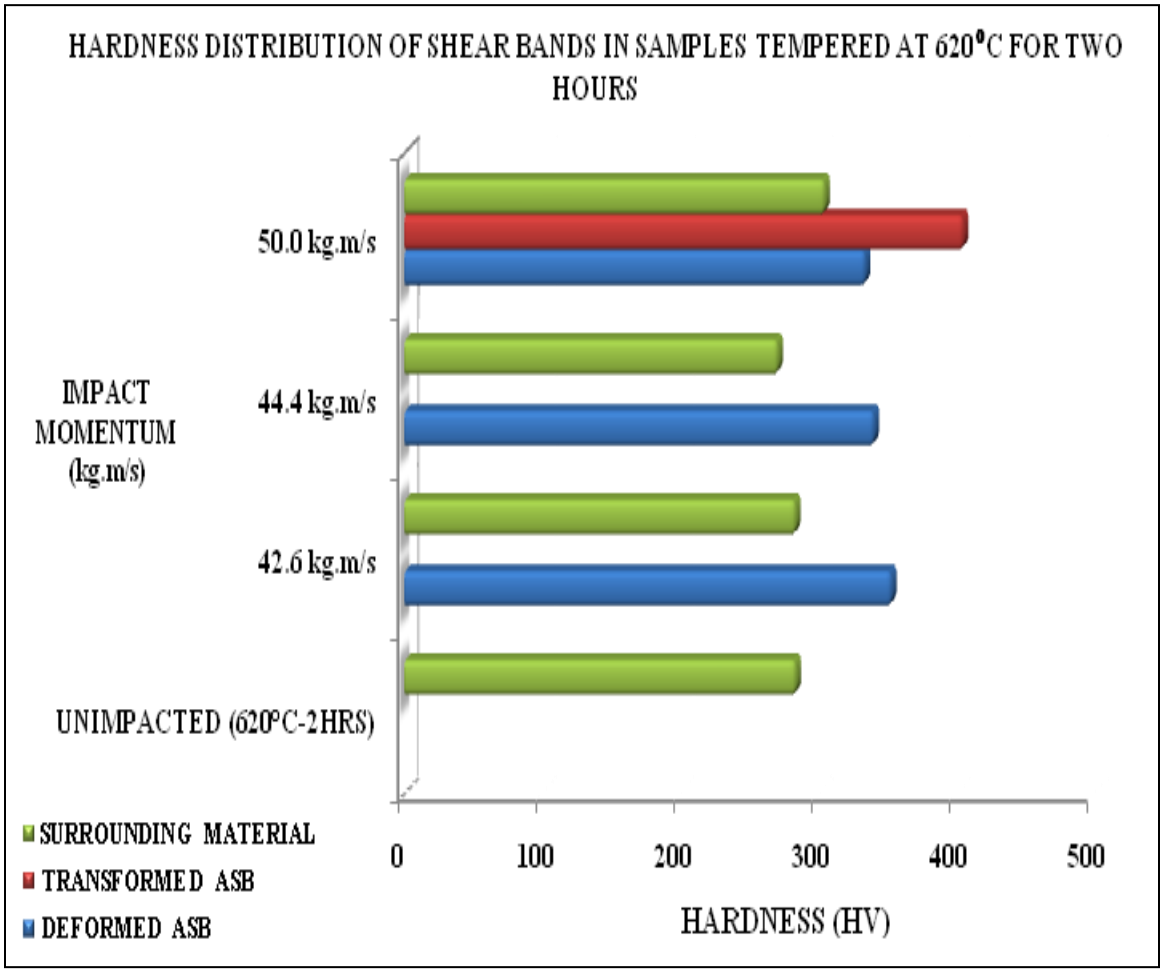

Figure 4.40: A Comparison of the Hardness of the Surrounding Material and the Shear Bands formed in Samples Tempered at 425^{O}C at 620^{O}C for 2 hours

The adiabatic shear bands formed are harder than the material surrounding the shear bands. The material surrounding the adiabatic shear bands are also harder than the unimpacted material.

The average hardness of the only transformed band formed in the sample impacted at 50.0 kg.m/s was higher than the hardness of all the deformed bands formed in each impacted sample. The hardness of the transformed band is approximately 43% higher than the hardness of the unimpacted sample. In addition, compared to the hardness of the material surrounding the shear band, the transformed band is 33% higher. In this group, the average hardness of the deformed shear bands decrease slightly as the impact momentums increase.

Tables 4.11 to 4.12 are summaries of the microscopic analysis done on the steel samples that were tempered at $620^{O}C$ for two hours. Table 4.11 shows the widths of the shear bands while table 4.12 shows the hardness variations in the shear bands and the surrounding materials.

Table 4.11: Widths of adiabatic shear bands in samples tempered at 620 ^{O}C for 2 hours

IMPACT MOMENTUM (kg.m/s)	DEFORMED BAND (μm)	TRANSFORMED BAND (μm)
42.6	119	
44.4	202	131
48.2	237	
50.0	143	32

Table 4.12: Hardness of adiabatic shear bands in samples tempered at 620 ^{O}C for 2 hours

IMPACT MOMENTUM (kg.m/s)	DEFORMED BAND (HV)	TRANSFORMED BAND (HV)	SURROUNDING MATERIAL (HV)
UNIMPACTED SAMPLE	284		
42.6	353		284
44.4	340		271
50.0	334	405	305

(4.2.4) FACTORS INFLUENCING THE THICKNESS OF THE ADIABATIC SHEAR BANDS FORMED IN THE STEEL SAMPLES

It was observed in the current study that the strength of the AISI 4340 steel and the microstructure affect the formation of adiabatic shear bands. The widths of the adiabatic shear bands formed in the impacted steel samples were influenced by the hardness of the parent steels used for the impact test. In addition, the impact momentum also had an influence on the width of the adiabatic shear bands.

At the same impact momentum, harder steel samples had adiabatic shear bands with smaller width after the impact tests compared to the relatively softer samples. As the hardness of the AISI 4340 steel samples increased, the width of the shear bands decreased at the same impact momentum. After tempering, before the impact tests, samples tempered at 315^{O}C were harder compared to those tempered at $425\ ^{O}$C and $620\ ^{O}$C. At the same impact momentum, the width of the shear bands formed in the steel samples tempered at 315^{O}C was smaller compared to the width of the shear bands formed in the samples tempered at 425^{O}C. At an impact momentum of 38.9 kg.m/s, the width of the transformed shear band in the harder steel sample tempered at 315^{O}C was 53 μm while that of the steel sample tempered at 425^{O}C was 66 μm. Again, at an impact momentum of 37.0 kg.m/s, the deformed band in the harder steel sample tempered at 315^{O}C was 80 μm whilst the deformed shear band in the steel sample tempered at 425^{O}C was 165 μm.

Increasing impact momentum decreased the width of the shear bands at the same tempering temperature. When the impact momentum of the steel sample tempered at 315^{O}C was 37.0 kg.m/s, the width of the shear band formed in the impacted steel sample was 80 μm. When the

impact momentum was increased to 38.9 kg.m/s, the width of the deformed band was 53 μm. Increasing the impact momentum of the steel samples tempered at 425 ^{O}C from 37.0 kg.m/s to 38.9 kg.m/s reduced the width of the shear band from 165 μm to 66 μm.

Figure 4.41 shows the influence of the hardness of the parent steel on the width of the adiabatic shear bands formed. Figure 4.42 shows the influence of impact momentum on adiabatic shear bands width.

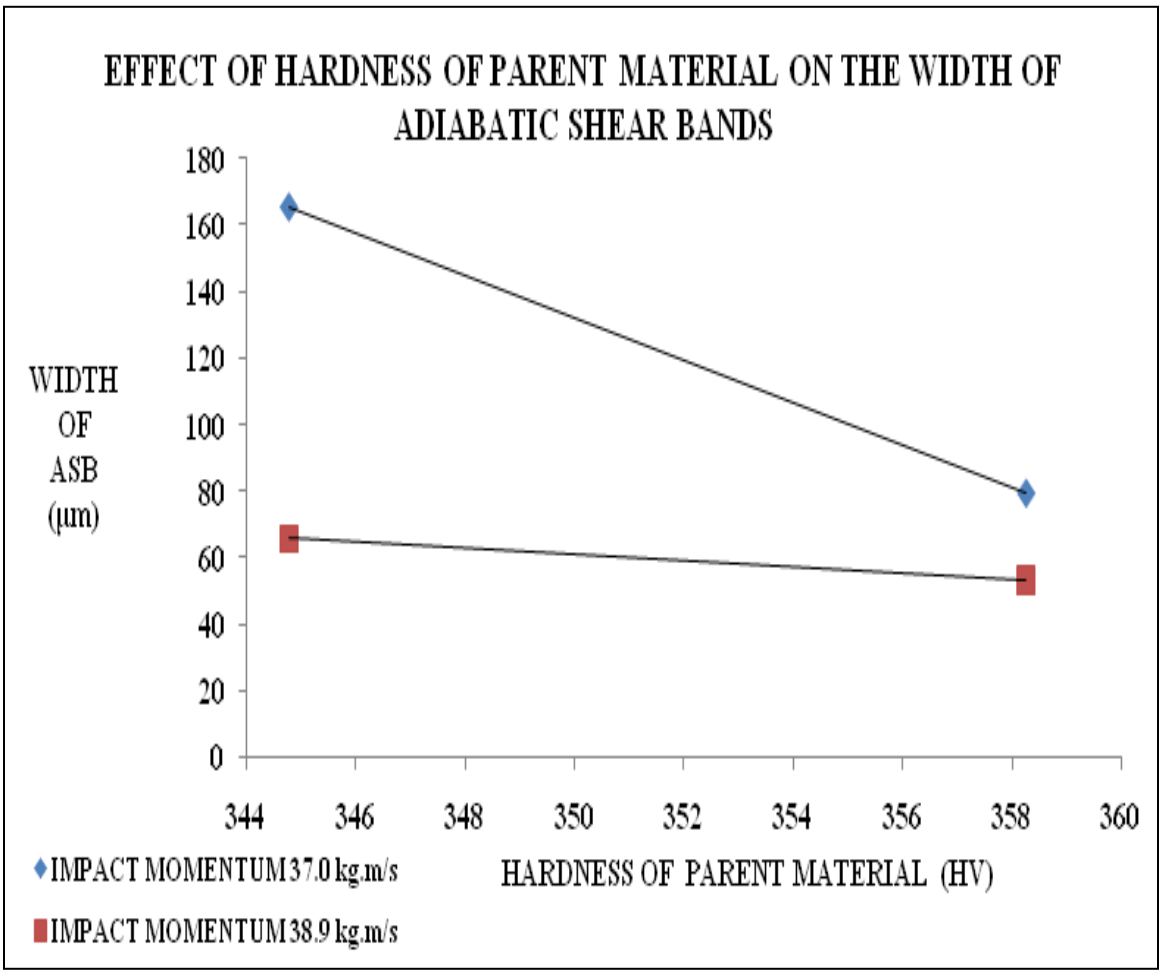

Figure 4.41: Effect of hardness of parent material on the width of adiabatic shear bands

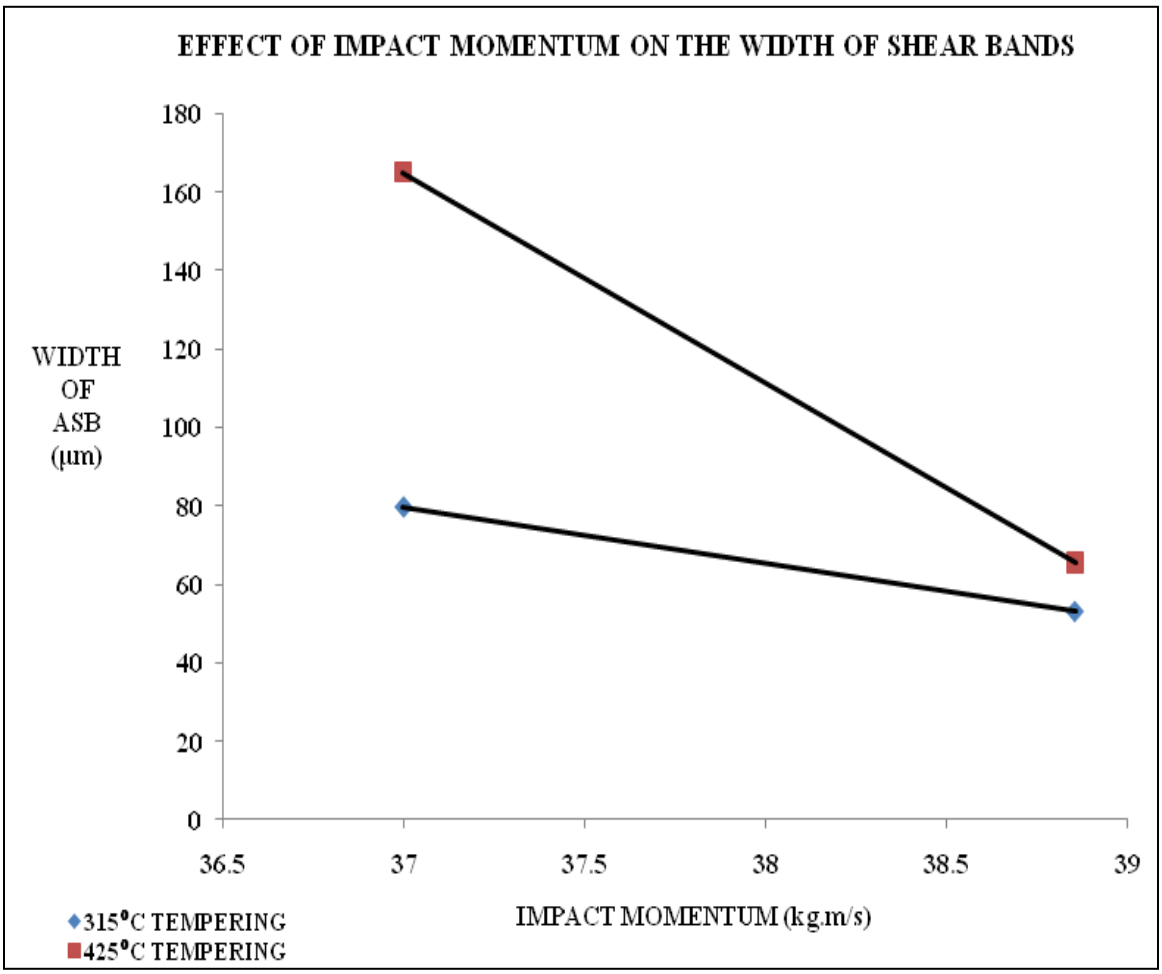

Figure 4.42: Effect of impact momentum on the width of adiabatic shear bands

(4.2.5) CRACKS PROPAGATING IN ADIABATIC SHEAR BANDS

The higher hardness of the adiabatic shear bands compared to the surrounding impacted material makes them susceptible to crack initiation and propagation during deformation. Many of the fractured samples had cracks propagating through shear bands formed in them during the impact tests. The transformed adiabatic shear bands are more susceptible to crack initiation and propagation than the deformed adiabatic shear bands. This is due to the hard nature of the transformed shear bands as compared to the deformed shear bands.

There were no cracks found in any of the deformed adiabatic shear bands formed in the impacted samples. However, cracks were propagated inside the transformed adiabatic shear bands in some of the impacted samples. This led to fracture of the impacted samples. Some fractured samples showed distinct cracks propagating in the transformed shear bands. Optical micrographs of some of the cracks found propagating though shear bands in the impacted samples are shown in figures 4.43 to 4.45.

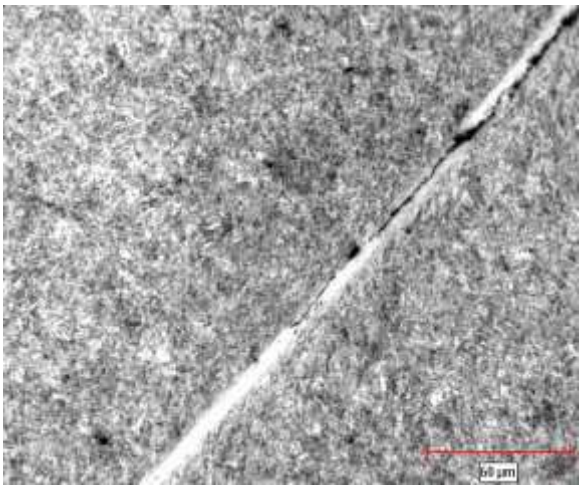

Figure 4.43: Crack propagating in a shear band in a sample tempered at 315^{O}C for 1 hour

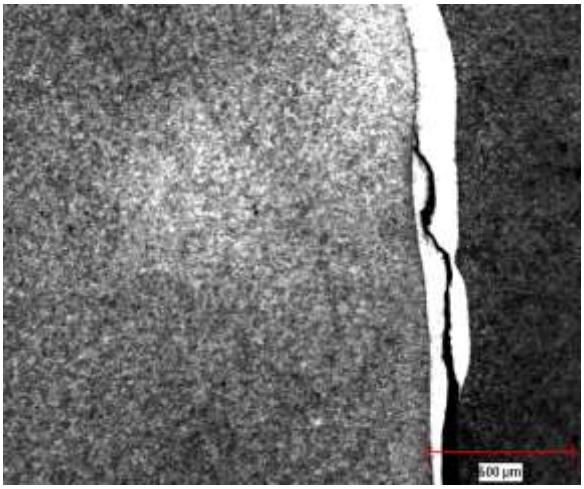

Figure 4.44: Crack propagating in a shear band in a sample tempered at 425 ^{O}C for 2 hours

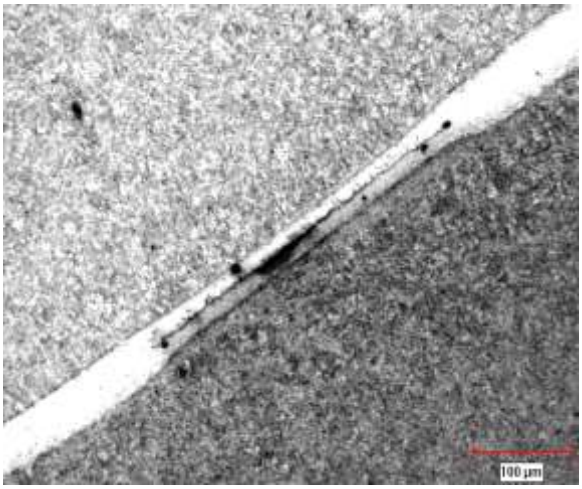

Figure 4.45: Crack propagating in a shear band in a sample tempered at 315 ^{O}C for 1 hour

(4.3) POST IMPACT ANNEALING OF AISI 4340 STEEL

Post-impact heat treatments of samples were used to determine the possibility of eliminating adiabatic shear bands from the microstructure of the steel samples. After impact, all the transformed shear bands formed in the samples were studied thoroughly under the optical microscope before proceeding with the post impact annealing process to document the properties of the shear bands. It was observed that the transformed shear bands appeared white and clear both at low and high magnifications on the optical microscope. The transformed shear bands were well developed and easily distinguishable from the adjoining material.

The impacted steel samples were soaked at 350 ^{O}C to 850 ^{O}C for periods ranging from 30 minutes to 4 hours. The steel samples that were annealed at temperatures of 650 ^{O}C to 850 ^{O}C were soaked at 30 minutes to 2 hours. On the other hand, steel samples that were annealed at temperatures of 350 ^{O}C to 550 ^{O}C were soaked at 2 hours to 4 hours. After each annealing procedure, the samples were mounted, ground, polished, etched and studied beneath the optical microscope.

Post impact annealing of the AISI 4340 steel samples revealed that annealing samples at 650 ^{O}C to 850 ^{O}C could have very significant effects on the properties of the adiabatic shear bands and the surrounding impacted material. However, annealing the impacted steel samples at 350 ^{O}C to 550 ^{O}C does not support reversing the properties of the adiabatic shear bands and the surrounding impacted material effectively.

In contrast, annealing at a temperature of 650 ^{O}C resulted in the white etching adiabatic shear bands appearing as a black band due to the effects of diffusion and strain. New material that resembled that of the surrounding impacted material developed in the shear bands when the

samples were observed under the microscope. The shear bands emerged as black bands but could still be distinguished from the surrounding bulk material. The hardness of the shear bands and the surrounding material decreased when the steel samples were annealed at higher temperatures.

In addition, annealing at 750 ^{O}C and 850 ^{O}C resulted in a total elimination of the shear bands from the impacted steel samples. There were no traces of the shear bands in the annealed samples at these temperatures. The shear flow patterns were obliterated and the microstructure of the steel became homogeneous with no traces of extensive deformation. Again, the hardness of the shear bands and the surrounding material both decreased and their properties became comparable

(4.3.1) POST IMPACT ANNEALING OF AISI 4340 STEEL SAMPLES TEMPERED AT 315^{O}C FOR ONE HOUR AND IMPACTED AT 44.4 kg.m/s

The impacted quench-hardened steel samples that were tempered at 315^{O}C were annealed at 350^{O}C, 450 ^{O}C and 650 ^{O}C after their impact. These steel samples were previously tempered at 315^{O}C for one hour after austenitizing at 855 ^{O}C, and impacted at 44.4 kg.m/s and annealed.

Table 4.13 is a summary of the average widths of the shear bands, the average hardness of the shear bands and the average hardness of the surrounding impacted material during the post impact annealing procedures of the steel samples tempered at 315^{O}C for one hour and impacted at 44.4 kg.m/s. The table gives the width and hardness of the shear bands after impact and after

post-impact annealing. The hardness of the surrounding material after impact and after post impact annealing are also given in the table.

Figures 4.46 to 4.48 are the optical micrographs of the steel samples tempered at 315^{O}C, impacted at 44.4 kg.m/s and annealed at 350^{O}C, 450 ^{O}C and 650 ^{O}C respectively after impact. Samples A, sample B and sample C were annealed at 350 ^{O}C, 450 ^{O}C and 650 ^{O}C respectively. All the three samples were tempered at 315^{O}C for one hour and impacted at 44.4 kg.m/s.

Figure 4.46 (a) shows a transformed shear band in sample A after impact and figure 4.46 (b) shows the transformed shear band after two hours post-impact annealing at 350 ^{O}C.

Figure 4.47 (a) shows a transformed shear band in sample B after impact and figure 4.47 (b) shows the transformed shear band after two hours post-impact annealing at 450 ^{O}C.

Figure 4.48 (a) shows a transformed shear band in sample C after impact and figure 4.48 (b) shows the transformed shear band after thirty minutes post-impact annealing at 650 ^{O}C. Figure 4.48 (c) shows the transformed shear band in sample C after two hours post-impact annealing at 650 ^{O}C.

Table 4.13: Variations in width and hardness of shear bands for samples tempered at $315^{O}C$

SAMPLES	THICKNESS OF TRANSFORMED SHEAR BANDS (μm)	HARDNESS OF TRANSFORMED SHEAR BANDS (HV)	HARDNESS OF SURROUNDING MATERIAL (HV)
"A" AFTER IMPACT	36	621	543
"A" AFTER 2 HRS ANNEALING AT 350°C	28	642	559
"B" AFTER IMPACT	31	628	575
"B" AFTER 2 HRS ANNEALING AT 450°C	15	599	520
"C" AFTER IMPACT	39	681	533
"C" AFTER 30 MINUTES ANNEALING AT 650°C	31	368	359
"C" AFTER 2 HRS ANNEALING AT 650°C	31	310	317

a) SAMPLE "A" AFTER IMPACT

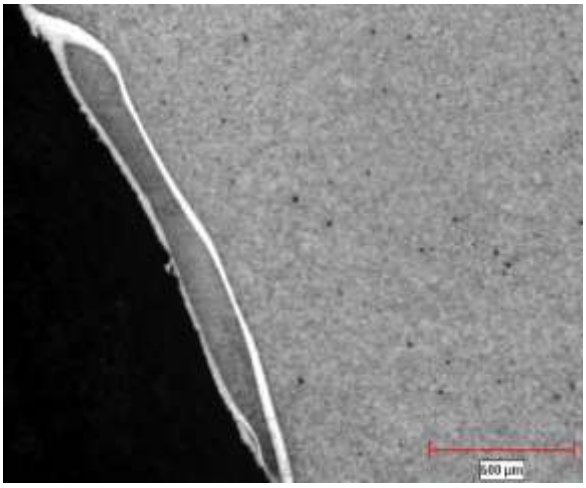

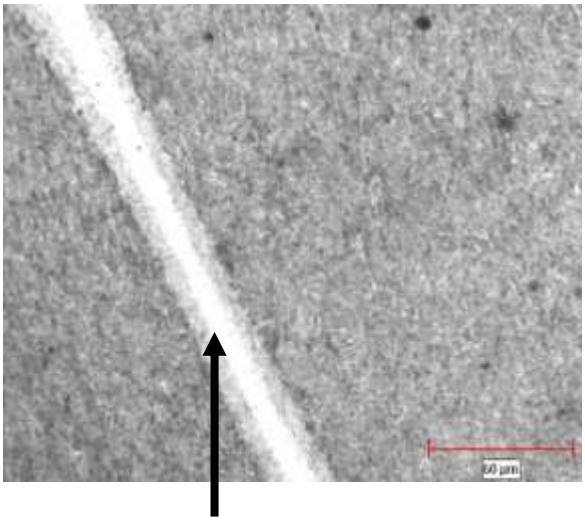

TEMPERED AT 315^{O}C FOR 1 HOUR
IMPACTED AT 44.4 kg.m/s
TRANSFORMED BAND
36 µm
621 HV
SURROUNDING MATERIAL
543 HV

b) SAMPLE "A" AFTER 2 HRS ANNEALING AT 350°C

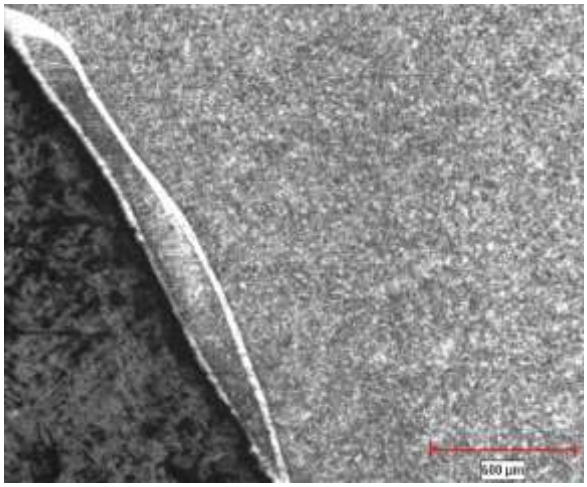

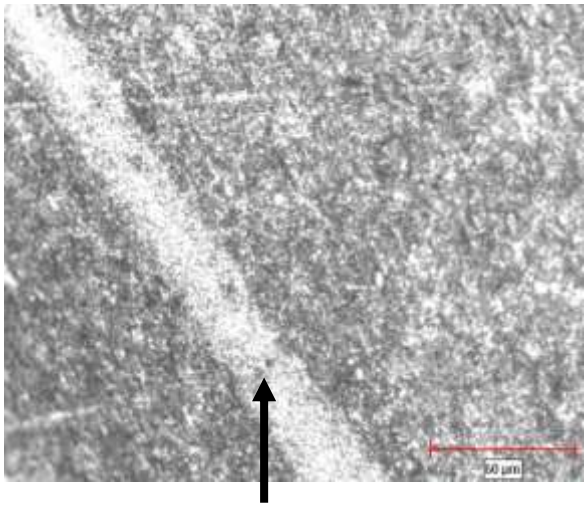

TEMPERED AT 315^{O}C FOR 1 HOUR
IMPACTED AT 44.4 kg.m/s
AFTER 2 HOURS ANNEALING AT 350 ^{O}C
TRANSFORMED BAND
28 µm
642 HV
SURROUNDING MATERIAL
559 HV

Figure 4.46: Steel Sample A (a) after impact (b) after 2 hours post-impact annealing at 350^{O}C

a) SAMPLE "B" AFTER IMPACT

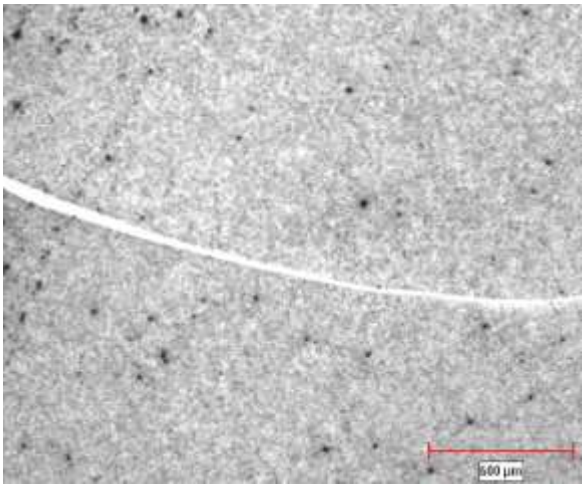

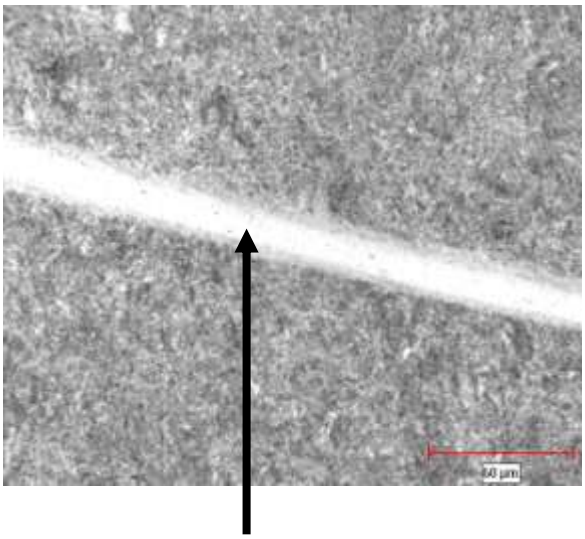

TEMPERED AT 315^{O}C FOR 1 HOUR
IMPACTED AT 44.4 kg.m/s
TRANSFORMED BAND
31µm
628HV
SURROUNDING MATERIAL
575 HV

b) SAMPLE "B" AFTER 2 HRS ANNEALING AT 450°C

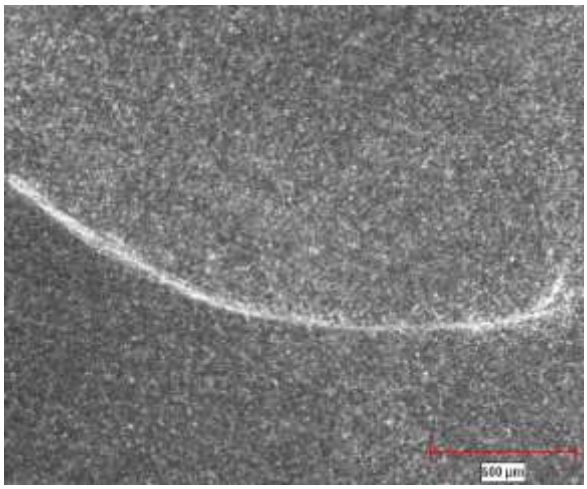

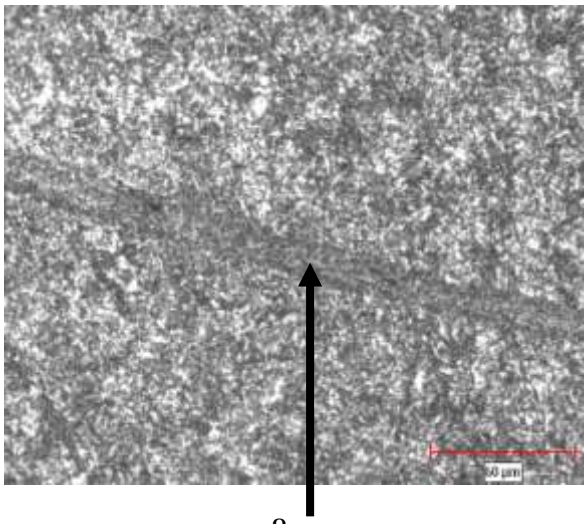

TEMPERED AT 315^{O}C FOR 1 HOUR
IMPACTED AT 44.4 kg.m/s
AFTER 2 HOURS ANNEALING AT 450 ^{O}C
TRANSFORMED BAND
15 µm
599 HV
SURROUNDING MATERIAL
521HV

Figure 4.47: Steel Sample B (a) after impact (b) after 2 hours post-impact annealing at 450^{O}C

a) SAMPLE "C" AFTER IMPACT

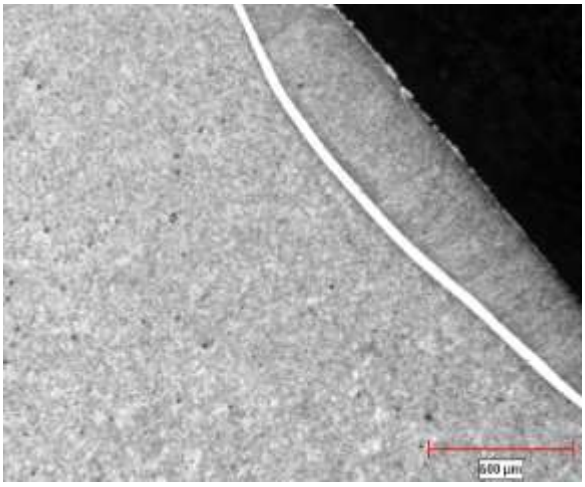

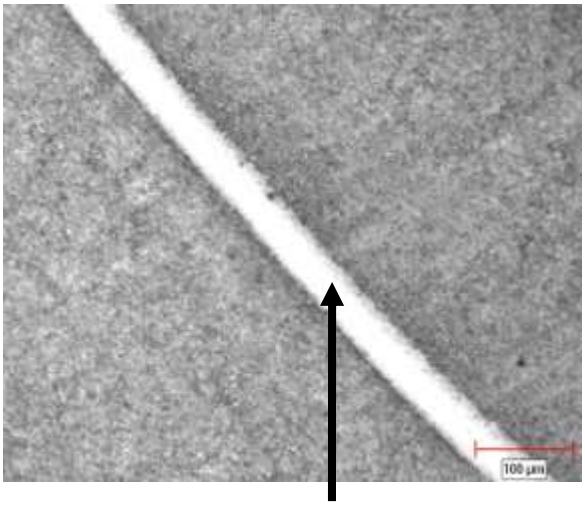

TEMPERED AT 315^{O}C FOR 1 HOUR
IMPACTED AT 44.4 kg.m/s
TRANSFORMED BAND
39 µm
681 HV
SURROUNDING MATERIAL
533 HV

b) SAMPLE "C" AFTER 0.5 HRS ANNEALING AT 650°C

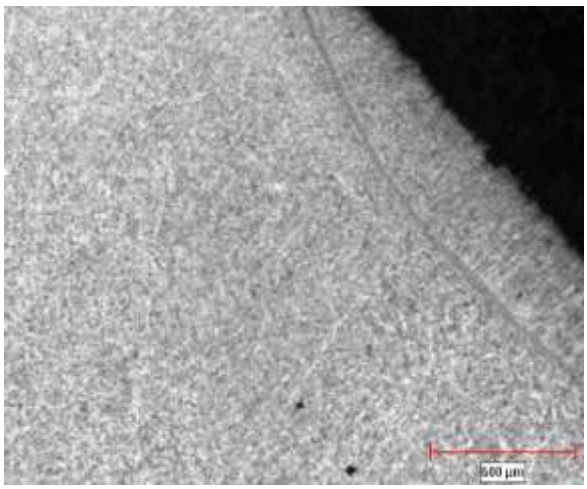

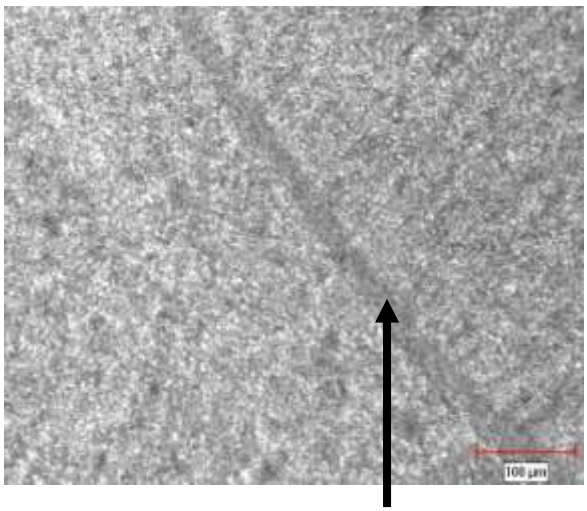

TEMPERED AT 315^{O}C FOR 1 HOUR
IMPACTED AT 44.4 kg.m/s
AFTER 30 MINUTES ANNEALING AT 650 ^{O}C
TRANSFORMED BAND
31 µm
368 HV
SURROUNDING MATERIAL
359 HV

Figure 4.48: Steel Sample C (a) after impact (b) after 0.5 hours post-impact annealing at 650OC

c) SAMPLE "C" AFTER 2 HOURS ANNEALING AT 650 ^{O}C

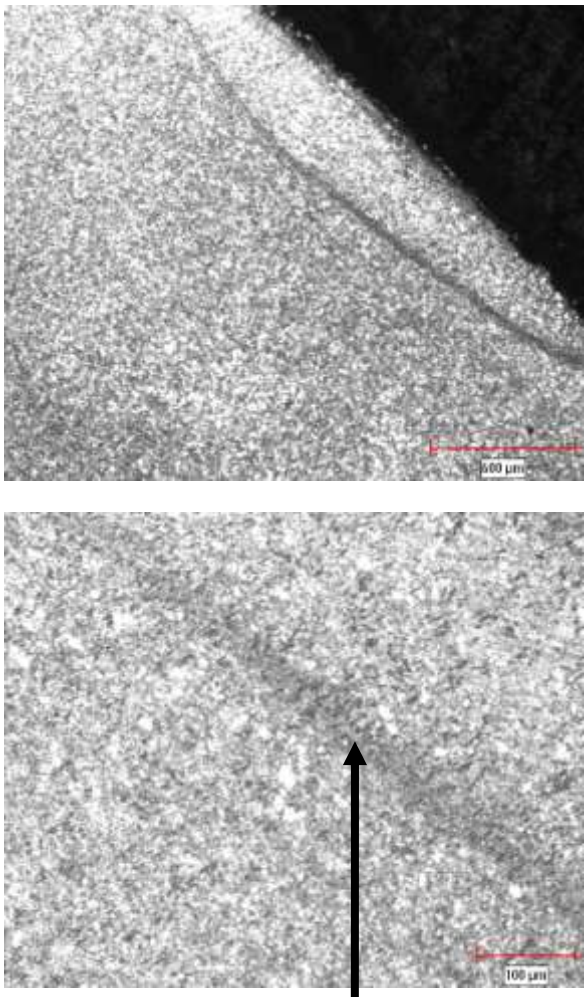

Figure 4.48 (c) Sample C after 2 hours post-impact annealing at 650OC

The thickness of the transformed shear band in the AISI 4340 steel sample "A" tempered at 315 ^{O}C and impacted at 44.43 kg.m/s decreased from 36 μm to 28 μm after post impact annealing at 350 ^{O}C for two hours as shown in table 4.13. The transformed shear band etched white at lower and higher magnifications after the post impact annealing as shown in figures 4.6 (a) and 4.6 (b). However, the brightness of the transformed shear band was reduced at higher magnifications as new materials resembling the surrounding impacted material were observed developing in the shear bands. This can be seen in the figure 4.6 (b) where the shear band is shown at a higher magnification after post-impact annealing at 350^{O}C. Hardness of the transformed shear band and the hardness of the surrounding impacted material in this sample increased after the post impact annealing at 350 ^{O}C as shown in figure 4.49.

The thickness of the transformed shear band in the sample "B" also decreased subsequently after post-impact annealing at 450 ^{O}C for two hours as shown by table 4.13. At lower magnifications of the optical microscope, the shear band etched dull white. At higher magnifications, the shear band emerged as a dark band with new material that bears a resemblance to the surrounding bulk material growing in it as shown in figure 4.47 (b). The hardness of both the shear band and the surrounding bulk materials decreased after the two hours post impact annealing at 450 ^{O}C as can be seen on figure 4.49.

The thickness of the shear band in the sample "C" after thirty minutes post impact annealing at 650 ^{O}C decreased from 39 μm to 31 μm. The white etching transformed shear band appeared as a black band both at lower and higher magnifications as can be seen in figure 4.48. New material that resembled the surrounding impacted material was observed in the shear band as shown in figure 4.48 (b) and 4.48 (c). There was a significant reduction in the hardness of the transformed shear band from 681 HV to 368 HV after the 30 minutes post impact annealing at 650 ^{O}C. After

2 hours post impact annealing at 650 ^{O}C, the thickness of the black band did not reduce but the hardness decreased further to 310 HV as shown on figure 4.49. The hardness of the neighboring bulk material also reduced significantly, such that after the 2 hours post impact annealing at 650 ^{O}C, the shear band and the surrounding material hardness was comparable. The shear band altered to a black band with the initial white grains replaced by materials resembling the surrounding bulk material. The black band also had hardness equal to the bulk material.

Figure 4.49 is a summary of the hardness distribution in the shear bands compared to the surrounding bulk material during the post impact annealing processes of samples tempered at 315 ^{O}C before impact at 44.4 kg.m/s.

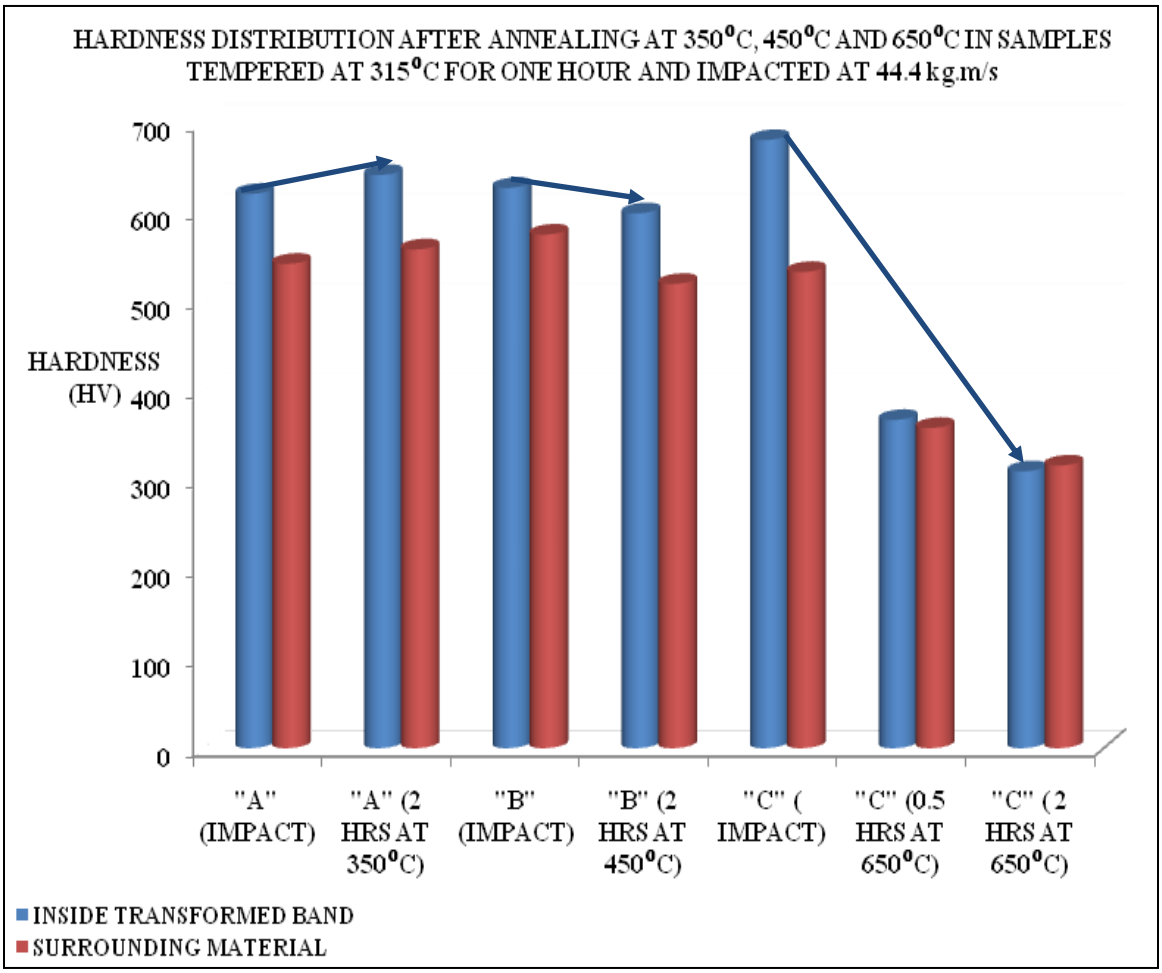

Figure 4.49: Hardness of shear bands and surrounding materials after impact and post-impact annealing

(4.3.2) POST IMPACT ANNEALING OF STEEL SAMPLES TEMPERED AT 425^{O}C FOR ONE HOUR AND IMPACTED AT 44.4 kg.m/s

The impacted steel samples that were tempered at 425^{O}C were annealed at 350^{O}C, 450 ^{O}C and 650 ^{O}C after their impact. These steel samples, after austenitizing at 855 ^{O}C, tempered at 425^{O}C for one hour, and impacted at 44.4 kg.m/s and subsequently annealed.

Table 4.14 is a summary of the average widths and hardness of the shear bands and the average hardness of the surrounding impacted material during the post impact annealing procedures of the steel samples tempered at 425^{O}C for one hour and impacted at 44.4 kg.m/s. The table gives the width and hardness of the shear bands after impact and after post-impact annealing. The hardness of the surrounding material after impact and after post impact annealing are also given in the table.

Figures 4.50 to 4.52 are the optical micrographs of the steel samples tempered at 425^{O}C, impacted at 44.4 kg.m/s and annealed at 350^{O}C, 450 ^{O}C and 650 ^{O}C respectively after impact. Samples A, B and C were annealed at 350 ^{O}C, 450 ^{O}C and 650 ^{O}C respectively. All the three samples were tempered at 425^{O}C for one hour and impacted at 44.4 kg.m/s.

Figure 4.50 (a) shows a transformed shear band in sample A after impact and figure 4.50 (b) shows the transformed shear band after two hours post-impact annealing at 350 ^{O}C. Figure 4.51 (a) shows a transformed shear band in sample B after impact and figure 4.51 (b) shows the transformed shear band after two hours post-impact annealing at 450 ^{O}C. Figure 4.52 (a) shows a transformed shear band in sample C after impact and figure 4.52 (b) shows the transformed shear band after thirty minutes post-impact annealing at 650 ^{O}C. Figure 4.52 (c) shows the transformed shear band in sample C after two hours post-impact annealing at 650 ^{O}C.

Table 4.14: Variations in width and hardness of shear bands for samples tempered at 425^{O}C

SAMPLES	THICKNESS OF TRANSFORMED SHEAR BANDS (μm)	HARDNESS OF TRANSFORMED SHEAR BANDS (HV)	HARDNESS OF SURROUNDING MATERIAL (HV)
"A" AFTER IMPACT	28	575	457
"A" AFTER 2 HRS ANNEALING AT 350°C	25	609	530
"B" AFTER IMPACT	289	667	470
"B" AFTER 2 HRS ANNEALING AT 450°C	25	579	507
"C" AFTER IMPACT	130	759	457
"C" AFTER 30 MINUTES ANNEALING AT 650°C	85	344	347
"C" AFTER 2 HRS ANNEALING AT 650°C	55	307	307

a) SAMPLE "A" AFTER IMPACT

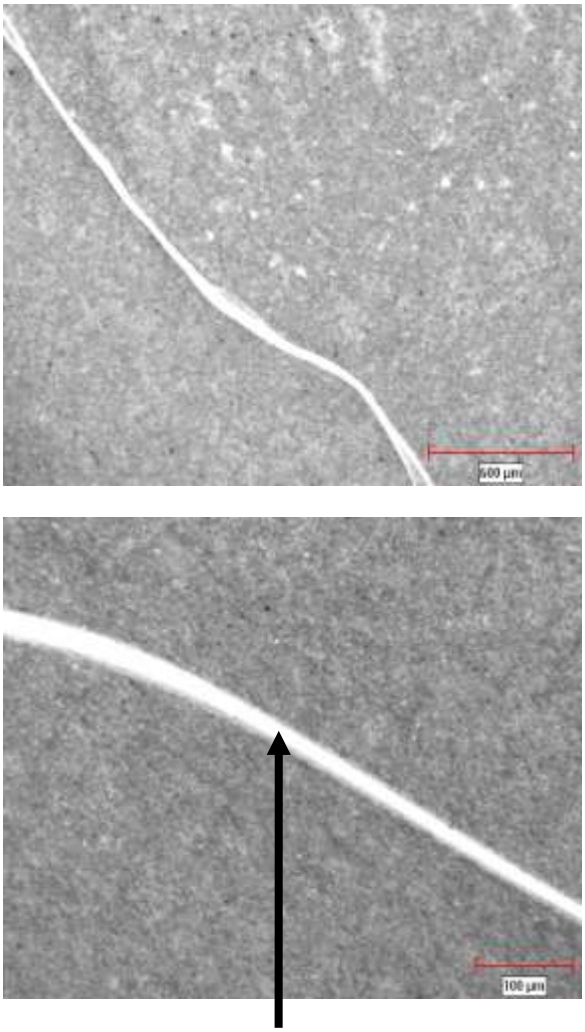

TEMPERED AT 425^{O}C FOR 1 HOUR
IMPACTED AT 44.4 kg.m/s
TRANSFORMED BAND
28µm
575HV
SURROUNDING MATERIAL
457HV

b) SAMPLE "A" AFTER 2 HOURS ANNEALING AT 350 ^{O}C

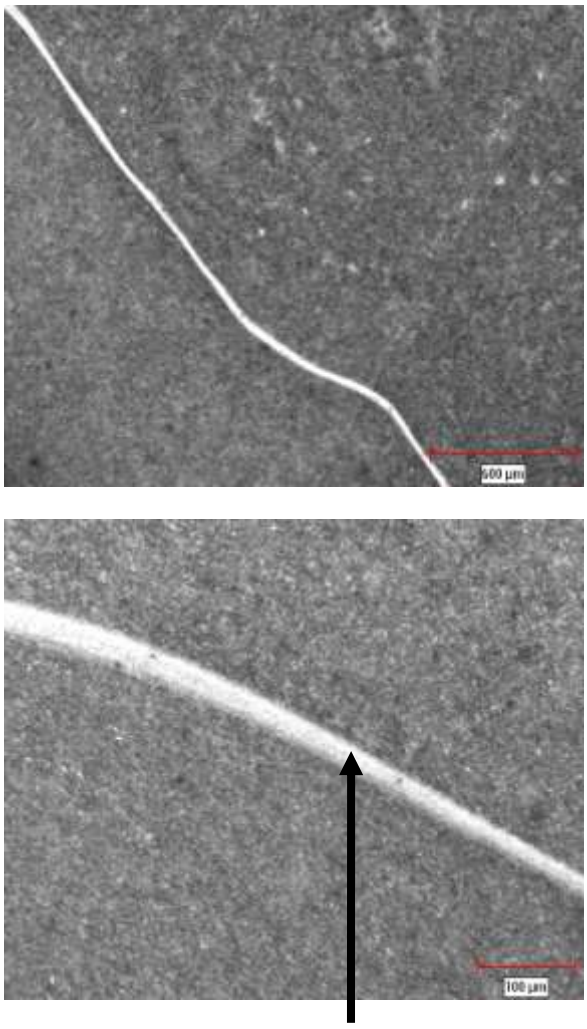

TEMPERED AT 425^{O}C FOR 1 HOUR
IMPACTED AT 44.4 kg.m/s
AFTER 2 HOURS ANNEALING AT 350 ^{O}C
TRANSFORMED BAND
25µm
609HV
SURROUNDING MATERIAL
530HV

Figure 4.50: Steel Sample A (a) after impact (b) after 2 hrs post-impact annealing at 350^{O}C

a) SAMPLE "B" AFTER IMPACT

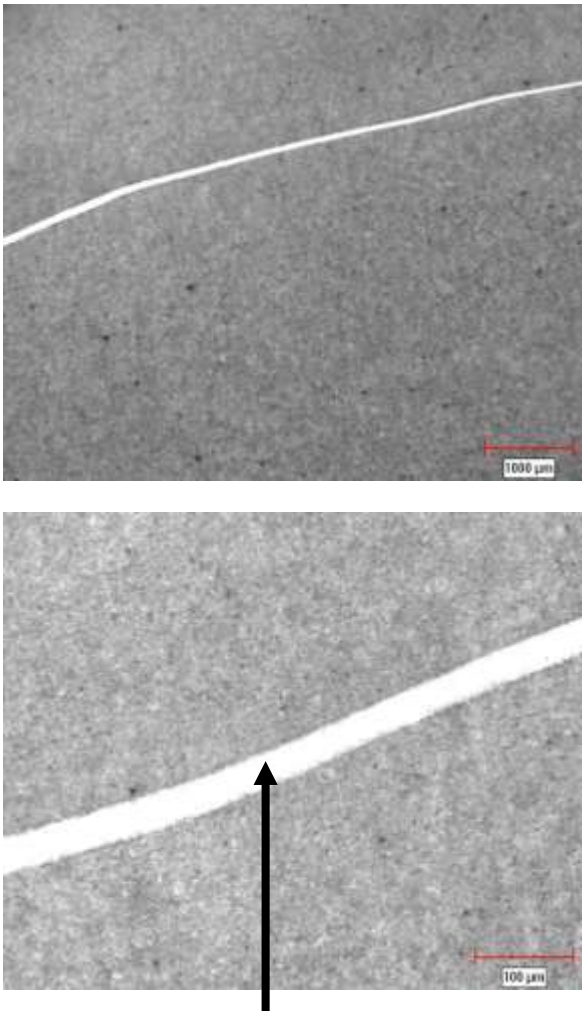

TEMPERED AT 425^{O}C FOR 1 HOUR
IMPACTED AT 44.4 kg.m/s
TRANSFORMED BAND
29µm
667HV
SURROUNDING MATERIAL
470HV

b) SAMPLE "B" AFTER 2 HRS ANNEALING AT 450^{O}C

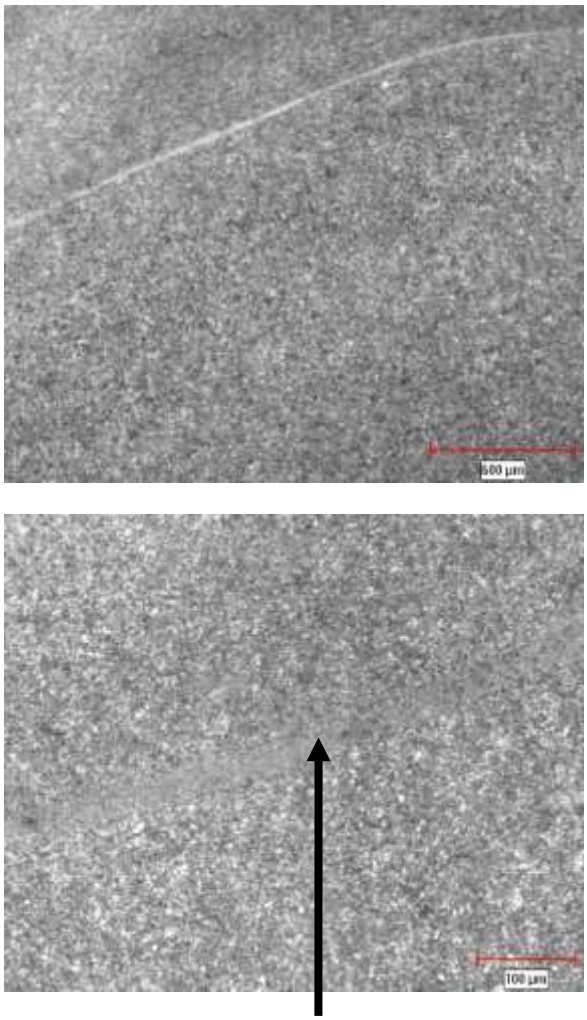

TEMPERED AT 425^{O}C FOR 1 HOUR
IMPACTED AT 44.4 kg.m/s
AFTER 2 HOURS ANNEALING AT 450 ^{O}C
TRANSFORMED BAND
25µm
579HV
SURROUNDING MATERIAL
507HV

Figure 4.51: Steel Sample B (a) after impact (b) after 2 hrs post-impact annealing at 450^{O}C

a) SAMPLE "C" AFTER IMPACT

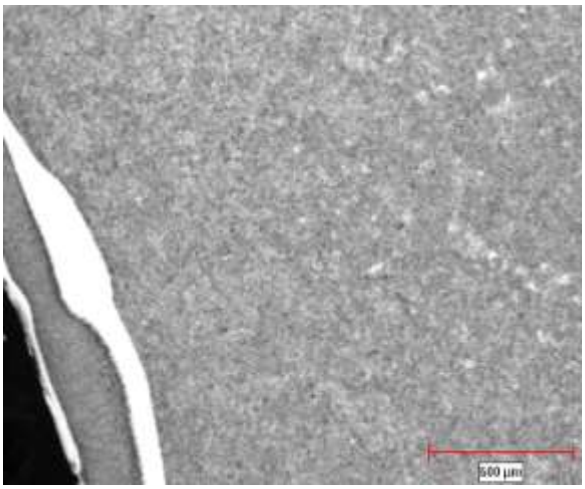

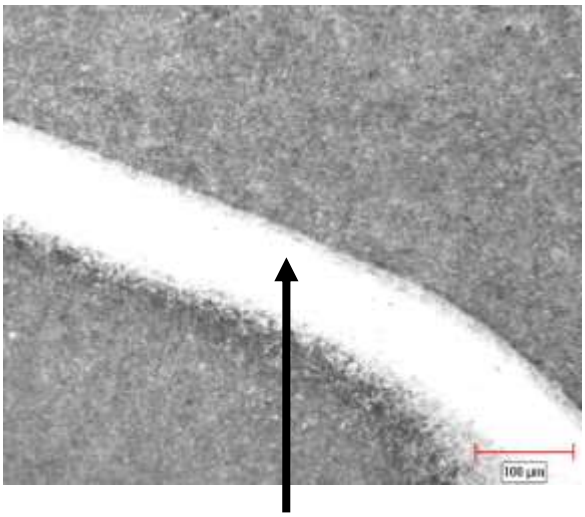

TEMPERED AT 425^{O}C FOR 1 HOUR
IMPACTED AT 44.4 kg.m/s
TRANSFORMED BAND
130µm
759HV
SURROUNDING MATERIAL
457HV

b) SAMPLE 'C' AFTER 0.5 HRS ANNEALING AT 650^{O}C

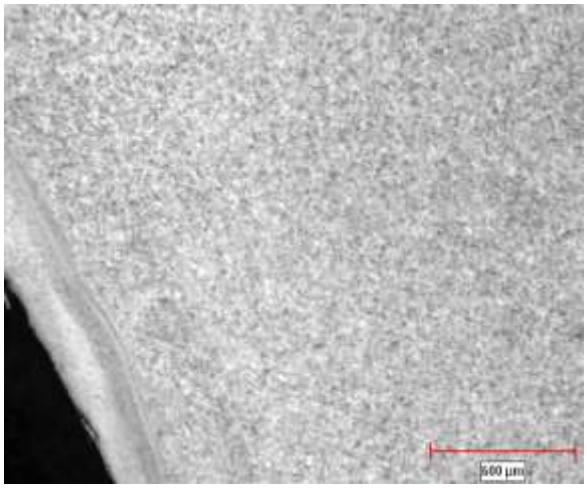

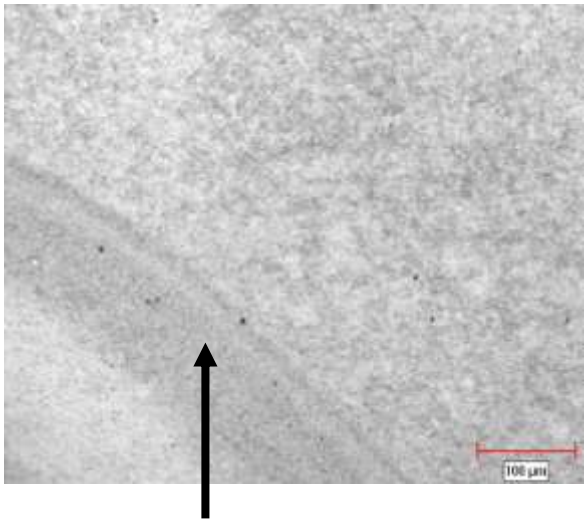

TEMPERED AT 425^{O}C FOR 1 HOUR
IMPACTED AT 44.4 kg.m/s
AFTER 30 MINUTES ANNEALING AT 650 ^{O}C
TRANSFORMED BAND
85µm
344HV
SURROUNDING MATERIAL
347HV

Figure 4.52: Steel Sample C (a) after impact (b) after 0.5 hrs post-impact annealing at 650^{O}C

c) SAMPLE "C" AFTER 2 HOURS ANNEALING AT 650 ^{O}C

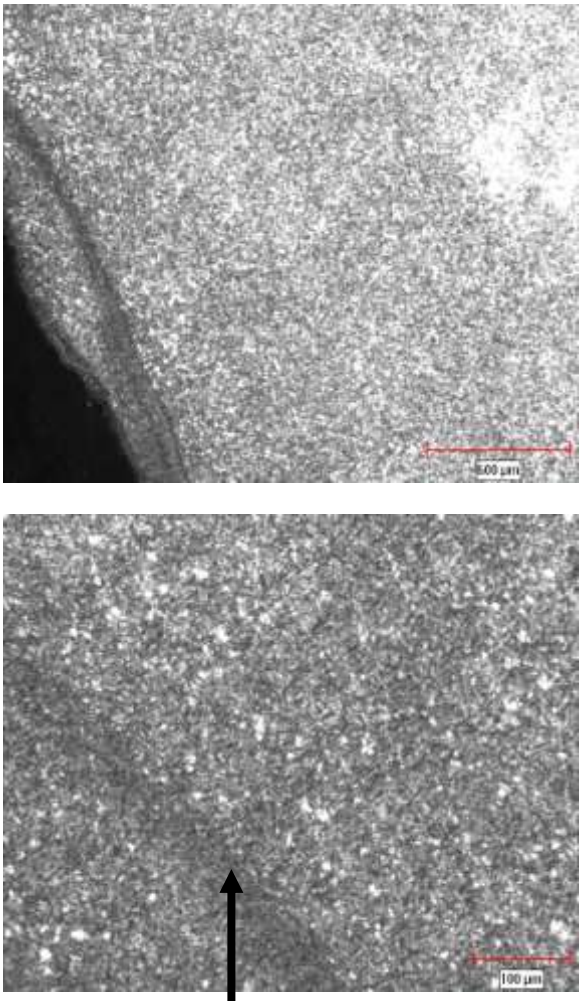

TEMPERED AT 425^{O}C FOR 1 HOUR
IMPACTED AT 44.4 kg.m/s
AFTER 2 HOURS ANNEALING AT 650 ^{O}C
TRANSFORMED BAND
55µm
307HV
SURROUNDING MATERIAL
307HV

Figure 4.52: (c) after 2 hrs post-impact annealing at 650^{O}C

The thickness of the transformed shear band in sample "A" decreased from 28 μm to 25 μm after the post impact annealing at 350 ^{O}C for two hours as shown on table 4.14. The transformed shear band etched white at both lower and higher magnifications on the optical microscope, which can be seen on, figures 4.50 (a) and 4.50 (b). Nevertheless, at higher magnifications, the brightness of the white transformed shear band reduced due to the development of new materials which resembled the surrounding impacted material as shown in figures 4.50 (b). The hardness of both the transformed shear band and the surrounding impacted material increased after the post impact annealing at 350 ^{O}C for two hours as shown in figure 4.53.

Thickness of the transformed shear band in the steel sample "B" in this group decreased from 29 μm to 25 μm after post impact annealing at 450 ^{O}C for two hours. The transformed shear band etched dull black at lower magnifications and etched as a black band at higher magnifications on the microscope, which can be seen in figure 4.51 (a) and (b). New materials resembling that of the surrounding materials developed in the shear band after the two hours post impact annealing as seen on figure 4.51 (b). The hardness of the transformed shear band reduced as that of the surrounding material increased.

The thickness of the shear band in the sample "C" after thirty minutes post impact annealing at 650 ^{O}C decreased from 130 μm to 85 μm. The white etching transformed shear band appeared as a black band both at lower and higher magnifications with new materials resembling that of the surrounding impacted material growing in the shear band as shown in figure 4.52. There was a significant reduction in the hardness of the transformed shear band from 759 HV to 344 HV after the 30 minutes post impact annealing at 650 ^{O}C. After 2 hours post impact annealing at 650 ^{O}C, the thickness of the black band decreased. The hardness also reduced further to 307 HV. The hardness of the surrounding bulk material reduced appreciably such that after the 2 hours post

impact annealing at 650 ^{O}C, the shear band and the surrounding material had comparable hardness as shown in figure 4.53. The black band had a hardness of 307 HV and the surrounding material was 307 HV after two hours annealing at 650 ^{O}C .The shear band changed to a black band with the early white grains replaced by new materials resembling the surrounding bulk material as shown in figure 4.52 (c).

Figure 4.53 is a summary of the hardness distribution in the shear bands compared to the surrounding bulk material during the post impact annealing processes of samples tempered at 425 ^{O}C before impact at 44.4 kg.m/s.

.

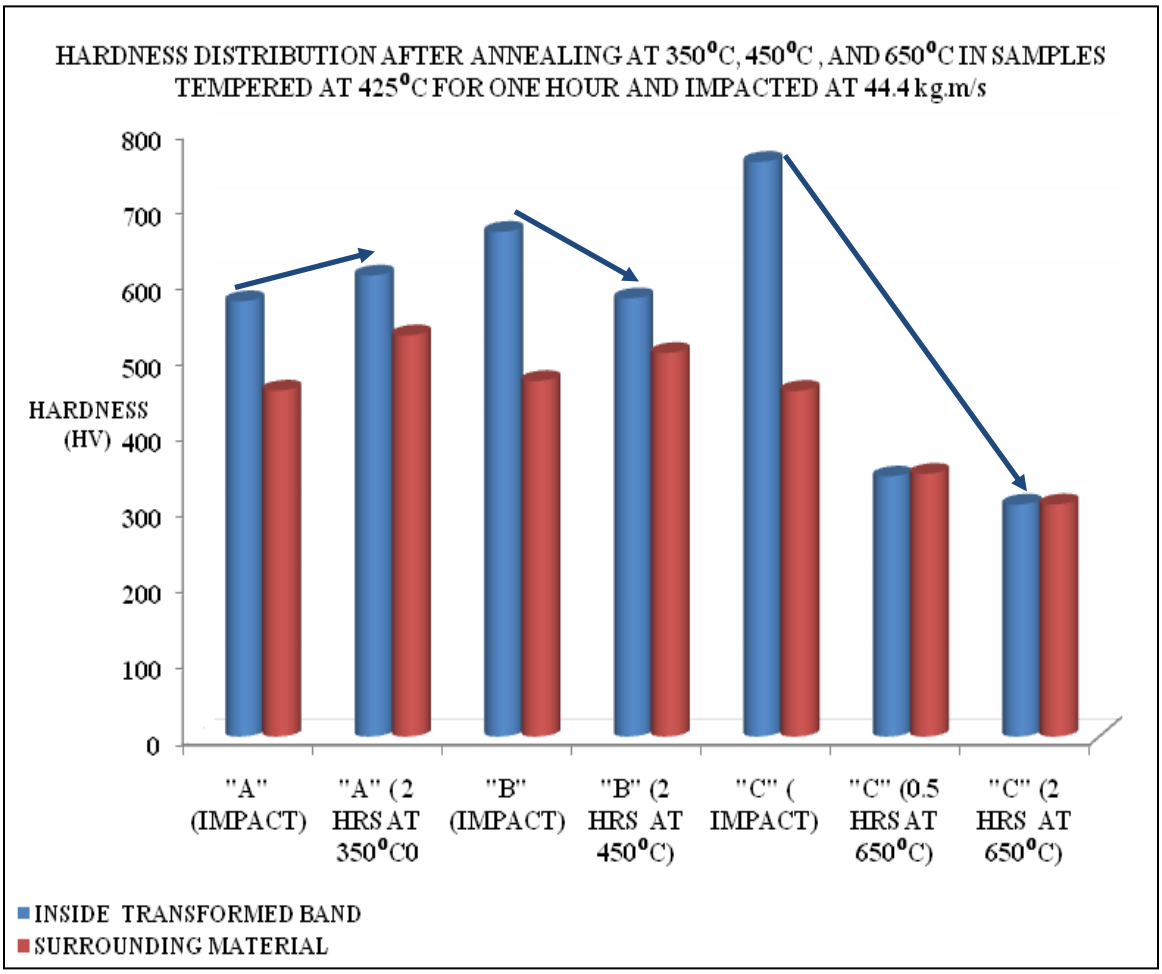

Figure 4.53: Hardness of shear bands and surrounding materials after impact and post-impact annealing

(4.3.3) POST IMPACT ANNEALING OF SAMPLES TEMPERED AT 620^{O}C FOR TWO HOURS AND IMPACTED AT 50.0 kg.m/s

The steel samples that were tempered at 620^{O}C before impact were annealed at 350^{O}C, 450 ^{O}C, 550, 650, 750 and 850 ^{O}C after their impact. The samples, after austenitizing at 855 ^{O}C, were tempered at 620^{O}C for two hours, and impacted at 50.0 kg.m/s and subsequently annealed.

Table 4.15 is a summary of the average widths and hardness of the shear bands and the average hardness of the surrounding impacted material during the post impact annealing of the steel samples tempered at 620^{O}C for two hours and impacted at 50.0 kg.m/s. The table gives the width and hardness of the shear bands after impact and post-impact annealing. The hardness of the surrounding material after impact and after post impact annealing is also given in the table.

Figures 4.54 to 4.59 are the optical micrographs of the steel samples tempered at 620^{O}C, impacted at 50.0 kg.m/s and annealed after impact. Samples A, B, C, D, E and F were annealed at 350^{O}C, 450 ^{O}C, 550 ^{O}C, 650 ^{O}C, 750 ^{O}C and 850 ^{O}C respectively after impact. All the three samples were tempered at 620^{O}C for two hours and impacted at 50.0 kg.m/s.

Figure 4.54 (a) shows a transformed shear band in sample A after impact, (b) shows the transformed shear band after two hours post-impact annealing at 350 ^{O}C and (c) shows the shear band after 4 hours post-impact annealing at 350 ^{O}C.

Figure 4.55 (a) shows a transformed shear band in sample B after impact, (b) shows the transformed shear band after two hours post-impact annealing at 450 ^{O}C and (c) shows the shear band after 4 hours post-impact annealing at 450 ^{O}C.

Figure 4.56 (a) shows a transformed shear band in sample C after impact, (b) shows the transformed shear band after two hours post-impact annealing at 550 ^{O}C and (c) shows the shear band after 4 hours post-impact annealing at 550 ^{O}C.

Figure 4.57 (a) shows a transformed shear band in sample D after impact, (b) shows the transformed shear band after half an hour post-impact annealing at 650 ^{O}C and (c) shows the shear band after 2 hours post-impact annealing at 650 ^{O}C.

Figure 4.58 (a) shows a transformed shear band in sample E after impact, (b) shows the transformed shear band after half an hour post-impact annealing at 750 ^{O}C and (c) shows the shear band after 1.5 hours post-impact annealing at 750 ^{O}C.

Figure 4.59 (a) shows a transformed shear band in sample F after impact and (b) shows the transformed shear band after half an hour post-impact annealing at 850 ^{O}C.

Table 4.15: Variations in width and hardness of shear bands for samples tempered at $620^{O}C$

SAMPLES	THICKNESS OF TRANSFORMED SHEAR BANDS (μm)	HARDNESS OF TRANSFORMED SHEAR BANDS (HV)	HARDNESS OF SURROUNDING MATERIAL (HV)
"A" AFTER IMPACT	70	366	316
"A" AFTER 2 HRS ANNEALING AT $350^{0}C$	28	499	403
"A" AFTER 4 HRS ANNEALING AT $350^{0}C$	29	539	416
"B" AFTER IMPACT	66	411	314
"B" AFTER 2 HRS ANNEALING AT $450^{0}C$	48	478	374
"B" AFTER 4 HRS ANNEALING AT $450^{0}C$	43	466	388

"C" AFTER IMPACT	73	452	308
"C" AFTER 2 HRS ANNEALING AT 550^0C	N/A	409	361
"C" AFTER 4 HRS ANNEALING AT 550^0C	67	387	370
"D" AFTER IMPACT	69	433	329
"D" AFTER 30 MINUTES ANNEALING AT 650^0C	70	288	320
"D" AFTER 2 HRS ANNEALING AT 650^0C	69	244	295
"E" AFTER IMPACT	75	524	298
"E" AFTER 30 MINUTES ANNEALING AT 750^0C	48	305	373

"E" AFTER 1.5 HRS ANNEALING AT 750^{0}C	N/A	387	450
"F" AFTER IMPACT	105	477	298
"F" AFTER 30 MINUTES ANNEALING AT 850^{0}C	N/A	313	313

a) SAMPLE "A" AFTER IMPACT

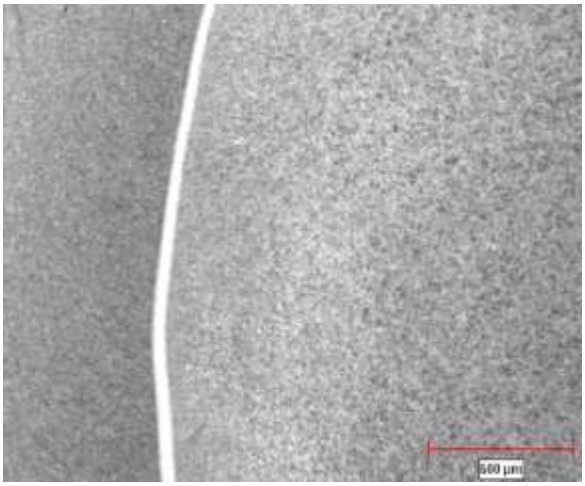

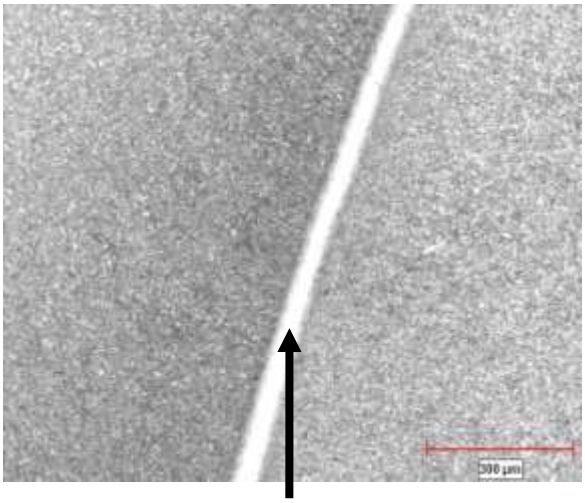

TEMPERED AT 620^{O}C FOR 2 HOURS
IMPACTED AT 50.0 kg.m/s
TRANSFORMED BAND
70µm
366HV
SURROUNDING MATERIAL
316HV

b) SAMPLE "A" AFTER 2 HRS ANNEALING AT 350 ^{O}C

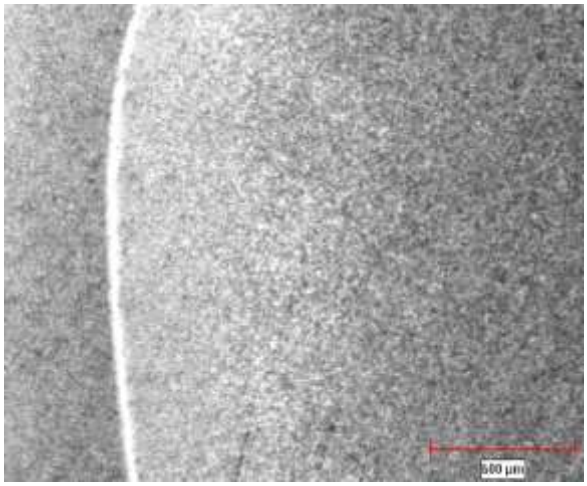

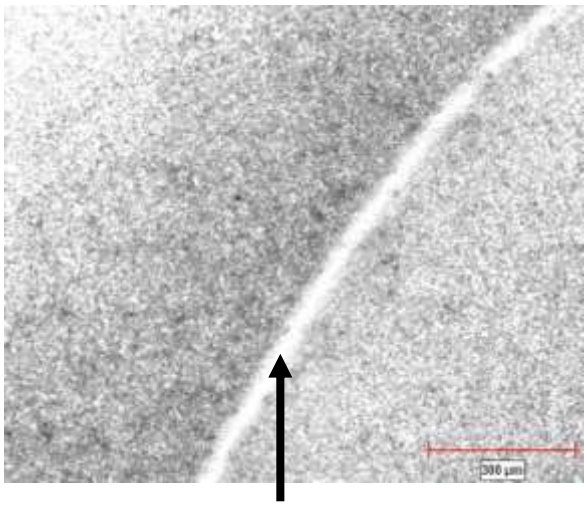

TEMPERED AT 620^{O}C FOR 2 HOURS
IMPACTED AT 50.0 kg.m/s
AFTER 2 HOURS ANNEALING AT 350 ^{O}C
TRANSFORMED BAND
28µm
499HV
SURROUNDING MATERIAL
403HV

Figure 4.54: Steel Sample A (a) after impact (b) after 2 hrs post-impact annealing at 350^{O}C

c) SAMPLE "A" AFTER 4 HOURS ANNEALING AT 350 ^{O}C

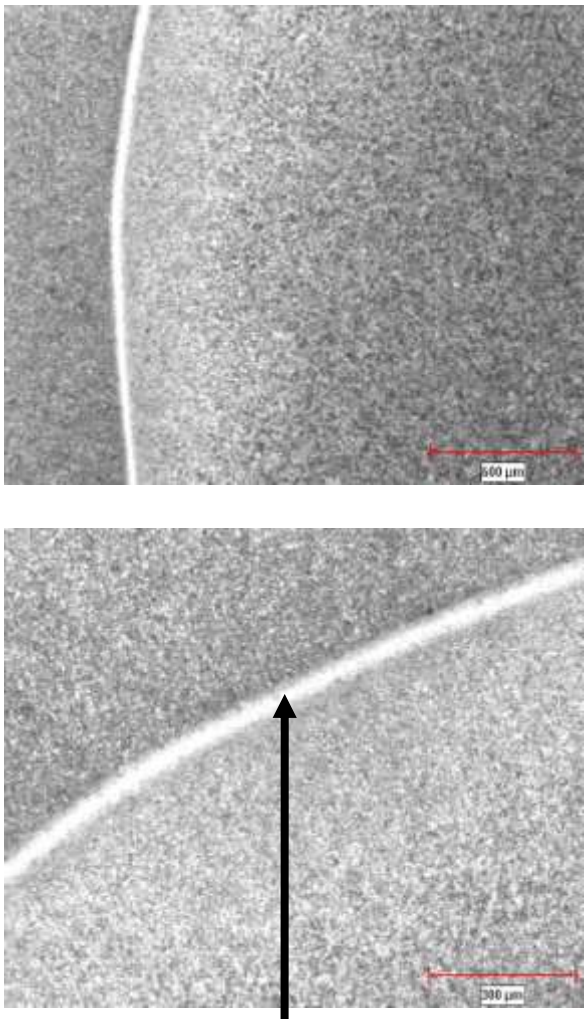

Figure 4.54: (c) after 4 hrs post-impact annealing at 350^{O}C

a) SAMPLE"B" AFTER IMPACT

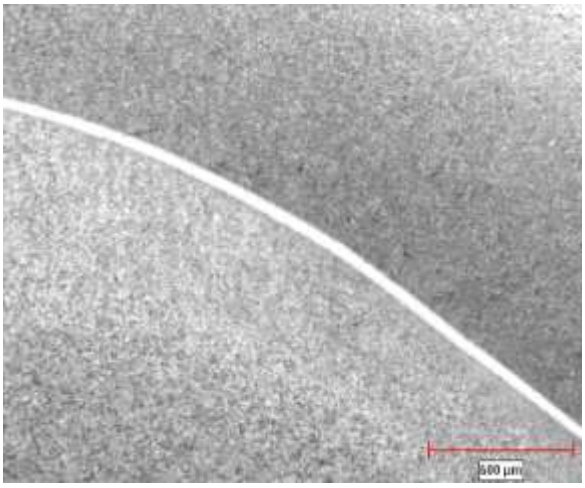

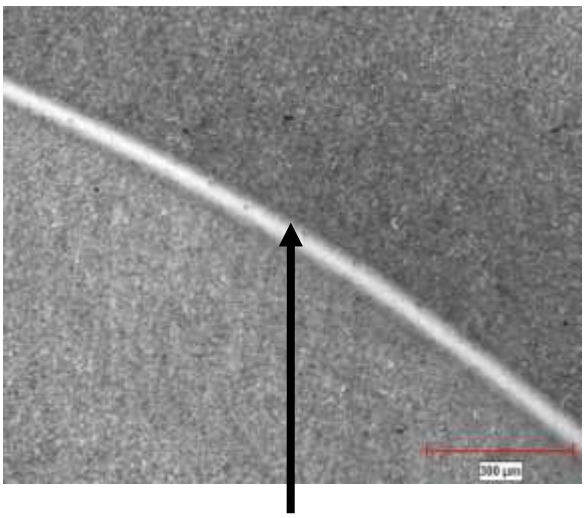

TEMPERED AT 620^{O}C FOR 2 HOURS
IMPACTED AT 50.0 kg.m/s
TRANSFORMED BAND
66µm
411HV
SURROUNDING MATERIAL
314HV

b)SAMPLE "B" AFTER 2 HOURS ANNEALING AT 450 ^{O}C

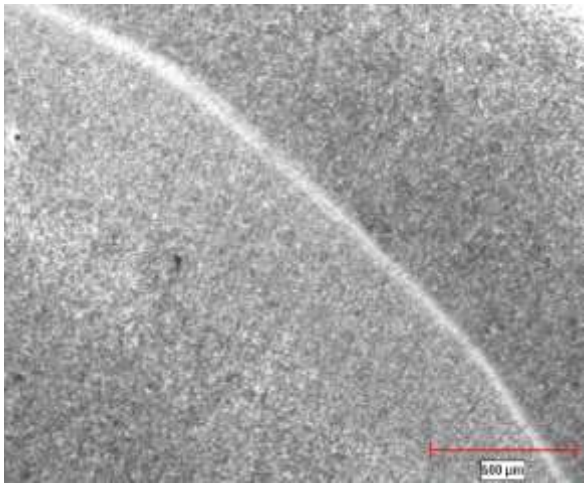

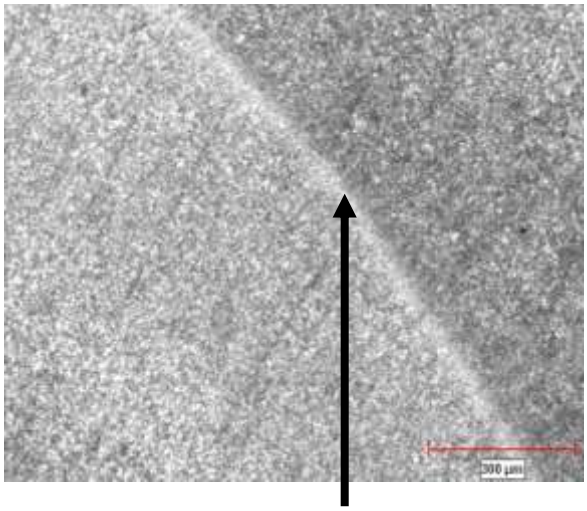

TEMPERED AT 620^{O}C FOR 2 HOURS
IMPACTED AT 50.0 kg.m/s
AFTER 2 HOURS ANNEALING AT 450 ^{O}C
TRANSFORMED BAND
48µm
478HV
SURROUNDING MATERIAL
374HV

Figure 4.55: Steel Sample B (a) after impact (b) after 2 hrs post-impact annealing at 450^{O}C

c) SAMPLE "B" AFTER 4 HOURS ANNEALING AT 450 ^{O}C

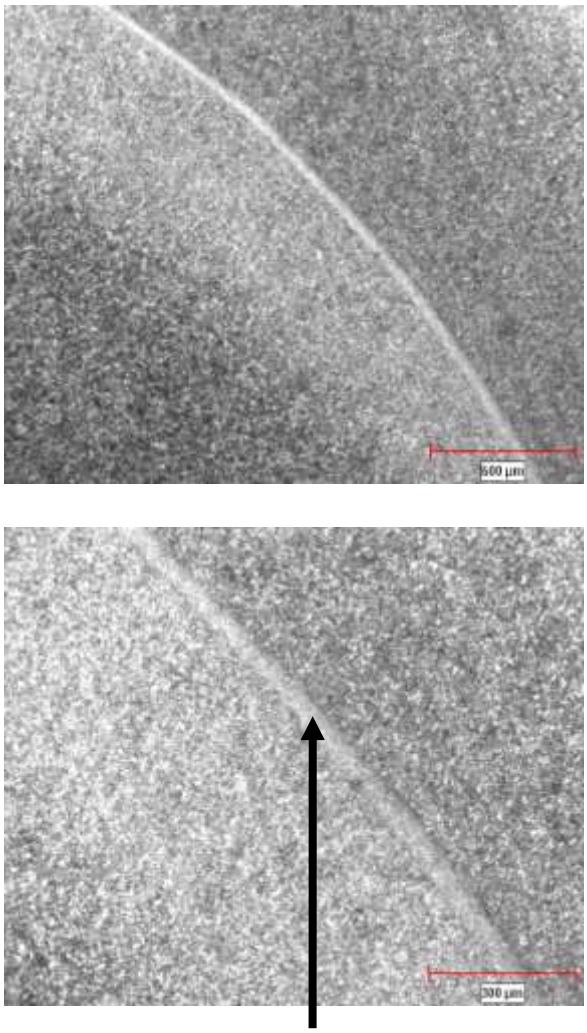

Figure 4.55: (c) after 4 hrs post-impact annealing at 450^{O}C

a) SAMPLE "C" AFTER IMPACT

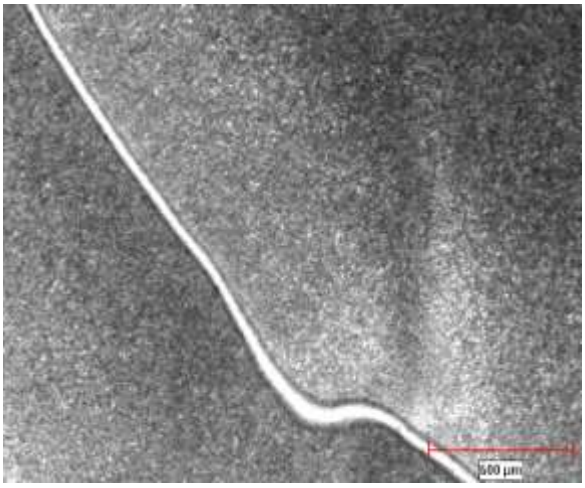

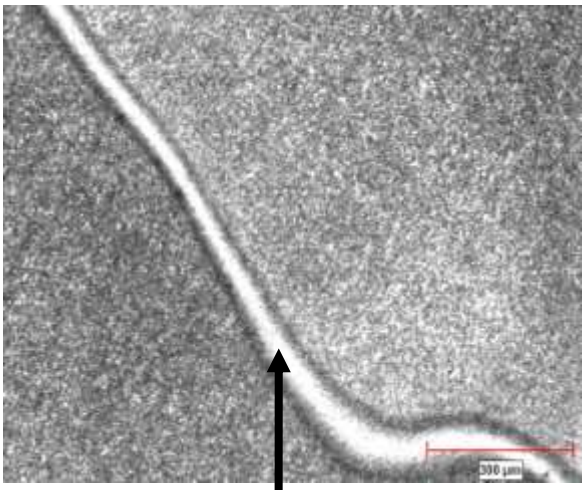

(1)TEMPERED AT 620^{O}C FOR 2 HOURS IMPACTED AT 50.0 kg.m/s
TRANSFORMED BAND
73µm
452HV
(2) SURROUNDING MATERIAL
308HV

b) SAMPLE "C" AFTER 2 HOURS ANNEALING AT 550 ^{O}C

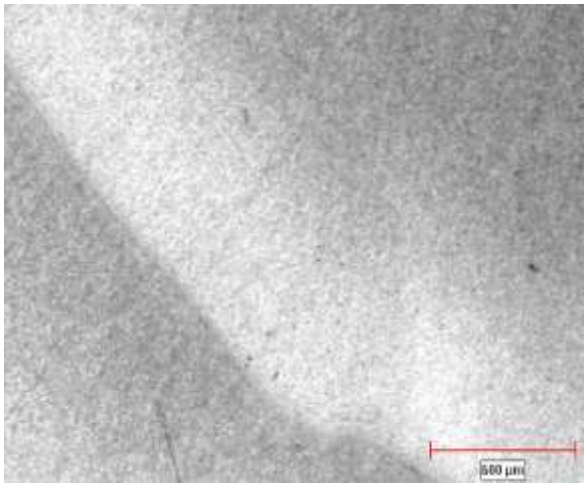

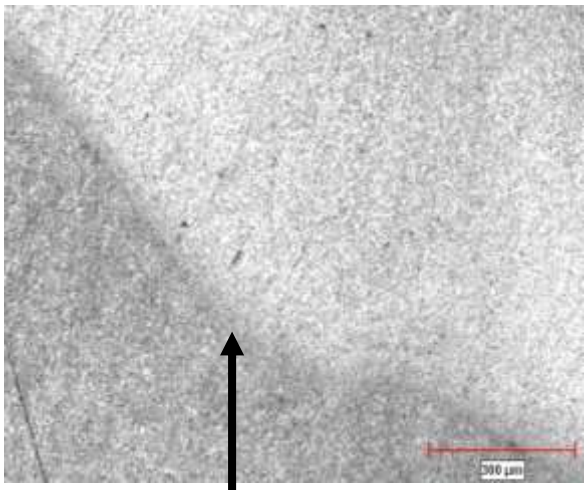

(1)TEMPERED AT 620^{O}C FOR 2 HOURS IMPACTED AT 50.0 kg.m/s
AFTER 2 HOURS ANNEALING AT 550 ^{O}C
TRANSFORMED BAND
409HV
(2) SURROUNDING MATERIAL
361HV

Figure 4.56: Steel Sample C (a) after impact (b) after 2 hrs post-impact annealing at 550^{O}C

c) SAMPLE "C" AFTER 4 HOURS ANNEALING AT 550 ^{O}C

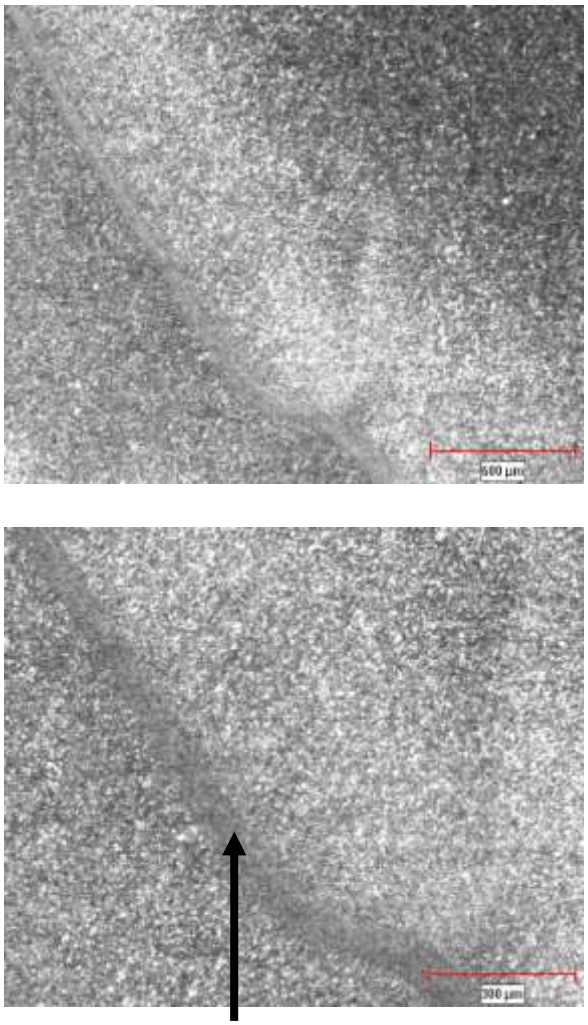

TEMPERED AT 620^{O}C FOR 2 HOURS
IMPACTED AT 50.0 kg.m/s
AFTER 4 HOURS ANNEALING AT 550 ^{O}C
TRANSFORMED BAND
67µm
387HV
SURROUNDING MATERIAL
370.4HV

Figure 4.56: (c) after 4 hrs post-impact annealing at 550^{O}C

a) SAMPLE "D" AFTER IMPACT

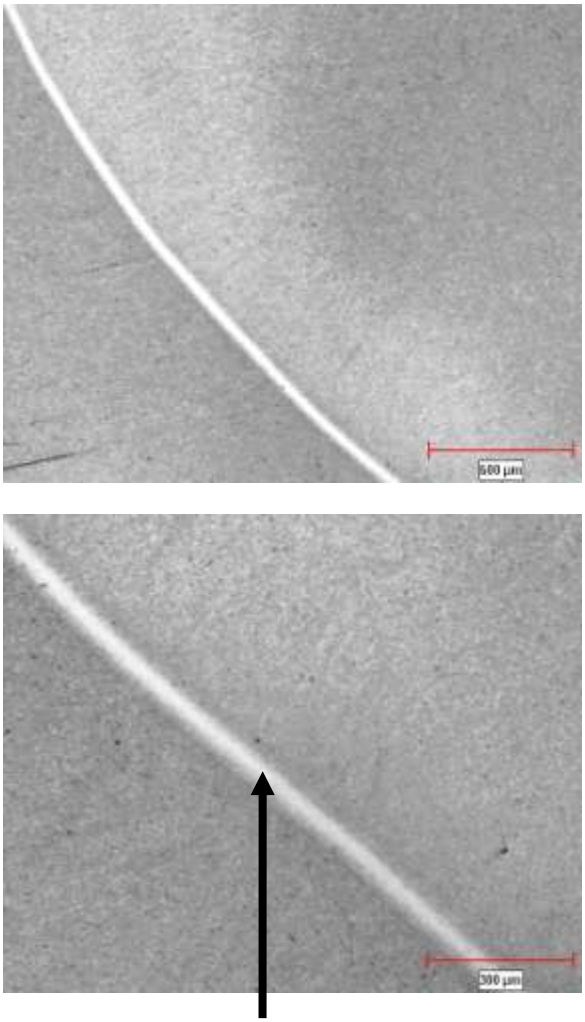

TEMPERED AT 620^{O}C FOR 2 HOURS
IMPACTED AT 50.0 kg.m/s
TRANSFORMED BAND
69µm
433HV
SURROUNDING MATERIAL
329HV

b) SAMPLE "D" AFTER 0.5 HOURS ANNEALING AT 650 ^{O}C

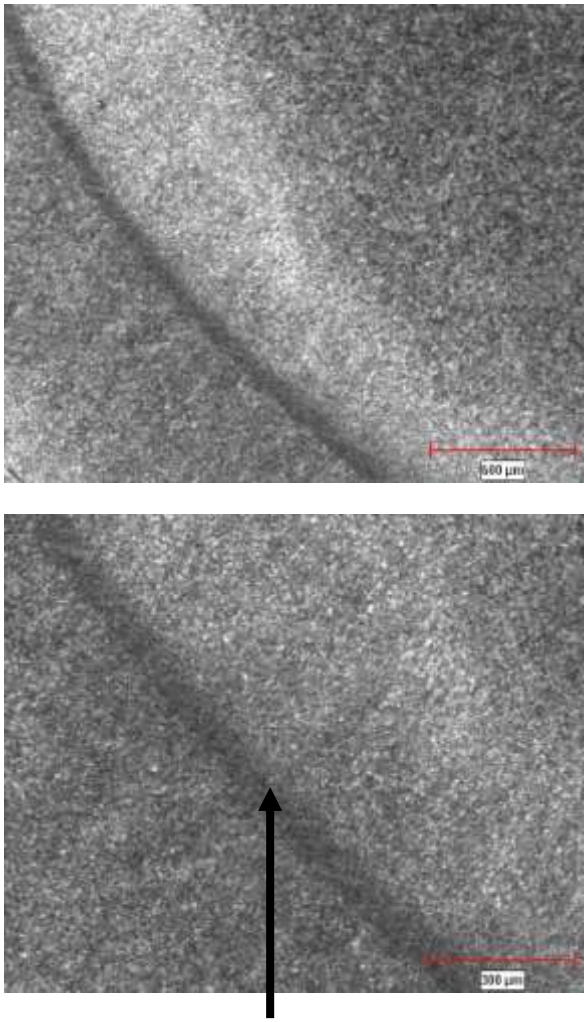

TEMPERED AT 620^{O}C FOR 2 HOURS
IMPACTED AT 50.0 kg.m/s
AFTER 0.5 HURS ANNEALING AT 650 ^{O}C
TRANSFORMED BAND
70µm
288HV
SURROUNDING MATERIAL
320HV

Figure 4.57: Steel Sample D (a) after impact (b) after 0.5 hrs post-impact annealing at 650^{O}C

c) SAMPLE "D" AFTER 2 HOURS ANNEALING AT 650 ^{O}C

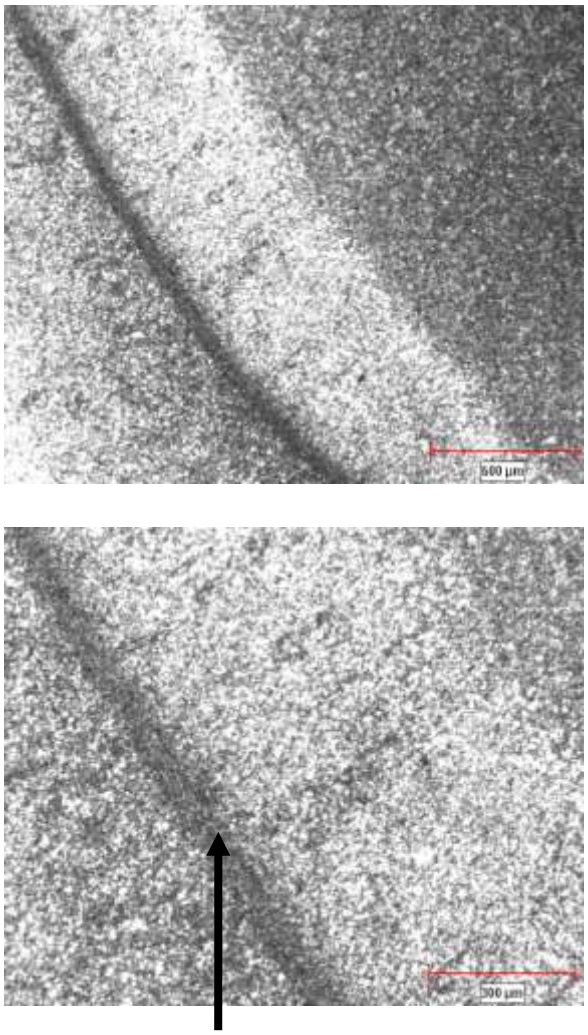

Figure 4.57: (c) after 2 hrs post-impact annealing at 650^{O}C

a) SAMPLE "E" AFTER IMPACT

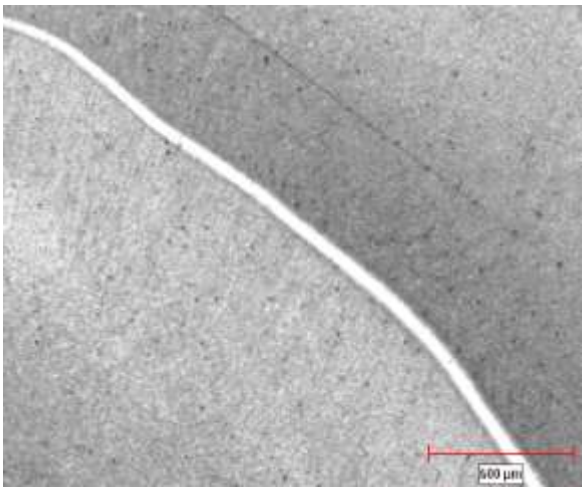

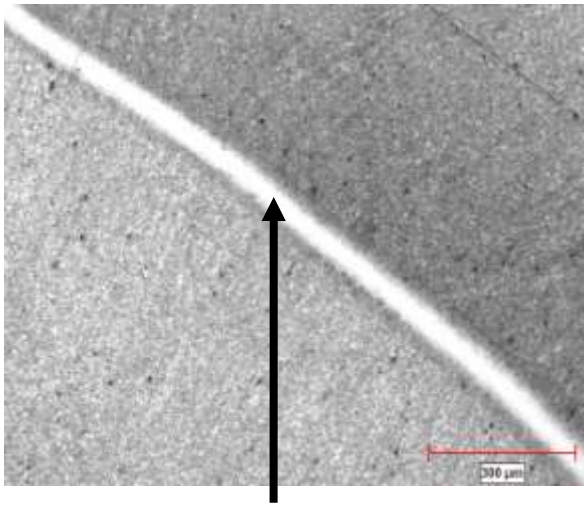

TEMPERED AT 620^{O}C FOR 2 HOURS
IMPACTED AT 50.0 kg.m/s
TRANSFORMED BAND
75µm
524HV
SURROUNDING MATERIAL
298HV

b) SAMPLE"E" AFTER 0.5 HOURS POST IMPACT ANNEALING AT 750^{O}C

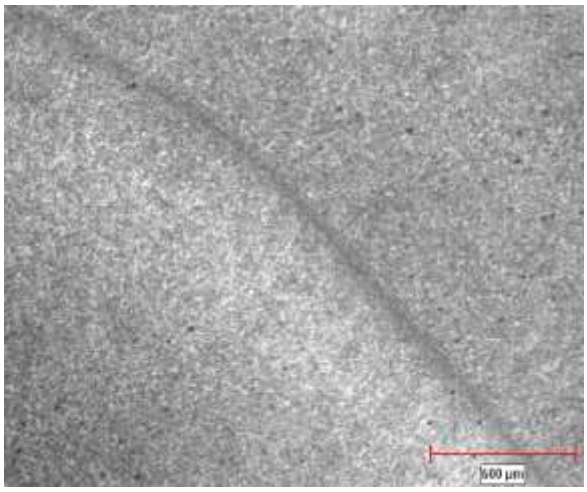

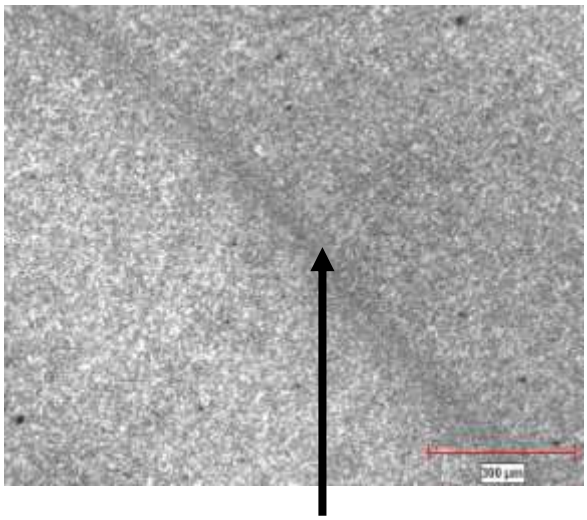

TEMPERED AT 620^{O}C FOR 2 HOURS
IMPACTED AT 50.0 kg.m/s
AFTER 30 MINUTES ANNEALING AT 750 ^{O}C
TRANSFORMED BAND
48µm
305HV
SURROUNDING MATERIAL
373HV

Figure 4.58: Steel Sample (a) after impact (b) after 0.5 hrs post-impact annealing at 750^{O}C

c) SAMPLE "E" AFTER 1.5 HOURS ANNEALING AT 750 ^{O}C

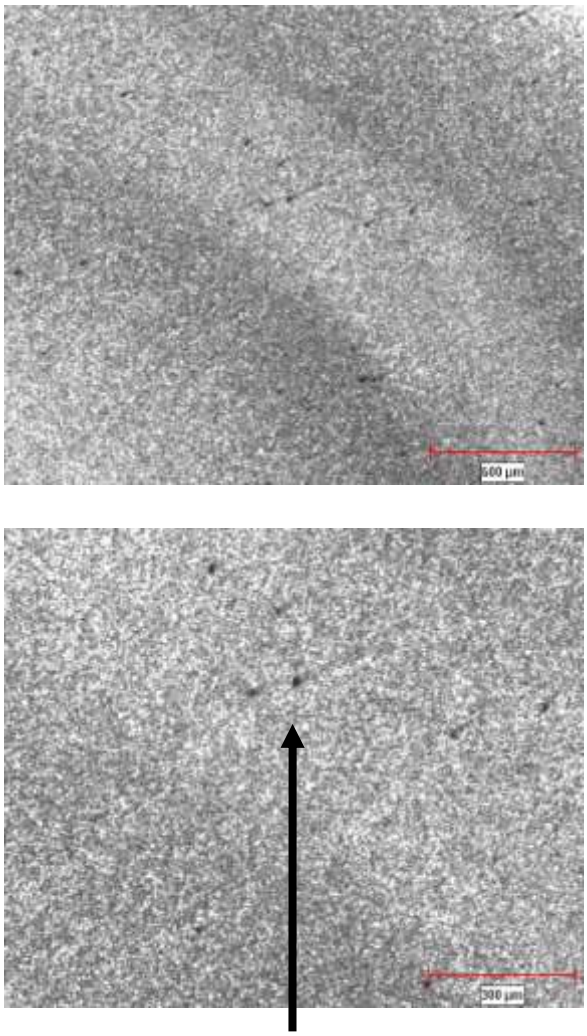

TEMPERED AT 620^{O}C FOR 2 HOURS
IMPACTED AT 50.0 kg.m/s
AFTER 1.5 HRS ANNEALING AT 750 ^{O}C
TRANSFORMED BAND
387HV
SURROUNDING MATERIAL
450HV

Figure 4.58: (c) after 1.5 hrs post-impact annealing at 750^{O}C

a) SAMPLE "F" AFTER IMPACT

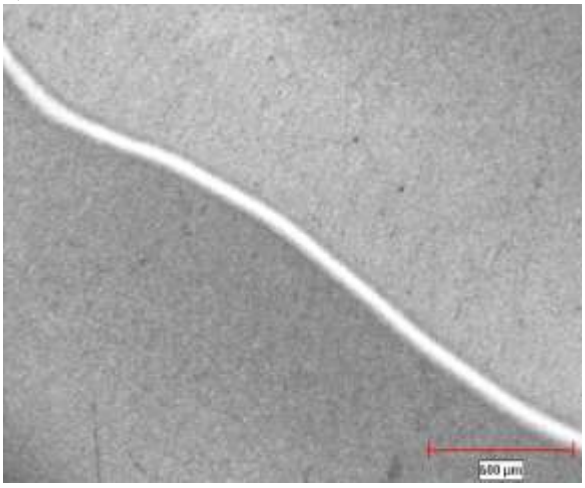

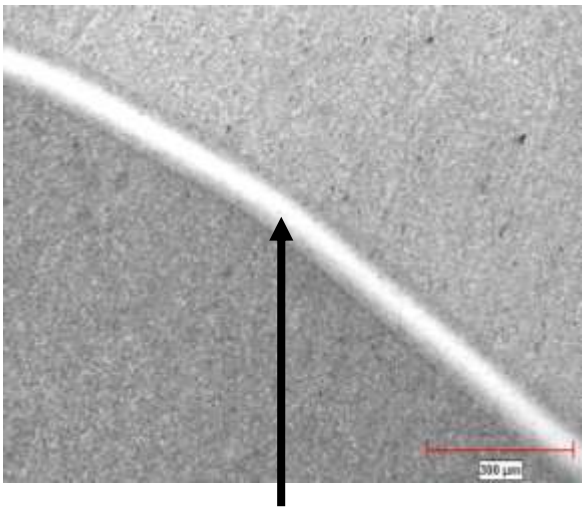

TEMPERED AT 620^{O}C FOR 2 HOURS
IMPACTED AT 50.0 kg.m/s
TRANSFORMED BAND
105µm
477HV
SURROUNDING MATERIAL
298HV

b) SAMPLE "F" AFTER 0.5 HOURS ANNEALING AT 850 ^{O}C

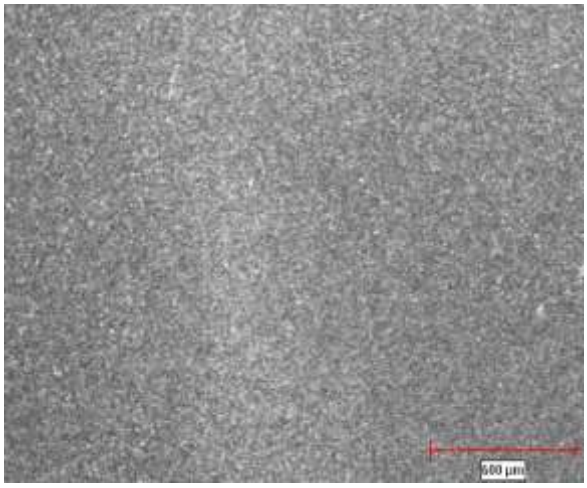

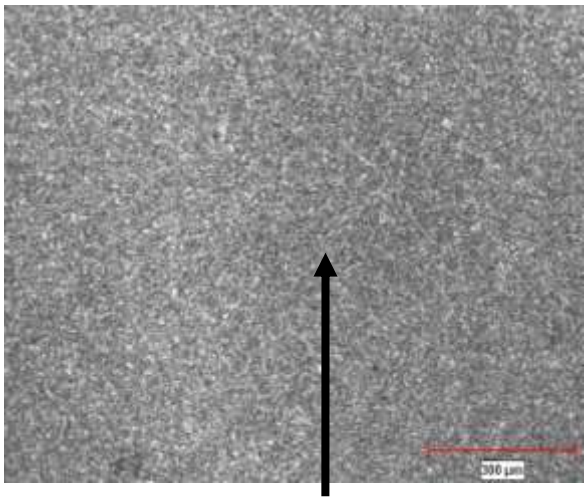

TEMPERED AT 620^{O}C FOR 2 HOURS
IMPACTED AT 50.0 kg.m/s
AFTER 0.5 HOURS ANNEALING AT 850 ^{O}C
TRANSFORMED BAND
313HV
SURROUNDING MATERIAL
313HV

Figure 4.59: Steel Sample F (a) after impact (b) after 0.5 hrs post-impact annealing at 850^{O}C

The thickness of the transformed shear band in sample "A", tempered at 620^{O}C for two hours

and impacted at 50.0 kg.m/s reduced from 70μm to 28μm after post impact annealing at 350 ^{O}C for two hours as shown on table 4.15. After four hours of post impact annealing at 350 ^{O}C, there was no additional reduction in thickness of the shear band. After the two hours and four hours post impact annealing at 350 ^{O}C, the shear band etched white as shown on figures 4.54 (b) and (c). The hardness of the shear band and that of the surrounding material increased after the two hours post impact annealing at 350 ^{O}C. The hardness of the transformed shear band increased from 366HV to 499HV at the same time as the hardness of the surrounding material also increased from 316HV to 403HV. The hardness of the shear band and the surrounding material continued to increase after four hours annealing at 350 ^{O}C as shown in figure 4.60. This means that the adiabatic shear bands in the impacted steel samples could not be eliminated by annealing at 350 ^{O}C, no matter the duration of the annealing at this temperature.

The thickness of the shear band in sample "B" decreased after post impact annealing at 450 ^{O}C as shown on table 4.15. The shear band etched dull white and at higher magnifications, new material akin to the surrounding material was observed nucleated and growing inside the shear band as shown on figures 4.55 (b) and (c). After two hours post impact annealing, the hardness in the shear band and the surrounding material increased. However, after four hours post impact annealing at 450 ^{O}C, the hardness of the shear band decreased as shown on figure 4.60.

The transformed adiabatic shear band in sample "C" could be seen fading after two hours post impact annealing at 550 ^{O}C as shown by figure 4.56 (b). The shear band became diffused and it resembled the bulk material. The hardness decreased and the shear band etched as a black band beneath the optical microscope.

Thirty minutes post impact annealing of sample "D" at 650 ^{O}C reduced the hardness of the shear band significantly as shown on table 4.15. The shear band etched as a black band and new material that resembled the surrounding bulk material developed in the shear band as can be seen in figure 4.57 (b) and (c).

In the post impact annealing of all the samples at 350 ^{O}C, 450 ^{O}C, 550 ^{O}C and 650 ^{O}C for periods ranging from 30 minutes to 4 hours the shear bands decreased in thickness, sometimes become a black band and at other times etch dull white. The shear bands also decreased in hardness and resembled the bulk-impacted material since new particles were observed which nucleated and grew inside them. However, a "scar" was always left in the deformed sample. The initial path of the transformed adiabatic shear band could be traced inside the deformed sample.

On the other hand, post impact annealing of the deformed samples at 750 ^{O}C and 850 ^{O}C erased the transformed adiabatic shear bands without a trace in the impacted steel samples. The hardness was reduced to that of the surrounding material and there were no "scars" left in the impacted samples as shown in figures 4.58 and 4.59. New strain-free particles developed in the shear bands and replaced all the fine strained particles in the transformed adiabatic shear bands because of recovery, recrystallization and grain growth mechanisms as shown by figures 4.58 (c) and 4.59 (b). After 30 minutes post impact annealing of sample "E" at 750 ^{O}C, the thickness of the shear band was reduced drastically as seen on table 4.15. After 1.5 hours post impact annealing, the shear band disappeared and was replaced by new particles as shown in figure 4.58 (c). There was no trace of the shear band in the sample. Thirty minutes post impact annealing of sample "F" at 850 ^{O}C erased all the shear bands. New material replaced the initial material in the shear band. There was no "scar" or trace of the transformed adiabatic shear band in the post impacted and annealed sample as shown by figure 4.59 (b).

Figures 4.60 and 4.61 are summaries of the hardness distribution in the shear bands compared to the surrounding bulk material during the post impact annealing processes of samples tempered at 620 ^{O}C for two hours before impact at 50.0 kg.m/s.

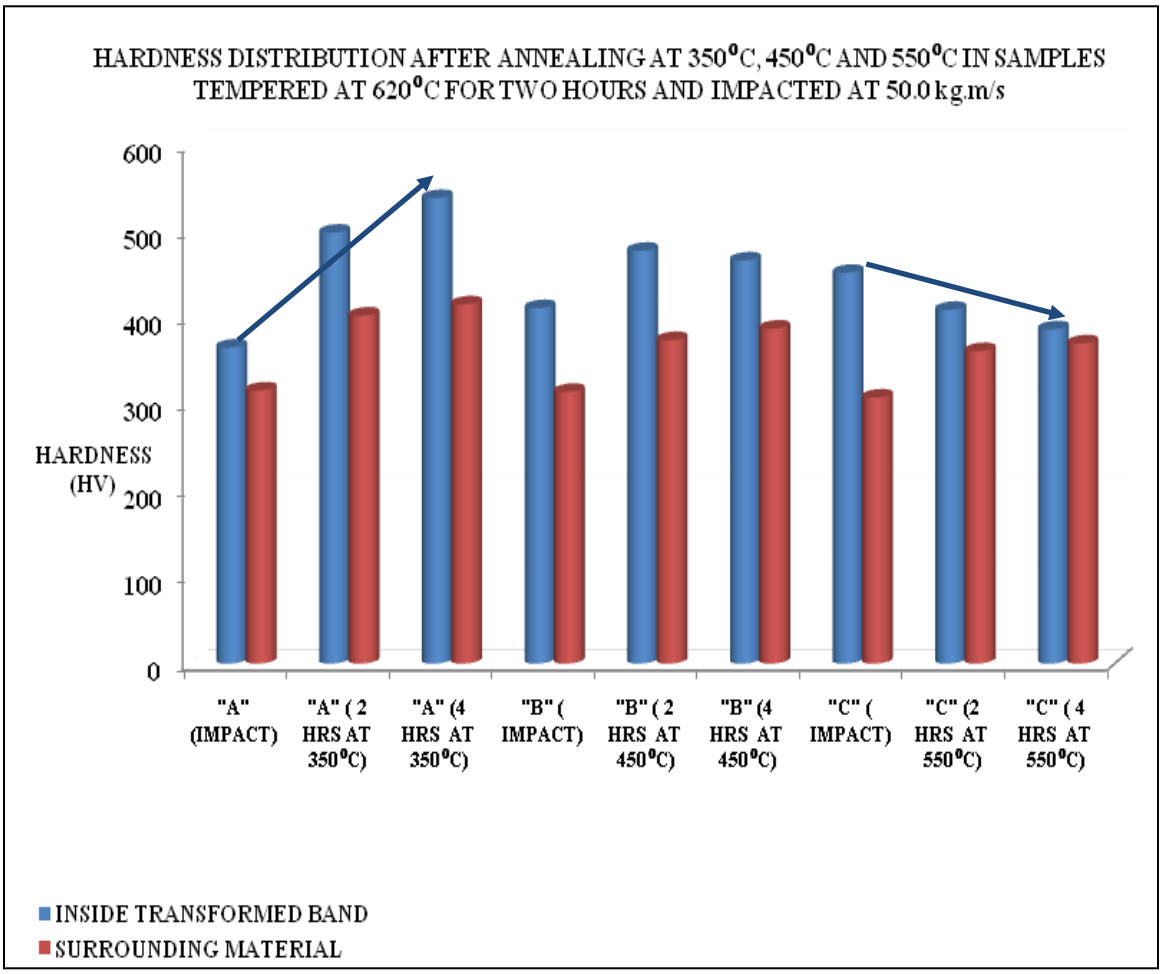

Figure 4.60: Hardness of shear bands and surrounding materials after impact and post-impact annealing

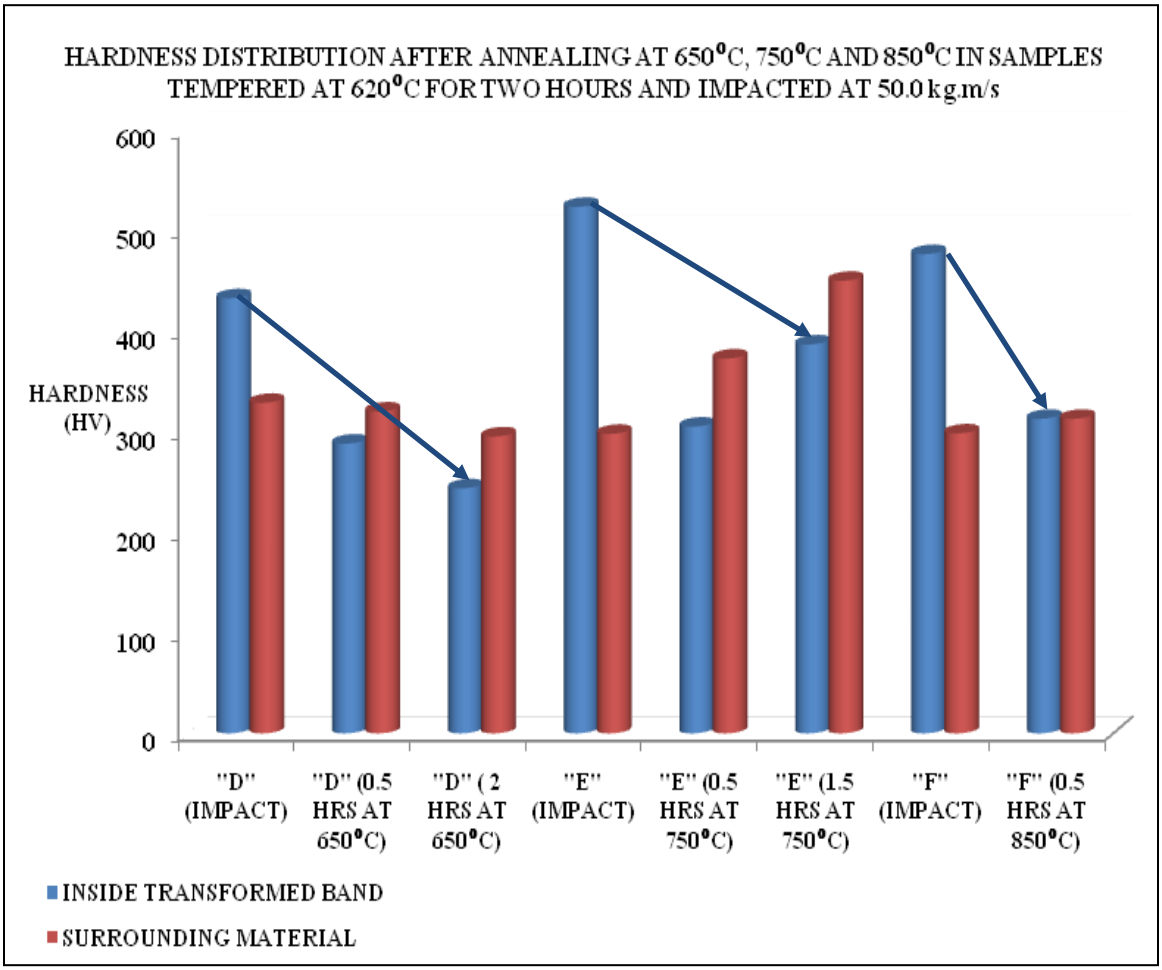

Figure 4.61: Hardness of shear bands and surrounding materials after impact and post-impact annealing

(4.3.4) TRENDS OBSERVED IN THE PROPERTIES OF THE STEEL SAMPLES DURING THE POST IMPACT ANNEALING PROCESSES

During the post impact annealing processes, it was observed that all the steel samples that were annealed at 350 ^{O}C had something in common even though they all had different properties. Post-impact annealing the steel samples at 350 ^{O}C for two hours increased the hardness of the transformed shear bands. This occurred in all the different steel samples that were annealed at this temperature. The steel samples that were annealed for four hours at this same temperature also resulted in a further increased in the hardness of the shear bands. In addition, the hardness of the surrounding bulk impacted materials also increased. In the steel sample "A", tempered at 620^{O}C for two hours and impacted at 50.0 kg.m/, the hardness of the transformed shear band increased from 366HV to 499HV even as the hardness of the surrounding material increased from 316HV to 403HV after two hours post impact annealing at 350 ^{O}C. There was further increase in hardness of the transformed shear band and the surrounding material after four hours post impact annealing at 350 ^{O}C. The hardness of the transformed shear band increased further from 499HV to 539HV whilst the hardness of the surrounding material increased further from 403HV to 416HV.

This increase in hardness of the transformed shear bands and the surrounding material when they are annealed at 350 ^{O}C can be attributed to the diffusion of carbon in the steel samples and because of insufficient recovery and recrystallization mechanisms.

Figure 4.62 shows the differences in hardness of the shear bands and the surrounding materials in the different steel samples when they were annealed at 350 ^{O}C after impact. The samples "A (315 ^{O}C)" and "A (425 ^{O}C)" are the steel samples tempered at 315 ^{O}C and 425 ^{O}C for one hour and

impacted at 44.4 kg.m/s respectively. They were annealed at 350 ^{O}C for two hours after impact. The steel sample "A (620 ^{O}C)" is the steel sample tempered at 620 ^{O}C for two hours, impacted at 50.0 kg.m/s, and was annealed at 350 ^{O}C for two hours and four hours respectively.

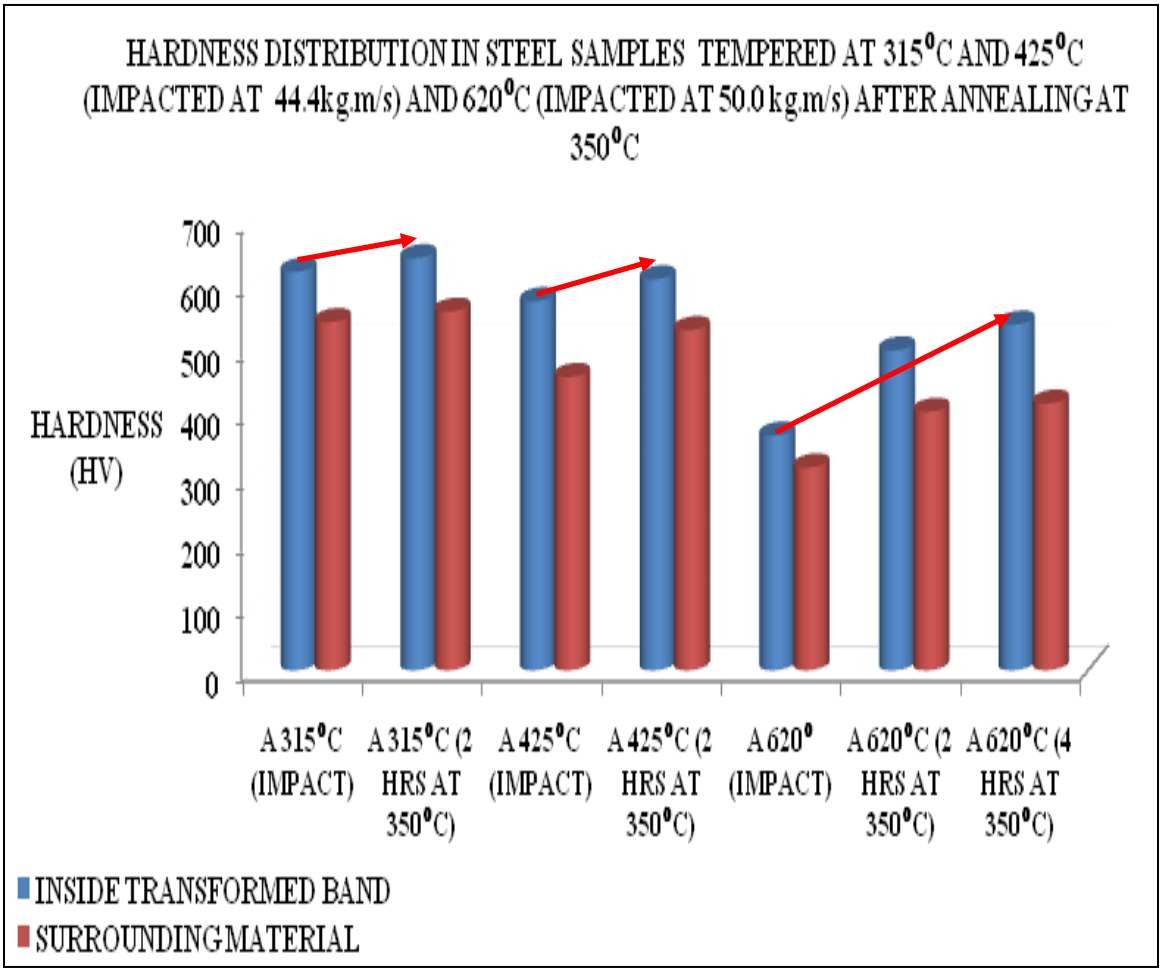

Figure 4.62: Increasing hardness during post-impact annealing

All the steel samples that were annealed at 650 ^{O}C after impact had decreasing hardness in the shear bands and the surrounding bulk impacted material. Irrespective of the duration of the annealing procedures, annealing at 650 ^{O}C resulted in a reduction in the properties of the shear bands and the surrounding bulk impacted material. New materials grew and replaced the shear bands. This new material resembled the bulk-impacted metal microstructure. The shear bands were replaced by a new microstructure that have properties correspondent to that of the surrounding material after the annealing. However, the microstructural development showed that there was a "scar" left by the shear bands in the deformed samples after the annealing procedures.

In general, during the post impact annealing procedures, the thickness of the shear bands was reduced after each annealing procedure as shown by table 4.13 to 4.15. It was observed that at lower temperatures, the shear bands thickness was reduced and there was no further reduction in thickness during any further annealing process. At higher temperatures, there was a reduction in the thickness of the shear bands and new materials were observed developed inside the shear bands.

Figure 4.63 shows the properties occurring in the shear bands and the surrounding impacted material for the different steel samples at the different testing conditions. It shows that the hardness of the shear bands and the surrounding material reduce during post-impact annealing at 650^{O}C regardless of the initial conditions before annealing.

Figure 4.64 shows the reduction in widths of the shear bands at the various temperatures during post-impact annealing.

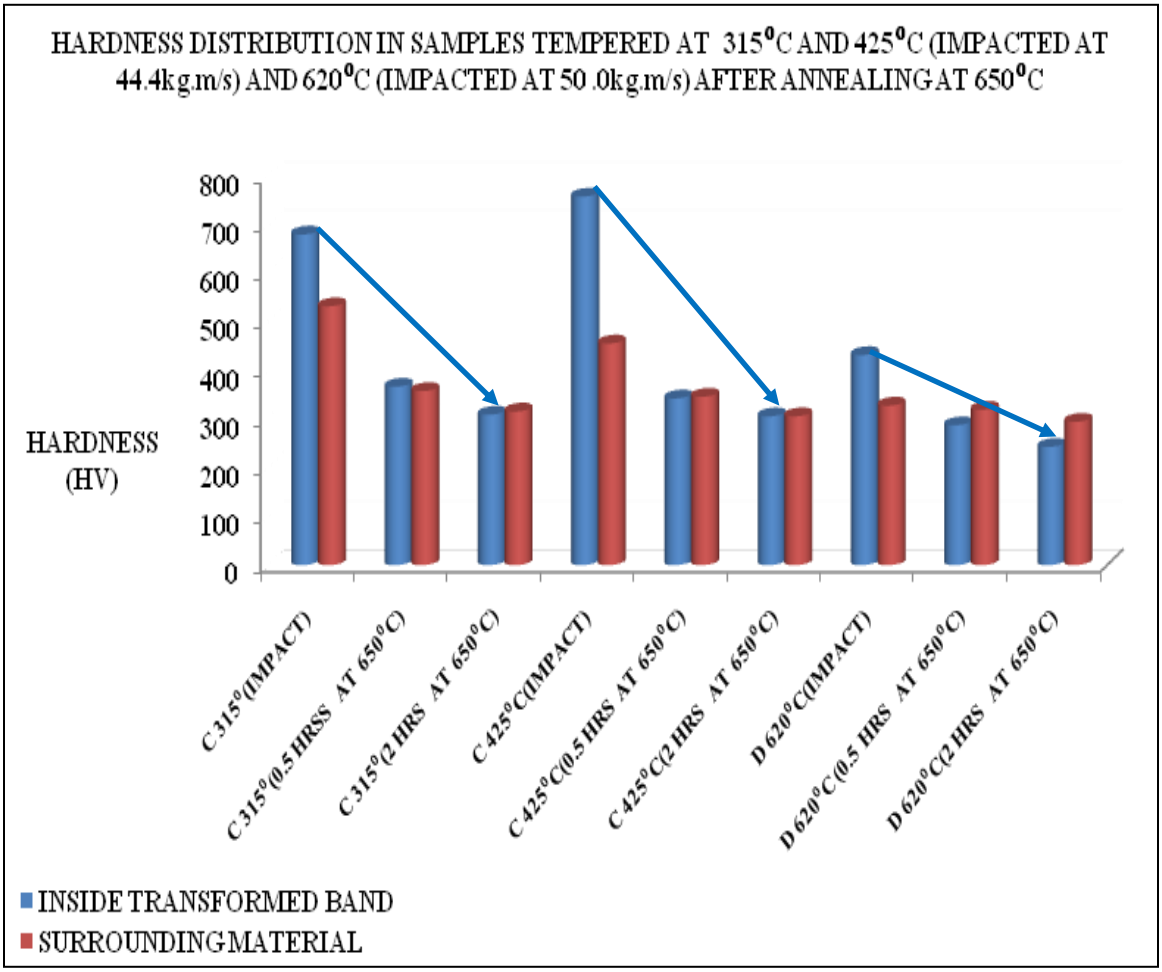

Figure 4.63: Decreasing hardness during post-impact annealing

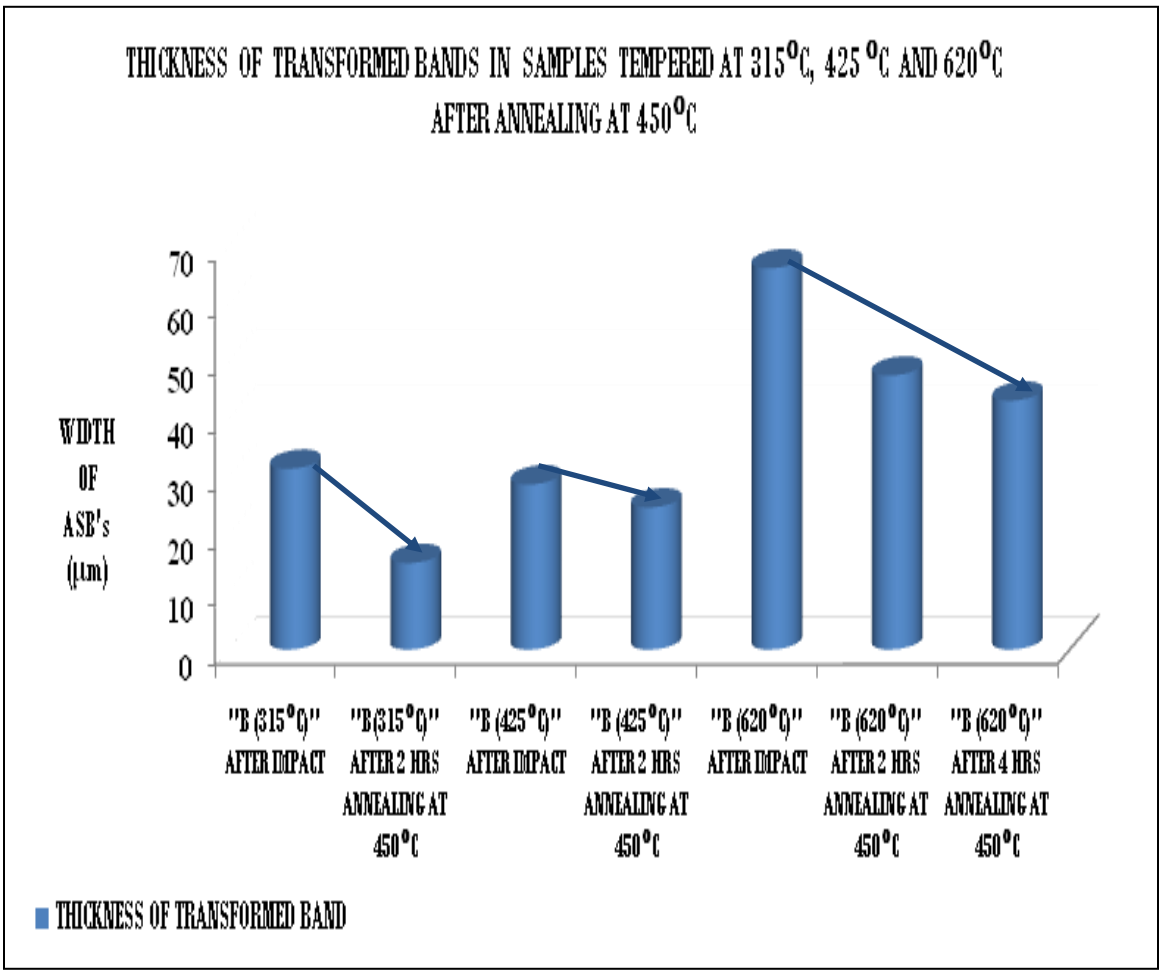

Figure 4.64: Width of shear bans during post-impact annealing

CHAPTER 5.0: DISCUSSION

(5.1)EFFECTS OF TEMPERATURE AND TIME OF TEMPERING ON THE DYNAMIC BEHAVIOR OF STEEL SAMPLES UNDER IMPACT

The mechanical properties of metals are extremely dependent on the microstructure, crystal structure and elemental composition [41 – 47]. The microstructure of martensitic steels, which includes dislocations, carbides and lath widths, depends largely on the temperature and time of tempering. Although martensitic steel samples have high strengths and hardness, they are brittle. The high strength and hardness are generally due to the lattice distortions caused by carbon atoms trapped in the octahedral sites of martensite and carbide formation during quenching [41-45, 47]. The highly distorted lattice of body-centered tetragonal martensite effectively blocks the motion of dislocations during deformation. During tempering, hardness and strength of steel decrease while ductility and toughness increase. The density of dislocations of martensitic steels also decrease with increasing temperature and increasing time of tempering [48].

At the same tempering time, samples tempered at 315^{O}C had higher strengths and hardness than those tempered at 425^{O}C. These are depicted in figures 4.17, 4.28 and 4.38. However, samples tempered at 425^{O}C had higher fracture resistance, defined as the energy absorbed without fracture during deformation, than those tempered at 315^{O}C. This is seen in table 4.1 and 4.2 where samples tempered at 425^{O}C could be deformed at higher impact momentums without fracturing compared to samples tempered at 315^{O}C that fractured at lower impact momentums. In addition, samples tempered at 620^{O}C had lowest strengths and hardness but highest fracture resistances as shown in tables 4.1 and 4.2. These results agree with the observations in [28, 41,

and 48]. During tempering of the martensitic steels, higher tempering temperatures lower the strength and hardness, increase the ductility, and fracture resistance.

Carbon atoms, dispersed in martensite, form carbide precipitates of increasing size during tempering [42]. The stages of tempering as summarized by [42, 43, 44, and 45] are:

(a) the formation of a transition carbide and the reduction of the carbon content in the martensite matrix
(b) the transformation of retained austenite to ferrite and cementite
(c) the replacement of the transition carbide and low-carbon martensite with cementite and ferrite

During the preliminary stages of tempering, carbon atoms segregate to various defects in the microstructure, martensite is converted to a low carbon martensite, and transition carbides are formed [42, 43]. The formation of transition carbides reduces the carbon content of the martensitic matrix. In the final stages of tempering, transition carbides dissolve and are replaced by cementite when the tempering temperatures are increased. Cementite is very hard and brittle. It has been reported that during tempering between 400^{O}C and 595^{O}C, carbides combine to form spheroidites [42, 43]. Spheroidites have lower surface energies and hardness as compared to the carbides. It is inferred that the steel samples tempered at 425^{O}C that were softer than the 315^{O}C tempered samples might be due to the coalescence of carbides into spheroidites in the 425^{O}C tempered samples. Cepus [28] in his study on the evolution of adiabatic shear bands, austenitized SPS-Plus steel samples at 850^{O}C, oil quenched and tempered them at 315^{O}C, 480^{O}C and 650^{O}C. He observed that as the tempering temperature increased, hardness of the steel samples decreased. Cepus studied the tempered samples using a scanning electron microscope (SEM) and observed that samples tempered at 315^{O}C had finer microstructures than samples tempered at

480^{O}C. The sizes of precipitates in the samples tempered at 480^{O}C were larger in size and more than the precipitates in the 315^{O}C tempered samples. Samples tempered at 650^{O}C had very coarse grains and very large precipitates compared to those tempered at 315^{O}C and 480^{O}C. Tempering from 595^{O}C to 704^{O}C could result in spheroidization and smaller particles could dissolve [42, 43, 45]. Thus, increasing the sizes of spheroidites could result in decrease in hardness. This could lead to a decrease in strength such that samples tempered at 620^{O}C become soft compared to the 315^{O}C and 425^{O}C tempered samples. Moreover, improvement in ductility and fracture toughness with higher tempering temperatures accounted for the higher impact momentums at which steel samples tempered at 620^{O}C were deformed without fracturing. The strength, hardness and strain-hardening exponent decrease with an increase in tempering temperature and holding time during tempering. However, higher tempering temperatures lead to higher ductility and fracture resistances. The results observed in the current study are similar to that observed by Lee and Su [41] and Bhat [49] when they studied the mechanical and microstructural properties of AISI 4340 steel under different tempering conditions.

It was observed in the current study that when the steel samples were tempered at 315^{O}C and 425^{O}C for one hour, they had improved fracture resistances than those tempered at 315^{O}C and 425^{O}C for two hours. This can be observed on tables 4.1 and 4.1 when the samples tempered at 315^{O}C and 425^{O}C for one hour were deformed at higher impact momentum values without fracturing while those tempered at 315^{O}C and 425^{O}C for two hours broke at these high impacts. These results reveal that, at these tempering temperatures 315^{O}C and 425^{O}C, the time of tempering is as significant as the tempering temperature. During heat treatment of steels, lower strength and hardness leads to higher ductility and toughness of a microstructure unless embrittlement occurs. In general, embrittlement is a reduction in the normal toughness of steel

due to a microstructural change and chemical effects during tempering. Tempered martensite embrittlement is thought to result from the combined effects of cementite precipitation on prior-austenite grain boundaries or interlath boundaries and the segregation of impurities at prior-austenite grain boundaries [42, 50, 51]. The reduced impact toughness associated with tempered martensite embrittlement is associated with three different modes of fracture that depend on the various carbon and phosphorus contents of the hardened steels. These are ductile, cleavage, and intergranular modes of fracture [42, 50, 51, 52, 53, and 54]. A general cause of tempered martensite embrittlement is the formation of carbide films from the interlath austenite after tempering. Tempering hardened carbon and low alloy steels for relatively long times or cooling slowly through the temperature 375 ^{O}C to 575 ^{O}C may lead to temper embrittlement [42, 43, 50, 51, 53, 55]. Other studies show temper embrittlement occurs in the temper range 400 ^{O}C to 600 ^{O}C. Temper embrittlement is caused by the presence of specific impurities such as manganese, Mn, and phosphorus, P, in the steel, which segregate to prior austenite grain boundaries during heat treatment. When embrittlement occurs, ductility and toughness are reduced as hardness and strength decreases. The lower fracture resistance of the samples tempered at 315$^{\mathbf{O}}$C and 425$^{\mathbf{O}}$C for two hours is attributed to the effects of embrittlement that occurs in the steels samples when they are tempered at these temperatures. It is inferred that the embrittlement occurring became severe when the samples were held longer at these temperatures.

(5.2)DYNAMIC BEHAVIOR OF QUENCH-HARDENED AND TEMPERED AISI 4340 STEEL SAMPLES DURING IMPACT

The response of a metal to external forces depends on factors that include the type of loading, temperature, strain rate and the metallurgical features of the metal [46]. In the current study, flow stress increases initially with strain at the beginning of the deformation. It reaches a maximum as the deformation continues and decrease with subsequent increase in strain. This trend was prevalent in all the impacted steel samples. According to Ludwik's equation [42, 46, 56, 57], the flow stress, σ, is related to the strain by:

$$\sigma = k\varepsilon^{n} \qquad 5.1$$

where k is the strength coefficient and n is the strain-hardening exponent. The true stress- true strain graphs for the steel samples used for the current study match closely to the Ludwik's equation above. The strength coefficient, k, and the strain-hardening exponent, n, illustrate the shape of the true stress- true strain graphs for the steel samples. It describes completely how the steel samples respond to the dynamic impacts during the deformation.

The formation of adiabatic shear bands results from strain localization during deformation. This occurs from the competition between strain hardening and adiabatic heating. Adiabatic heating, resulting in a local rise in temperature, wins over strain hardening in the latter stages of the deformation. The dislocation density in a metal increases with deformation or cold work due to dislocation multiplication or the formation of new dislocations. During the preliminary stages of the deformation, stress varies linearly with strain. After the uniform deformation stages, continuous deformation leads to a nonlinear relationship between flow stress and strain. This is the point where plastic deformation begins. As plastic flow continues, the density of dislocations

and dislocation-dislocation interactions are increased. Consequently, the average distance of separation between dislocations decreases thus positioning dislocations closer together. As a result, the motion of a dislocation is hindered by the presence of other dislocations. Additionally, the interaction of dislocations with interfaces such as grain boundaries increases. Dislocation movements are halted when they interact with grain boundaries [58]. Dislocations begin to build up at the grain boundaries and may lead to the creation of dislocation tangles. As the dislocation build up increases, a back stress develops that opposes the motion of additional dislocations. This gives rise to an increase in strength with increasing deformation known as work hardening or strain hardening. The increase in strength is a direct result of dislocation multiplication and dislocation-dislocation interactions.

Considering a given dislocation distribution, the shear flow stress, T, is related to the dislocation density, ρ, by [56]

$$T = T_{O+} \alpha G b \rho^{1/2} \qquad 5.2$$

where α is a material specific constant, G is the shear modulus, b is the Burgers vector and T_O is the flow strength in the absence of work hardening. Dislocation tangles or cell structures form at high strains after which the strengthening becomes more a function of cell size than of dislocation length. The value of the constant in the Ludwik's equation, k, indicates the level of strength of the material whilst the rate of work hardening, n, provides a measure of the ability of the material to resist localization of deformation.

Additionally, the strength of a metal is coupled with the movement of dislocations [58]. If dislocations move without restraint in the metal, the strength of the metal and the rate of work hardening will be low. On the other hand, if the movement of dislocations in the metal is

restrained, it leads to an increase in strength. Obstacles or barriers such as grain boundaries, sessile dislocations and large precipitates in the microstructure of the metal can inhibit the movement of dislocations [58]. In the present study, the steel samples tempered at 315^{O}C were found to be the strongest and hardest of all the steels used for this experiment. This is illustrated in figure 4.6 where steel samples tempered at 315^{O}C, 425 ^{O}C and 620 ^{O}C were all impacted at the same momentum of 37.0 kg.m/s. This is because the steel samples tempered at 315^{O}C were able to prevent dislocations from moving freely in the microstructure during the deformation. On the other hand, the steel samples tempered at 620 ^{O}C were relatively soft and low in strength because dislocations move freely in the microstructure of these samples as is illustrated in figures 4.5 and 4.6.

In a polycrystalline aggregate, the boundaries between grains are regions of disturbed lattice. There are rapid changes in the crystallographic orientation in passing from one grain to the next grain across the grain boundary. Grain boundaries act as preferential sites for solid-state reactions such as diffusion, phase transformations, and precipitation reactions due to their high energy. Due to restrictions enforced by the grain boundaries during deformation, slip occurs on several systems and on planes that are not closely packed. Grain boundaries act as obstacles to the motion of dislocations [39, 46, 57]. Decreasing grain size leads to an increase in the strength of the metal in line with the Hall-Petch equation

$$\sigma = \sigma_O + kd^{-1/2} \qquad 5.3$$

where σ_o is the intrinsic strength of the metal, k is a coefficient and d is a grain diameter or the size of the grain. The Hall-Petch equation shows that increasing the grain size leads to a decrease in the stress concentration at the grain boundaries that result in reduced strengthening compared

with fine-grained materials. The likelihood of dislocation-dislocation interaction leading to dislocation pile-up that result in a larger resistance to dislocation motion at the grain boundaries increases at small grain sizes [58]. The resistance to dislocation motion due to back stresses associated with dislocation tangles that form at grain boundaries reduces when the grain size increases because of the larger distances between grain boundaries. The strain hardening of a fine-grain-size metal will be greater than in a coarse-grain polycrystalline aggregate. Tempering eliminates many of the smaller martensitic laths and replaces the laths with coarse, spherical cementite particles at prior austenite grain boundaries and within the packets. The tempering temperature and holding time of steels determines the distances between layers or lamellae of the grains in the microstructure. The effects of replacing many of the martensitic laths with coarse, spherical particles become rigorous when tempering temperatures are increased. If the tempering temperature is low, the microstructure has fine layers or lamellae resulting in higher strengths [59]. These observations are in line with those made by Cepus [28] when he used SEM to investigate the microstructure of tempered SPS-Plus steels. In the steels tempered at $620^{O}C$, the cementite formed small spheroids or globules dispersed in ferrite matrix. The interlamellae spacing of the steel samples in this group were wider than in the other groups. The grain sizes were larger for the steel samples in this group than in the other groups. According to the Hall-Petch equation, when the grain size increases, the strength decreases. This analysis shows why the flow stresses in the steel samples tempered at $620\ ^{O}C$ were lower than in the other groups because they had larger grain sizes. This can be seen by comparing figures 4.2, 4.4, 4.5 and 4.6. Higher tempering temperature results in larger grain sizes and lower strengths for the steel samples tested [28, 59].

Thermal softening because of the conversion of impact energy to thermal energy dominates the latter stages of the deformation leading to observed drop in flow stress at high strain values. This is the point of stress collapse, which is due to the rapid thermal softening effect of adiabatic heating leading to strain localization. This is illustrated in figure 4.3 where a "kink" in the flow stress graph is indicated as the point of stress collapse. Thus, the point of stress collapse indicates the occurrence of localized adiabatic shearing which leads to the formation of adiabatic shear bands.

(5.3)EFFECTS OF HIGH STRAIN RATE AND LARGE STRAINS ON THE IMPACTED STEEL SAMPLES

The finger prints of directly impacting materials under large strains and high strain rates are the formation of adiabatic shear bands. Strain localization precedes the formation of adiabatic shear bands at high strain rates of deformation. At the initial stages of the deformation, there is no plastic deformation occurring. The competing processes of strain hardening and adiabatic heating occur in the microstructure of the samples as deformation continues. Strain hardening dominates the deformation process due to dislocation multiplication and dislocation-dislocation interactions. The adiabatic heating occurs by the conversion of most of the deformation energy into thermal energy that leads to thermal softening (adiabatic heating). As deformation continues, adiabatic heating leading to localized increase in temperature becomes critical. This occurs when the local rate of heat generation due to plastic flow exceeds the rate of heat dissipation into the surrounding material [24]. Additional heat generated in this zone softens the material and

increases deformation in the region. At a critical strain, there is stress collapse that leads to localization of strain in narrow bands which results in the formation of adiabatic shear bands. Material defects, geometric defects and temperature changes are essential for adiabatic shear band initialization [24]. The defects are attributed to inhomogeneities in the microstructure and composition of the steel samples. The above explanation for the formation of adiabatic shear bands has been confirmed by other investigators [21, 24]. Bassim and Odeshi [21] analyzed the occurrence of adiabatic shear bands in different materials using finite element approach and suggested that shear bands form at inhomogeneities such as second phase particle and precipitates in the microstructure of materials and results from the competition between strain hardening and adiabatic heating. Bassim et al [17, 21, 24], in their studies of adiabatic shear bands in steels, concluded that evolution of adiabatic shear bands proceed in three stages that include:

(a) no plastic deformation in the early stages of the deformation
(b) strain hardening and material softening competing with each other in the second stage
(c) thermal softening wins over strain hardening and dominates the deformation leading to a drop in stress resistance and strain localization

The formation of adiabatic shear bands in samples after impact is influenced by strain rate and impact momentum. This is evident in the results obtained where deformed bands and transformed bands formed in samples depending on the strain rate, impact momentum and the microstructure. However, the current study also demonstrates that the initial condition of the steel sample before impact have a strong influence on the type of shear band that is formed in the sample after impact. It has been reported in the literature that steel samples tempered at relatively

low temperatures usually form transformed shear bands while samples tempered at higher temperatures usually form deformed bands. This is seen in the steel samples tempered at 315^{O}C and those tempered at 620^{O}C. Transformed shear bands formed mostly in the samples tempered at 315^{O}C while deformed shear bands formed mainly in the samples tempered at 620 ^{O}C. Other investigators have verified these results in their studies on adiabatic shear bands in tempered martensitic steel samples [6, 29]. Zhang et al [29], in their studies on adiabatic shear bands in impact wear using low-alloy steel, observed white adiabatic shear bands in samples tempered at 200 ^{O}C -400 ^{O}C while deformed shear bands were formed in samples tempered at 650 ^{O}C . However, it was observed in the current study that although the formation of deformed shear bands dominated steel samples tempered at higher temperatures, at very high strain rates, transformed shear bands were formed. This can be seen in figure 4.36 where a transformed shear band formed in a sample tempered at 620^{O}C for two hours after it has been impacted at 50.0 kg.m/s. All the shear bands formed in this group, (samples tempered at 620^{O}C for two hours), were of the deformed shear bands type. However, after impacting at a very high momentum, a transformed shear band was formed. This demonstrates that regardless of the initial conditions of the steel samples, at very high strain rates, transformed shear bands will be formed during impact.

It was observed that well-developed distinct shear bands were formed in samples tempered at 315^{O}C and 425 ^{O}C for one hour than in the samples tempered at 315^{O}C and 425 ^{O}C for two hours. The shear bands were mostly diffused in the microstructure of the samples tempered at 315^{O}C and 425 ^{O}C for two hours. In the study by Bassim and Odeshi [21], they observed that the distance between precipitates limits the width of the adiabatic shear band formed in alloy steels containing fine precipitates. They determined that adiabatic shear bands formed in

microstructures that were reinforced by the presence of hard precipitates or second phase particles were narrow in shape and confined to narrow spacings between hard precipitates. The narrow shear bands have very large strains within them leading to micro crack formations. It is suggested that the well-developed distinct shear bands formed in samples tempered at 315^{O}C and 425 ^{O}C for one hour might be due to the presence of hard precipitates and particles in the samples in this group. Bassim and Odeshi suggested that wider bands with lower total strains that were less susceptible to damage were formed in steel samples with homogeneous microstructures. The two hours tempering time might have made the microstructure of the steel samples in this group more homogeneous than in the group that were tempered for one hour leading to the formation of very wide and diffused shear bands. Cepus [28] observed that when the tempering time of SPS-Plus steel samples were increased from 315^{O}C to 480 ^{O}C and 650 ^{O}C, the martensite grain sizes increased (coarsening) and the number and size of precipitates also increased and ferrite was much more uniformly distributed throughout the matrix. Increasing temperature during tempering is synonymous to increasing time of tempering. As suggested by Bassim and Odeshi, shear bands formed in homogenous microstructures are wider with less total strains. The wider and diffused shear bands in samples tempered at 2 hours are attributed to the homogeneous microstructure formed due to longer tempering times. Smaller particles and precipitates can dissolve during prolonged heat treatments [42, 43, and 45]. It is suggested that if the particles and precipitates that define the width of shear bands dissolve during the heat treatment, then diffused and scattered shear bands can form because there might not be any boundaries and limitations that will confine the widths of the shear bands. This might account for the diffused nature of the shear bands formed in steel samples tempered for 2 hours than those tempered for 1 hour.

In addition, the hardness of the parent material was found to influence the thickness of the shear bands as is depicted in figure 4.41. At the same impact momentum, the width of the shear bands formed in impacted samples decreased as the hardness of the parent steel increase. The size of grains, particles and precipitates in steel samples tempered at lower temperatures are finer compared to samples tempered at higher temperatures. Increasing tempering temperature increases the size of grains leading to a decrease in strength and hardness. At the same impact momentum, narrower shear bands formed in harder samples are attributed to the finer grain sizes, particles and precipitates that limit the widths of the shear bands. These results confirm those observed by other investigators [21, 60]. Panic [60], studied high strain rate induced failure in steels at high shear strains and suggested that harder materials could not deform plastically at high strain rates in the absence of enough heat. In the absence of enough heat to soften the material, deformation is restricted to the narrow region under the influence of adiabatic heating. Increasing impact momentum decreases the width of the shear bands at the same tempering temperature as depicted in figure 4.42. In addition, at the same impact momentum, increasing tempering temperature increases the widths of the shear bands formed. This can be related to the hardness and the microstructure of the parent materials as suggested by Bassim and Odeshi [21]. At higher tempering temperatures, material hardness decreases and grain sizes are larger. Particles and precipitates in the microstructure become coarser with larger spacings than at lower tempering temperatures. These distances between particles and precipitates that confine the width of the shear bands during initialization and formation of adiabatic shear bands become larger resulting in increase in the width of shear bands as compared to finer particles and precipitates in samples tempered at lower temperatures. This is similar to Cepus' observation during his study on the evolution of adiabatic shear bands [28]. Cepus observed that as the

tempering temperature increases; there is an increase in the width of shear bands regardless of test temperature. It should be emphasized here that, irrespective of the tempering temperature and time, the width of the transformed bands were always narrower than the deformed shear bands regardless of impact momentum, tempering temperature and hardness of parent materials.

Transformed shear bands formed in the impacted samples were harder compared to deformed shear bands due to the very large total strains within them. Transformed bands have been reported in the literature to have higher tendency to cracking than deformed bands. There were no cracks observed in any of the deformed bands formed in the impacted samples. However, some impacted samples had transformed bands with cracks propagating within them. The formation of these cracks within transformed bands is attributed to the very hard and brittle nature of the bands. Fractured samples failed along cracks propagating within the shear bands. Lower total strains were observed in the deformed shear bands compared to the total strains in the transformed shear bands. The deformed shear bands consisted of highly distorted grains when compared to the surrounding matrix because of the large strains in the bands [6, 8, 9, and 10]. Transformed shear bands showed white after etching whereas deformed shear bands appeared as a dark band. Many researchers have reported that the transformed shear bands have very fine equiaxed sub-grains with a very high dislocation density with cell boundaries that are different from the surrounding matrix [29, 30, 31, 32].

(5.4)POST IMPACT ANNEALING OF STEEL SAMPLES

Plastic deformation increases the dislocation density of a material. Impact at large strains and high strain rates increases the density of dislocations leading to the formation of dislocation tangles and networks in the impacted material. The structure of adiabatic shear bands have been reported to consists of equiaxed fine sub grains and dislocation tangles with cell boundaries [29, 30, 31, 32]. A characteristic feature of deformed samples is the formation of cellular substructures in which high dislocation density tangles form the cell walls [46]. The generation and interaction of dislocations during deformation result in an increase in internal energy and higher stored strain energy in the deformed samples. The deformed samples with their dislocation cell structures are mechanically stable but thermodynamically unstable and as temperature increases, the structures become more unstable [46].

In the current study, selected impacted steel samples with well-developed transformed shear bands were soaked at 350 ^{O}C to 850 ^{O}C for periods ranging from 30 minutes to 4 hours. Temperature and time of annealing, initial character of material structure before deformation, and the amount of deformation influence the properties of the microstructure of samples after annealing [61, 62, 63, and 64]. It was observed in the current study that when impacted samples were annealed at 350 ^{O}C, hardness of the shear bands and the surrounding impacted material increased regardless of the heat treatment before impact, amount of deformation, and the time of annealing as shown in figure 4.62. The adiabatic shear bands were still white and distinct in the annealed samples. This implies that annealing impacted steel samples at 350 ^{O}C will not reduce the hardness of the shear bands and hence 350 ^{O}C cannot be used to eliminate shear bands. In addition, it signifies that recrystallization does not occur at this temperature because if recrystallization were occurring, hardness would have decreased. There exists some critical

degree of cold work below which recrystallization cannot be made to occur. Wingrove [32] studied the structure of adiabatic shear bands in steels and observed that tempering the steel samples at 473 ^{O}K produced very slight changes in the etching characteristics of shear bands. In general, the higher the amount of deformation of a material before annealing, the lower the initial temperature of recrystallization [46, 57, 64, 65]. This demonstrates that even the higher amount of deformation in the samples tempered at 620 ^{O}C is not enough to attain the initial recrystallization temperature of the deformed samples during annealing. Lee et al [66] investigated the effects of post-deformation annealing conditions on the behavior of lamellar cementite and the occurrence of delamination in cold drawn steel wires. They observed that post-deformation annealing of the steel wires between 425 ^{O}C to 475 ^{O}C for 30 seconds resulted in an increase in tensile strength. They attributed the increase in tensile strength during the post-deformation annealing to age hardening. They observed that age hardening occurring during annealing does not cause any noticeable changes in the microstructure of the samples. Schindler et al investigated the effect of cold rolling and annealing on mechanical properties of a HSLA steel [64]. They observed that annealing the steel samples to 530 ^{O}C and 580 ^{O}C after deformations of up to 40% led to a slow increase in hardness and strength. This increase in hardness and strength was attributed to partial recrystallization of the samples. Janošec et al [63] studied the properties of Nb-V-Ti micro alloyed steel influenced by cold rolling and annealing. They observed a slow increase in strength and hardness with rising strain up to ε=30% when steel samples were annealed to 530 ^{O}C and 600 ^{O}C. Al- Ameeri [26] studied the effect of heat treatment on adiabatic shear bands in AISI 4340 steel samples and observed that annealing impacted samples at 315 ^{O}C after impact do not produce any noticeable change in the hardness of shear bands. She suggested that recrystallization process at 315 ^{O}C was either nonexistent or very

slow. Park et al [67] determined that the increase in tensile strength during post deformation annealing at low temperatures (200 ^{O}C to 300 ^{O}C) was due to age hardening when they studied the effects of annealing temperature and time on the microstructural evolution and corresponding mechanical properties of cold-drawn steel wires. The observed increase in hardness of the steel samples during the post-impact annealing at 350 ^{O}C in the current study is attributed to age hardening or strain aging. The mechanism of age hardening was described by Watte et al [68] as occurring in two stages that include:

(a) Partial decomposition of lamellar cementite during annealing

(b) Segregation of carbon atoms to ferrite dislocations

Some of the cementite in the deformed steel samples decompose during the annealing process. This increases the amount of dissolved carbon atoms that diffuse into lamellar ferrite and pins dislocations. The pinning of dislocations blocks movement of the dislocations and results in an increase in strength. It is suggested that partial decomposition of cementite occurring during post-impact annealing at 350 ^{O}C accounts for the increase in hardness of shear bands and surrounding impacted materials. Sample "A" in figure 4.49 indicates that as the post-impact annealing time is increased at 350 ^{O}C, more cementite breaks up and increases the content of the dissolved carbon atoms that pins dislocations. This results in a further increase in hardness of the shear bands and the surrounding material.

Strength or hardness properties of materials usually decrease with increasing temperature of annealing. Post-impact annealing of the steel samples at 650 ^{O}C, regardless of the annealing time, initial conditions before deformation, and the amount of deformation, resulted in a significant reduction in hardness of the adiabatic shear bands and the surrounding material. This is shown in figure 4.52 where three different steel samples, tempered at different temperatures and deformed

at different impact momentums, were annealed at 650 ^{O}C for 30 minutes and 2 hours. The hardness of the shear bands and the surrounding material both decreased and their properties became comparable. Al-Ameeri [26] attributed the significant hardness reduction of shear bands and surrounding impacted materials to nucleation and growth of spheroidal cementite when she studied the structure of impacted steel samples under a Scanning Electron Microscope (SEM) after annealing at 650 ^{O}C. She suggested that the reduction in hardness was due to a significant reduction in dislocation density because of recrystallization and growth of strain free and coarse carbide grains. It was observed in the current study that since the amount of deformation in the steel samples tempered at 620 ^{O}C were greater than the other samples tempered at 315 ^{O}C and 425 ^{O}C, the reduction in hardness of shear bands and the bulk-impacted material were higher. This observed higher reduction in hardness when the amount of deformation is higher is in line with the observations made by Dedek [65] and Prasad et al [69]. During a post deformation annealing, Lee et al [66] attributed the decrease in hardness of cold drawn steel wires to age softening that involved

(a) the break-up and spheroidization of lamellar cementite

(b) the growth of cementite particles and

(c) recovery or recrystallization of lamellar ferrite

They suggested that the decrease in strength with annealing time was due to increased degree of age softening. Janošec et al [63] concluded that annealing at high temperatures after cold rolling results in decrease in strength of steel wires due to recrystallization processes and coarsening of precipitates. Coalescence of dissolved fine carbides in the shear bands could lead to a change in hardness since coalescence of carbides will lead to a decrease in surface energy. It is suggested that the reduction in hardness of both the adiabatic shear bands and the surrounding impacted

material is due to recovery and recrystallization processes which leads to reduction in dislocation density and spheroidization of cementite. During the post-impact annealing, recovery leads [70-71] to

(a) increased diffusion

(b) increased dislocation motion

(c) decrease in dislocation density by annihilation

(d) formation of low-energy dislocation configurations and

(e) relieve of the internal strain energy

Recovery sets in with the nucleation and growth of strain free grains with low-density dislocations [70-71] leading to a reduction in hardness of both the shear bands and the surrounding impacted material. Coalescence of sub grains, which involves re-orientation or rotation such that the orientation of two neighboring sub grains become equal resulting in the disappearance of the boundaries separating them leads to the formation of new strain free grains with reduced hardness.

The microstructure of the deformed steel samples became homogeneous after the post impact annealing at 650 ^{O}C. A "signature" or the path travelled by the shear bands during impact could still be traced in the annealed microstructures although the materials in the shear bands had been replaced with new strain free grains. It was only after annealing the deformed samples above 750 ^{O}C that complete elimination of the traces of the shear bands occurred. The microstructure became homogenous with no traces of deformation or shear bands in them. This can be seen in the post-impact annealed photomicrographs of samples tempered at 620 ^{O}C. The shear bands were completely erased from the microstructure with no traces left. Spheroidization occurred at

these high temperatures and recrystallized strain free grains coarsened and further reduction in the hardness occurred.

It is possible to eliminate adiabatic shear bands formed in impacted steel samples using heat treatment. Post-impact annealing heat treatment can be used to eliminate adiabatic shear bands; however, choosing the proper temperature of annealing is the most critical parameter. Choosing low annealing temperatures can deteriorate the properties of the adiabatic shear bands such as was observed in the impacted samples annealed at 350 ^{O}C in the present study. A higher annealing temperature ensures the elimination of adiabatic shear bands from the impacted steel samples. Post impact annealing of the steel samples should be done above 650 ^{O}C because the hard brittle transformed adiabatic shear bands are replaced by a more ductile and soft material.

CHAPTER 6.0: CONCLUSIONS

The stability of adiabatic shear bands using post impact annealing was investigated in this study. The heat treatment was used to determine the possibility of eliminating shear bands from the microstructure of severely deformed AISI 4340 steel specimens. The Direct Impact Hopkinson Pressure Bar (DIHPB), developed at the University of Manitoba, was used to impact the steel samples at large strains and high strain rates to generate adiabatic shear bands in the samples. Selected impacted steel samples with distinct transformed shear bands were soaked at 350 ^{O}C to 850 ^{O}C for periods ranging from 30 minutes to 4 hours to investigate how temperature and time affects the structure of adiabatic shear bands. The following is concluded from the current study:

(a) Extensive deformation by direct impact at large strains and high strain rates is required for the generation of adiabatic shear bands in the steel samples.

(b) Although impact momentum and strain rates affect the formation of shear bands, the initial condition (tempering temperature and time) of the steel samples before impact also has a significant influence on the formation of the shear bands.

(c) The initial conditions of the steel samples influence the type of adiabatic shear band that will be formed after impact as to whether the adiabatic shear bands will be well developed and distinct from the microstructure or diffused and scattered.

(d) White etching transformed shear bands and dull / black etching deformed shear bands were observed in most of the steel samples after impact at extensively large strains and at high strain rates.

(e) Tempering the steel samples at 315^{O}C and 425^{O}C for 1 hour led to the formation of distinct and well-developed adiabatic shear bands after impact than tempering at 315^{O}C and 425^{O}C for 2 hours. Diffused deformed and transformed adiabatic shear bands were formed in the steel samples tempered at 315^{O}C and 425^{O}C for 2 hours.

(f) Tempering the steel samples at high temperatures before impact resulted in the formation of mostly deformed shear bands than transformed shear bands after impact. Nevertheless, at high strain rates and impact momentum values, transformed shear bands were formed in the steel samples after severe deformation.

(g) Adiabatic shear bands, when formed in the steel samples, have a much higher hardness compared to the surrounding impacted materials. Transformed shear bands were always harder than deformed shear bands. Adiabatic shear bands were seen as preferred paths for crack initiation and propagation due to their hard and brittle nature.

(h) Transformed shear bands are hard and brittle compared to deformed shear bands and surrounding impacted materials. The very hard nature of the transformed shear bands made them very brittle. In some impacted samples, cracks propagated in the transformed shear bands. There were no cracks observed in deformed shear bands formed in the impacted samples.

(i) Fractured samples showed that the impacted steels failed along cracks that propagated in the shear bands. The paths of failure were where the shear bands cross paths with propagating cracks.

(j) Post impact annealing heat treatment can be used to eliminate adiabatic shear bands from impacted steel samples. The temperature of annealing of the impacted steel samples is the most critical parameter.

(k) Annealing impacted steel samples at lower temperatures, (less than $350^{O}C$) does not favor the elimination of adiabatic shear bands. The properties of the shear bands become worse at these temperatures during post impact annealing. However, annealing the impacted steel samples at higher temperatures (greater than 650 ^{O}C) eliminates shear bands from the samples.

(l) When impacted steel samples are annealed at $350^{O}C$, the hardness of the shear bands and the surrounding impacted material increases regardless of the heat treatment before impact, amount of deformation, and the time of annealing. This is explained by the effects of strain aging or age hardening. Age hardening does not cause significant changes in microstructure but causes an increase in hardness due to the segregation of carbon atoms to ferrite dislocations and partial decomposition of lamellar cementite during post impact annealing. More cementite breaks up and increases the content of the dissolved carbon atoms that pins dislocations.

(m) Post-impact annealing at 450 ^{O}C and 550 ^{O}C results in a decrease in hardness and thickness of the shear bands irrespective of the heat treatment of the samples before impact, the amount of deformation, and the time of annealing.

(n) Post impact annealing of steel samples at 650 ^{O}C for 30 minutes and 2 hours results in a significant decrease in the hardness of the shear bands and the surrounding material and their properties become similar due to the effects of recovery and recrystallization.

(o) Although the properties of the shear bands and the surrounding impacted material became comparable after post-impact annealing at 650 ^{O}C, there was a "signature" left in the microstructure of the samples. The material in the "signature" looked like the surrounding material and had approximately the same hardness. However, the initial path of the shear bands in the deformed steel samples could be traced through the "signature" left after the post-impact annealing.

(p) At higher temperatures of post deformation annealing (750 ^{O}C and 850 ^{O}C), the microstructure of the steel samples appeared as homogenous with no traces of the shear bands. The "signatures" which were used to trace the path of the shear bands were erased and the hardness of the samples became uniform.

(q) Adiabatic shear bands can be eliminated from deformed steel samples by annealing heat treatment. However, the post-impact annealing should be performed above 650 ^{O}C.

REFERENCES

1. J. A. Zukas et al, Impact Dynamics, John Wiley & Sons Inc. 1982

2. J. Hopkinson, Original Papers by J. Hopkinson, B. Hopkinson, Ed, Cambridge, At the University Press Volume 2 (1901), 316-324

3. B. Hopkinson, The Effects Of Momentary Stress In Metals, Proc. R. Soc. (London) A Volume 74 (1905), 498

4. H. Tresca, Further Applications Of The Flows Of Solids, Proceedings of the Institution of Mechanical Engineers Volume 30 (1878), 301

5. C. Zener, J. H. Hollomon, Effect Of Strain Rate Upon Plastic Flow Of Steel, Journal of Applied Physics Volume 15 (1944), 22-32

6. M. N. Bassim, A. G. Odeshi, Shear Strain Localization And Fracture In High Strength Structural Materials, Archives of Material Science and Engineering Volume 31 Issue 2 (June 2008), 69-74

7. A. G. Odeshi, M. N. Bassim, S. Al-Ameeri, Effect Of Heat Treatment On Adiabatic Shear Bands In High Strength Low Alloy Steel, Materials Science and Engineering A Volume 419 (2006), 69–75

8. K. A. Zurek, The Study Of Adiabatic Shear Band Instability In A Pearlitic 4340 Steel Using A Dynamic Punch Test, Metallurgical Transactions A Volume 25 (1994), 2483

9. K. M. Cho, S. Lee, S. R. Nutt and J. Duffy, Low Absorbed Energy Ductile Dimple Fracture In Lower Shelf Region In An Ultra Fine Grained Ferrite/Cementite Steel, Acta Metall Mater. Volume 41 (1993), 923

10. C. L. Wittman, M. A. Meyers , H. R. Pak, Observation Of An Adiabatic Shear Band In AISI 4340 Steel By High-Voltage Transmission Electron Microscopy, Metallurgical Transactions A Volume 21 (1990), 707

11. R. W. Armstrong and F. J. Zerilli, Dislocation Mechanics Aspects Of Plastic Instability And Shear Bending, Mechanics of Materials Volume 17 (1994), 319-327

12. S. E. Schoenfeld, T. W. Wright, A Failure Criterion Based On Material Instability. International Journal of Solids and Structures Volume 40 (2003)

13. D. C. Erlich, L. Seaman, D. A. Shockey, D. R. Curran, Development And Application Of A Computational Shear Band Model, BRL-CR-00416 (1980)

14. M. N. Raftenberg, C. D. Krause, Metallographic Observations Of Armor Steel Specimens From Plates Perforated By Shaped Charge Jets, International Journal of Impact Engineering Volume 23 (1999), 757–770

15. ASM Metals Handbook, Mechanical Testing & Evaluation Hard bound, ISBN: 0-87170-389-0, Volume 8, 427-554

16. X. W. Chen, Q. M. Li, S. C. Fan, Initiation Of Adiabatic Shear Failure In A Clamped Circular Plate Struck By A Blunt Projectile, International Journal of Impact Engineering Volume 31 (2005), 877-893

17. M. N. Bassim, Study Of The Formation Of Adiabatic Shear Bands In Steels, Journal of Materials Processing Technology Volume 119 (2001), 234-236

18. J. Duffy, Y. C. Chi, On The Measurement Of Local Strain And Temperature During The Formation Of Adiabatic Shear Bands, Materials Science and Engineering A Volume 157 (1992), 195–210

19. Y. Bai, B. Dodd, Adiabatic Shear Localization, Pergamon Press, New York, (1992)

20. A. G. Odeshi, M. N. Bassim, Effects Of Microstructure On The Dynamic Shear Failure Of A High Strength Low Alloy Steel In Compression At High Strain Rates

21. M. N. Bassim, A. G. Odeshi, Microstructural Model For Occurrence Of Adiabatic Shear Bands, AES-Advanced Engineering solutions (Ottawa, Canada) ATEMA (2007)

22. J. Duffy, Y. C. Chi, On The Measurement Of Local Strain And Temperature During The Formation Of Adiabatic Shear Bands, Materials Science and Engineering A Volume 157 (1992), 195–210

23. A. M. Merzer, Modeling Of Adiabatic Shear Band Development From Small Imperfections, Journal of the Mechanics and Physics of Solids Volume 30 (1982), 323–338

24. H. Feng, and M. N. Bassim, Finite Element Modeling Of The Formation Of Adiabatic Shear Bands In AISI 4340 Steel, Material Science and Engineering A Volume 266 (1999), 255-260

25. M. N. Bassim, Study Of The Formation Of Adiabatic Shear Bands In Steels, Journal of Materials Processing Technology Volume 119 (2001), 234-236

26. S. Al-Ameeri, The Effect Of Heat Treatment On The Adiabatic Shear Bands In AISI 4340 Steel At High Strain Rate, M.Sc. Thesis, University of Manitoba, (2005)

27. R. Nakkalil, Formation Of Adiabatic Shear Bands In Eutectoid Steels In High Strain Rate Compression, Acta. Metall. Mater. Volume 39 (1991), 2553-2563

28. E. Cepus, Evolution Of Adiabatic Shear Bands In High Strength Steels At High Shear Strain Rates, M.Sc. Thesis, University of Manitoba (1995)

29. B. Zhang, W. Shen, Y. Liu, Adiabatic Shear Bands In Impact Wear, Journal of Material Science Volume 17 (1998), 765-767

30. X. W. Chen, Q. M. Li, S. C. Fan, Initiation Of Adiabatic Shear Failure In A Clamped Circular Plate Struck By A Blunt Projectile, International Journal of Impact Engineering Volume 31 (2005), 877-893

31. R. C. Glenn and W. C. Leslie, The Nature Of "White Streaks" In Impacted Steel Armor Plate, Metallurgical Transactions Volume 2 (1971), 2945-2947

32. A. L. Wingrove, A Note On The Structure Of Adiabatic Shear Bands In Steel, Department of supply, Australian Defense Scientific Service, Defense Standard Laboratories, Tech. Memo Volume 33 (1971)

33. S. B. Newcomb and W. M. Stobb, A Transmission Electron Microscopy Study Of The White-Etching Layer On A Rail Head, Material Science Engineering Volume 66 (1984), 195

34. G. A. Li, L. Zhen, C. Lin, R. S. Gao, X. Tan, C. Y. Xu, Deformation Localization And Recrystallization In TC4 Alloy Under Impact Condition, Materials Science and Engineering A Volume 395 (2005) 98-101

35. C. R. Mason, M. J. Worswick and P. J. Gallagher, Adiabatic Shear In Remco Iron And Quenched And Tempered 4340 Steel, Journal of Physics IV France Volume 7 (1997), 827

36. M. E. Backmann and S. A. Finnegan, Metallurgical Effects At High Rates Of Strain, Plenum Press, New York (1973), 531-543

37. F. Yazdani, M. N. Bassim, A. G. Odeshi, The Formation Of Adiabatic Shear Bands In Copper During Torsion At High Strain Rates, Procedia Engineering (2008)

38. Z. H. Chen, L .C. Chan, T. C. Lee, C. Y. Tang, An Investigation On The Formation And Propagation Of Shear Band In Fine-Blanking Process, Journal of Materials Processing Technology Volume 138 (2003) 610–614

39. J. T. Black, A. K. Ronald, Materials And Processes In Manufacturing, 10th edition ,John Willey &sons, Inc. 71-117

40. G. Krauss, Steels, Processing, Structure And Performance, ASM International (2005), 55-83, 396-402

41. W. S. Lee, T. T. Su, Mechanical Properties And Microstructural Features Of AISI 4340 High-Strength Alloy Steel Under Quenched And Tempered Condition, Journal of Materials Processing Technology Volume 87 (1999), 198-206
42. F. C. Campbell, Elements Of Metallurgy And Engineering Alloys, ASM International,
43. G. Krauss, Steels, Processing, Structure And Performance, ASM International (2005), 327-402
44. B. S. Lement, B. L. Averbach, and M. Cohen, Microstructural Changes On Tempering Iron-Carbon Alloys. Trans. ASM. Volume 46 (1954), 851-881
45. M. A. Grossmann and E.C. Bain, Principles Of Heat Treatment, 5th edition. American Society of Metals, (1964)
46. G. E. Dieter, Mechanical Metallurgy, 3rd edition, McGraw-Hill Book Company, (1986)
47. N. Wan, W. Xiong and J. Suo, Mathematical Model For Tempering Time Effect On Quenched Steel Based On Hollomon Parameter, Journal of Material Science and Technology Volume 21 (2005)
48. E. Wakai, T. Taguchi, T. Yamamoto, F. Takada, Effects Of Tempering Temperature And Time On Tensile Properties Of F82H Irradiated By Neutrons, Journal of Nuclear Materials (2004) 329-333, 1133-1136
49. M. S. Bhat, Microstructure And Mechanical Properties Of AISI 4340 Steel Modified With Aluminum And Silicon, Lawrence Berkeley National Laboratory, LBNL Paper LBL-6046 , (2010)
50. ASTM STP 407, Temper Embrittlement In Steels, A symposium presented at a meeting of committee A-1 on steel, American Society for Testing and Materials, Philadelphia, 3rd to 4th October, (1967), 1-19

51. ASTM STP 499, Temper Embrittlement Of Alloy Steels, American Society for Testing and Materials, Atlantic City, N. J, 27th June to 2nd July, (1971), 1-33
52. T. Ishiguo, Y. Murakami, K. Ohnishi, and J. Watanabe, 2.25%Cr-1%Mo Pressure Vessel Steels With Improved Creep Rupture Strength, Proceedings of the symposium on Applications Of 2.25%Cr-1%Mo Steel For Thick-Wall Pressure Vessels, ASTM STP 755, (1980), 129-147
53. D. H. Herring, The Embrittlement Phenomena In Hardened & Tempered Steel, The International Journal of Thermal Technology (2006)
54. A. Reguly, T. R. Strohaecker, G. Krauss, and D. K. Matlock, Quench Embrittlement Of Hardened 5160 Steel As A Function Of Austenitizing Temperature, Metallurgical & Materials Transactions A Volume 35 (2004), 153
55. R. M. Bruscato, Embrittlement Factors For Estimating Temper Embrittlement In 2.25Cr:1Mo, 3.5Ni-1.75Cr-0.5Mo-0.1V And 3.5Ni Steels, ASTM Conference, Miami, Florida, (1987)
56. H. Baker, Structure And Properties Of Metals, Metals Handbook Desk Edition, 2nd Edition, ASM International, (1998), 85-121
57. W. D. Callister Jr, Material Science And Engineering, An Introduction, 3rd Edition, John Wiley & Sons, Inc., 148-176
58. D. Hull and D. J. Bacon, Introduction To Dislocations, Pergamon Press, London, (1984)
59. J. W. Martin, Micromechanisms In Particle Hardened Alloys, Cambridge University Press, (1980)
60. N. Panic, High Strain Rate Induced Failure In Steels At High Shear Strains, M.Sc. Thesis, University of Manitoba, (1999)

61. J. Adamczyk, A. Grajcar, Effect Of Heat Treatment Conditions On The Structure And Mechanical Properties Of DP-Type Steel, Journal of Achievements in Materials and Manufacturing Engineering Volume 17 (2006), 305-308
62. T. Gladman, The Physical Metallurgy Of Micro Alloyed Steels, The Institute of Materials, London, (1997)
63. M. Janošec, I. Schindler, J. Palát, L. Cížek, V. Vodárek, E. Místecký, M. Ružicka, L. A. Dobrzanski, S. Rusz, P. Suchánek, Properties Of A Nb-V-Ti Micro Alloyed Steel Influenced By Cold Rolling And Annealing, Journal of Achievements in Materials and Manufacturing Engineering Volume 20 (2006), 251-254
64. I. Schindler, M. Janosec, E. Mistecky, M. Ruzicka, L. Cizek, L. A. Dobrzanski, S. Rusz, P. Suchanek, Effect Of Cold Rolling And Annealing On Mechanical Properties Of HSLA Steel, Archives of Material Science and Engineering Volume 36 (2009), 41-47
65. V. Dedek, Heat Treatment Of The Cold Rolled Steel Strips, SNTL, Praha, (in Czech) (1964)
66. J. W. Lee, J. C. Lee, Y. S. Lee, K. T. Park, W. J. Nam, Effects Of Post-Deformation Annealing Conditions On The Behavior Of Lamellar Cementite And The Occurrence Of Delamination In Cold Drawn Steel Wires, Journal of Materials Processing Technology Volume 209 (2009), 5300–5304
67. D. B. Park, J. W. Lee, Y. S. Lee, K. T. Park and W. J. Nam, Effects Of The Annealing Temperature And Time On The Microstructural Evolution And Corresponding The Mechanical Properties Of Cold-Drawn Steel Wires, Metals and Materials International Volume 14 (2008), 59-64

68. P. Watte, J. V. Humbeeck, E. Aernoudt, and I. Lefever, Strain Ageing In Heavily Drawn Eutectoid Steel Wires, Scripta Mater. Volume 34 (1996), 89-95
69. N. Prasad, S. Kumar, P. Kumar, S. N. Ojha, Mechanical Properties Of Cold-Rolled Annealed HSLA Steel, Journal of Materials Science Volume 26 (1991), 5158-5162
70. A. K. Sinhar, Recovery Recrystallization And Grain Growth In Ferrous Metallurgy, Butterworth's Publishers, Stoneham, USA (1989) 43-76
71. H. Hu, and L. Himmel, Recovery And Recrystallization Of Metals, Interscience, New York, (1963), 311